Texas A&M University
Mechanical Engineering Department

Thermohydrodynamic Analysis of Cryogenic Liquid Turbulent Flow Fluid Film Bearings.

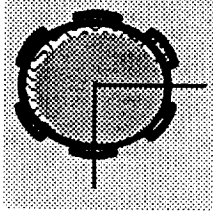

NASA Grant NAG3-1434

Annual Research Progress Report to
NASA Lewis Research Center

Contract Monitor: Mr. James Walker

Luis San Andres
Associate Professor

December 1993

Period of performance: January 1 to December 31, 1993

TABLE OF CONTENTS

THERMOHYDRODYNAMIC ANALYSIS OF CRYOGENIC LIQUID TURBULENT FLOW FLUID FILM BEARINGS

Annual Report to NASA-Lewis Research Center
NASA Grant NAG3–1434
Contract Monitor: Mr. James Walker

P.I.: Dr. Luis San Andres (Associate Professor)
(December 31, 1993)

Mechanical Engineering Department
Texas A & M University
College Station, Texas 77843
Telephone: 409-845-0160 Telefax: 409-845-1835

ABSTRACT

A thermohydrodynamic analysis is presented and a computer code developed for prediction of the static and dynamic force response of hydrostatic journal bearings (HJBs), annular seals or damper bearing seals, and fixed arc pad bearings for cryogenic liquid applications. The study includes the most important flow characteristics found in cryogenic fluid film bearings such as flow turbulence, fluid inertia, liquid compressibility and thermal effects. The analysis and computational model devised allow the determination of the flow field in cryogenic fluid film bearings along with the dynamic force coefficients for rotor-bearing stability analysis.

Journal model: ASME JOURNAL OF TRIBOLOGY.

ACKNOWLEDGEMENTS

This research was sponsored by the NASA-Lewis Research Center under NASA Grant NAG3-1434, with Mr. James Walker of NASA as the technical monitor. Acknowledgement is due to NASA-LeRC for its support, and in particular to Mr. James Walker for his interest on this work.

Thanks to Dr. Zhou Yang who worked as a Research Associate for the project until September 1993. Dr. Yang was responsible for most of the computer code programming. Thanks also to Dr. Dara Childs at Texas A&M University for his continued interest and encouragement on this research.

List of Tables

List of Figures

List of Figures (continued)

EXECUTIVE SUMMARY

A thermohydrodynamic analysis and computer code for the prediction of the static and dynamic force response of fluid film bearings for cryogenic applications have been completed on 1993. The current technological needs require reliable and resilient fluid film bearing designs to provide maximum operating life with optimum rotordynamic characteristics at the lowest cost. The analysis and code constitute practical tools for the prediction of performance and design of cryogenic liquid hydrostatic journal bearings, annular pressure seals or damper bearings, and cylindrical pad hydrodynamic bearings.

The motion of a cryogenic liquid on the thin film annular region of a fluid film bearing is described by a set of mass, momentum conservation, and energy transport equations for the primitive turbulent bulk-flow variables, and accompanied by thermophysical state equations for evaluation of the fluid material properties. Zeroth-order equations describe the fluid flow field for a journal static equilibrium position, while first-order linear equations govern the fluid flow for small amplitude journal center translational motions and journal axis conical motions. Solution to the zeroth-order flow field equations provides the bearing flow rate, load capacity, restoring moments and torque. Solution to the first-order equations determines the rotordynamic force and moment coefficients due to journal lateral and angular motions. The analysis includes the effects of flow turbulence, fluid inertia, liquid compressibility and thermal energy transport on the performance of cryogenic liquid bearings.

The numerical predictions from the computational program (*hydrosealt*) correlate favorably with experimental results available in the literature. Numerous examples are provided to demonstrate the effectiveness of the program to analyze cryogenic fluid film bearings as well as conventional viscous lubricant bearings.

INTRODUCTION

Hydrostatic Journal Bearings (HJBs) are the ideal candidates to replace roller bearings as support elements in cryogenic turbomachinery. These bearings along with hydrostatic annular seals will be used for primary space-power applications due to their long lifetime, low friction and wear, significant load capacity, and large direct stiffness and damping force coefficients. HJBs, unlike rolling element bearings, have no DN limit. Rotating machinery free of this constraint can operate at larger speeds with better efficiency and reduced overall weight and size. Durability in HJBs is assured by the absence of contact between stationary and moving parts during steady-state operation, while long life reduces the frequency of required overhauls. Despite these attractive features, fluid film bearing stability considerations and thermal phenomena along with two-phase flow operation are a primary concern for high speed operation with large pressure differentials. Fluid film bearing stability is essentially related to hydrodynamic and liquid compressibility effects, while thermal effects are of importance due to flow turbulence with substantial energy dissipation.

A comprehensive literature review on the subject of hydrostatic bearings and annular seals relevant to cryogenic liquid applications has been presented elsewhere (San Andres, 1990a-c, 1991a-c, 1992a, 1993a). A brief discussion of the relevant literature pertaining to the analysis, design and testing of fluid film bearings for cryogenic applications over the last few years follows.

Reddecliff and Vohr (1969) initially studied HJBs for use in high-pressure cryogenic rocket engine turbopumps. The inertia effect at the edges of the recesses changed the pressure distribution, reduced the flow rate but did not affect the total bearing load capacity. The non linear fluid advective inertial terms could not be accounted for due to numerical difficulties. Variable fluid properties were

treated as linear between those at the supply and discharge pressures, and steady-state predictions were reported to agree well with experimental results. The scatter in the measured recess pressures was attributed to variations in bearing clearance caused by **temperature** differences between the bearing and shaft and to measurement inaccuracies.

Artiles et al. (1982) presented a numerical solution to the static and dynamic performance characteristics of hydrostatic journal bearings. A turbulent Reynolds equation with **constant** fluid properties was solved by the column–matrix method, while a Newton-Raphson scheme was implemented for efficient calculation of the recess pressures. Turbulent-to-laminar flow power-loss ratios were reported to be in the range of 25 to 30 for the Reynolds numbers considered. Even though there were neither energy considerations nor thermal effects in the analysis, large temperature rises (up to 24.5$^{\circ}C$) in the fluid film were reported for LO_2 bearings, while temperature **rises** in LH_2 bearings were negligibly small.

Braun et al.(1987a,b) introduced a comprehensive THD analysis for cryogenic liquid hydrodynamic and hydrostatic journal bearings. On the fluid film region, a variable–properties Reynolds equation was coupled to a 2-D energy transport equation. The heat transfer to the bounding solids (shaft and bush) was analyzed in its three dimensional complexity. Bulk-flow heat transfer coefficients were used to represent the boundary conditions at the fluid/solid interfaces, and fluid inertia effects were considered only at the pocket's edges with no recess volume-liquid compressibility effects. Braun et al.'s analysis regard the fluid flow as **laminar**, although large pressure differentials and rotational speeds were considered in the applications studied. For a liquid hydrogen HJB, a small temperature increment was found in the fluid film, and thermal effects were shown to be minimal relative to a constant properties liquid model. Calculations for a liquid oxygen

hydrodynamic journal bearing showed a large temperature rise ($13°K$) for eccentric operation at 14,000 rpm with a profound impact on the mass flow rate and load capacity. The numerical predictions presented show circumferential flow Reynolds numbers as large as 100,000 with a laminar flow model. No definite conclusions in regard to the effect of heat transfer from the fluid film to the bounding solids are extracted from the analysis.

San Andres (1990a) introduced the first full inertial, fully developed turbulent bulk-flow model for the analysis of incompressible liquids hydrostatic bearings. This model revealed the importance of flow turbulence and fluid inertia at the film lands and at the recess boundaries of typical high speed hydrostatic bearings. Results of the analysis show that a fluid inertia flow model when compared to a classical viscous model determines reduced leakage rates and hydrostatic forces while increasing the hydrodynamic force due to journal rotation. These effects then lead to the generation of larger direct damping and cross-coupled stiffness coefficients whith a reduction in the direct stiffness coefficients and the appearance of significant inertia force coefficients for liquids of large density such as water and liquid oxygen. San Andres (1991b) shows that moderate to large journal eccentricities have a pronounced effect on the force coefficients of HJBs with large hydrodynamic effects (high rotational speeds). For large journal center static excursions, the hydrodynamic effect produces force coefficients similar in form to those of a conventional circular journal bearing. Furthermore, orifice back-flow accompanied by a sudden drop on direct stiffness is likely to occur at large journal eccentricity operation.

A study of the laminar flow field on a recess-land region of a typical high speed hydrostatic bearing geometry is given by San Andres and Velthuis (1992). Computational experiments revealed a substantial hydrodynamic pressure

generation on the downstream side of a recess followed by a sharp pressure drop at the recess edge next to a film region of small clearance. Calculated recess-edge entrance factors and recess shear coefficients form the basis of a simplified one-dimensional recess bulk-flow model implemented for the analysis of finite length hydrostatic bearings. Other recent analysis and numerical predictions studying the same flow geometry are given by Braun et al. (1993), and Hill et al. (1993).

The Texas A&M hydrostatic bearing test facility directed has provided with a wealth of experimental data for the static and dynamic force characteristics of water lubricated hydrostatic bearings. Experimental measurements are routinely performed for bearings of different geometries and at journal speeds ranging from 10,000 to 25,000 rpm and pressure supplies from 4 to 7 MPa. The test facility accomodates state of the art instrumentation and control, and possesses the most efficient and accurate bearing parameter identification method based on a real-time process and frequency domain algorithms. Kurtin et al. (1993) reported experimental data for the static performance characteristics of a 5 recess, water HJB for the operating conditions noted and three different bearing clearances. The experimental results correlate very well with predictions from the numerical model developed by San Andres (1990a, 1992a). It is noted also that accurate theoretical results depend greatly on the knowledge of the bearing operating clearance, and most importantly, on the orifice discharge coefficients.

The stability characteristics of a simple rotor-bearing system are defined by the threshold speed of instability and the whirl frequency ratio. This instability is of the "hydrodynamic" type and solely due to the effect of journal rotational speed on the flow field of a bearing under dynamic journal motions. The threshold speed represents the journal rotational speed at which the bearings loose their effective damping and any small perturbation from an equilibrium position determines

unbounded rotor motions according to linear vibrations theory. The rotor-bearing first natural frequency (critical speed) depends on the bearing equivalent stiffness and the shaft stiffness. It is also well known that flexible rotors do present natural frequencies much lower than rigid rotors. The whirl frequency ratio denotes the ratio between the onset whirl frequency (typically the system first critical speed) and the threshold speed of instability. This ratio is independent of the flexibility of the rotating shaft and, it provides information on the stability characteristics of the fluid film bearings within the desired range of operation of a typical machine. Plain cylindrical journal bearings show a characteristic whirl frequency ratio equal to 0.50 for operation at small to moderate eccentricities (light loads) and hence denote that a simple rotor-bearing system will become unstable at a rotational speed equal to twice the system first critical speed.

The results presented by San Andres (1990c, 1991b) have shown that, contrary to generalized intuition, incompressible liquid hydrostatic bearings present a whirl frequency ratio identical to that of plain journal bearings. This condition then limits severely the application of HJBs to high speed, light weight turbomachinery. Furthermore, cross-coupled inertia force coefficients for large density fluids have an adverse effect on the threshold speed of instability The experimental results from the Hydrostatic Bearing Test Program at Texas A&M University verify closely the theoretical predictions and show, in some circumstances, the whirl frequency ratio to increase above 0.50 for low rotational speeds and large supply pressures (Franchek et al., 1993, Mosher, 1993).

Approximate theoretical models for prediction of the dynamic force response of hydrostatic bearings at the centered position have been reported also by San Andres (1990b,1991a,1992b). Approximate analytical solutions to the turbulent flow field bring insight into the understanding of the flow mechanics and provide

a fast and efficient tool for the preliminary design of hydrostatic journal bearings. Results of the analyses show the importance of recess volume fluid compressibility effects on the rotordynamic force response of typical HJB for cryogenic applications. In brief, HJBs handling highly compressible liquids such as LH_2 for example, are prone to show a self-excited type instability of the "pneumatic hammer" type and could produce negative damping force coefficients for low frequency excitations. Dynamic operation under these conditions will then result in a whirl frequency ratio greater than 0.50, and consequently, it aggravates the "hydrodynamic" instability problem since it reduces even further the safe range of operating speeds of a rotor-bearing system. This important result, although first reported by Redecliff and Vohr (1969), has been largely overlooked until recently.

Hydrostatic bearings for cryogenic liquids of low viscosity require large levels of external pressurization to provide adequate load capacity and stiffness support. Typical pressure drops across a HJB can be as large as 30MPa and under these conditions the material properties of cryogenic liquids present substantial variations. These considerations lead San Andres (1992a) to develop a complex analysis for variable properties liquid HJBs. The fluid is regarded as barotropic with material properties, density and viscosity, as functions of a characteristic temperature and the local absolute pressure within the bearing flow region. Note that the designation of barotropic applies only to the fluid and not to the flow process within the fluid film bearing. The numerical model extracts the cryogenic liquid properties from accurate 32-term thermophysical state equations as given in the data base of McCarty(1986). Predictions of the isothermal analysis for a typical liquid hydrogen HJB show that the fluid properties affect considerably the static and dynamic force characteristics of the bearing and determine a whirl frequency ratio much larger than 0.50 for centered journal operation. This result

is a direct consequence the fluid compressibility effect at the recess volumes and at film lands. Sump pressures are relatively low at the discharge side of the bearing and determine small values of LH_2 density with a consequent increase in the axial velocity of the fluid. This effect then induces a large exit Mach number (M approaching 0.60 to 0.80) which shows that the bearing operates close to sonic conditions and may be accompanied by fluid vaporization. Dynamic operation of a liquid bearing at such large Mach numbers is entirely unknown, and thus, there is the urgent need to determinate experimentally whether test measurements produce a similar dynamic force response as the numerical predictions indicate.

The barotropic–isothermal fluid model for turbulent flow HJBs has been extended to include journal misalignment and dynamic journal axis conical motions. The complex analysis determines rotordynamic force and moment coefficients due to journal center displacements and journal axis rotations (San Andres, 1993a). An approximate analysis for the HJB force and moment dynamic response at the centered position is also available (San Andres, 1992b). Numerical predictions show that journal misalignment angles in line with the journal center displacement cause a reduction in load capacity due to the loss in available film thickness. Journal axis misalignment increases slightly the flow rate and produces significant restoring couples for large angular displacements as well as large moment coefficients for large angular motions. The whirl frequency ratio for conical motions is equal to 0.50 in the absence of rotor gyroscopic effects, and therefore, identical to that of plain journal bearings.

It is well known in fluid film lubrication theory and rotordynamics that there exists a trade off between the magnitude of the bearing static load capacity and its dynamic stability characteristics. In general, a bearing designer "sees" the need to reduce the former to improve the latter, or viceversa. Approximate

formulae for the calculation of a break frequency above which stiffness hardening and reduced damping occur in a compressible liquid HJB are available in the literature (San Andres, 1990b, 1991a, 1992b). Criteria to reduce the posibility of "pneumatic hammer" and to eliminate the reduced damping factor due to liquid compressibility effects are also formulated. In brief, improved dynamic characteristics (low values of the whirl frequency ratio) are attained for bearings with small recess volumes and very low values of the ratio between the pressure differential across the bearing and the liquid bulk modulus. Other recommended fixes to improve the dynamic characteristics of a hydrostatic bearing are:

o Use of large scale roughened bearing surfaces to reduce the cross-coupled stiffness coefficients which are the direct leading agents in promoting hydrodynamic bearing instability. Experimental results at Texas A&M show that a test HJB with a rough knurled-pattern bearing surface has a WFR as low as 0.30 but with a reduced load capacity and direct stiffness when compared to a smooth surfaces HJB (Franchek et al., 1993).

o Use of wear rings (Scharrer et al., 1992b) or end seal restrictions (San Andres, 1992b) to control bearing leakage, reduce the pressure differential across the bearing and increase the damping coefficients. Wear rings can also add a degree of safety for start-up and shut-down transient operation with potential shaft to bearing contact. The operating principle of end seals has been taken from the theory of shrouded pump-impellers (Childs, 1989). However, these wear ring seals in HJBs can lead to a substantial reduction of the direct force stiffness coefficient and static load support. Nonetheless, end seals of variable (controlable) restriction may prove in the future to be very valuable as active devices capable of producing load support and damping characteristics as desired within the environment of a "smart" control rotor-bearing system.

o Use of tangential liquid injection opposing journal rotation to reduce the development of the circumferential flow velocity and to practically eliminate the cross-coupled stiffness coefficients.This concept yet lacks firm theoretical modeling but has proved to be useful in some applications while disastrous in others. However, recent experimental results at the hydrostatic bearing test facility at Texas A&M University have shown succesfully that a tangential injection HJB has a very low whirl frequency ratio without reducing the hydrostatic stiffness and load capacity (Franchek et al., 1993). These experiments add to our knowledge a conceptually simple fluid film bearing free of stability problems. Issues of concern for this especial bearing geometry are related to increased power losses and the posibility of inducing backward whirl in lightly loaded rotating structures. Braun et al. (1993) and Hill et al. (1993) have recently presented simplified numerical analysis relevant to non-radial fluid injection in laminar flow hydrostatic recess regions.

o Bearing circumferential asymmetry has long been known to provide a minimal reduction in the whirl frequency ratio of cylindrical journal bearings. Elliptical and multi-lobe fixed pad bearing geometries have been the subject of past interest until the advent of tilt-pad bearings which are inherently stable. These bearings however are of large size, mechanically complex and present moving pivoted pads which need to be frictionless to operate efficiently. Furthermore, tilt-pad bearings present a dynamic response variable with frequency and coupled to the pads motion. So far these considerations have prevented conventional tilt-pad bearings to become suitable candidates as support elements in cryogenic turbomachinery. The flexure pivot tilt pad bearing introduced by KMC Inc. may overcome these problems (Zeidan, 1992). However, this type of bearing has yet to be tested for identification of its dynamic force coefficients.

Experimental results for the orifice discharge flow coefficients in a hydrostatic bearing (no journal rotation) for laminar and turbulent flows in freon, oil and gaseous nitrogen are given by Scharrer and Hibbs (1990). The experimental results point out to the complex nature of the flow field in the orifice and recess of a hydrostatic bearing and show that the orifice discharge coefficient is highly dependent on the Reynolds number with no evident correlation to the bearing clearance. The data presented is of utmost importance for the correct sizing of orifices for hydrostatic bearings in a cryogenic application. Scharrer, Hecht and Hibbs (1991a) present numerical results on the effects of bearing surface wear on the rotordynamic force coefficients in a HJB. The analysis is based on the solution of the turbulent flow Reynolds equation as given by the simplified model of Artiles et al. (1982). The results show that bearing performance is relatively unaffected by amounts of wear less than 10 percent of the bearing clearance. Direct stiffness and damping coefficients are found to decrease dramatically with increased wear while the cross-coupled stiffness is relatively unaffected. No results are presented in terms of the whirl frequency ratio to determine if bearing surface wear degrades the dynamic stability characteristics of a hydrostatic bearing.

Scharrer and Henderson (1992a) present a detailed study on the specification and design of hydrostatic bearings for the STME fuel turbopump. The paper describes the important characteristics of the turbopump and addresses with detail to the major advantages of HJBs when compared to conventional roller bearings. HJBs are selected to provide maximum life and design flexibility at the minimum turbopump cost. A similar study for the design of a annular hydrostatic bearing to be incorporated into the SSME HPOTP is given also by Scharrer et al.(1992c). This bearing package designed to act both as a load support element and a wear ring seal will replace the duplex ball bearing which

has been the primary life limiting component in the turbopump. The analyses of the static and rotordynamic characteristics of the hydrostatic bearings and the annular hydrostatic bearings are based on the numerical models developed by San Andres (1991c) and Yang et al.(1993a).

Fundamental transient operation tests for liftoff and touch-down operation in a liquid nitrogen HJB are given by Scharrer, Tellier and Hibbs (1991b). A test apparatus simulating the transients found in a typical cryogenic turbopump was used in the investigation. Profiles of speed, pressure and radial load in the tester reproduce those determined from an instrumented SSME HPOTP. The experimental results show that a soft bearing material promotes early liftoff when used in conjuntion with a journal of hard coating. Post experimental inspection of the test especimens revealed unmeasurable wear for combinations of hard journal with soft bearing materials; and, conclusively that hydrostatic bearings are capable of surviving (repeated) start transients with similar loads as those found in actual turbopumps. A similar experimental procedure for the start transient performance of an annular hydrostatic bearing in liquid oxygen has been reported recently by Scharrer et al. (1992d). The experimental results showed that the fluid film bearing supported effectively the radial loads impossed and that liftoff occured at speeds very close to predictions obtained using the analysis of Yang et al.(1993a,b).

Although cryogenic liquids offer very small viscosities, the trends toward higher rotational speeds and larger pressure differentials, as well as the implementation of intentionally roughened surfaces to improve fluid film bearing dynamic stability, provide unique flow characteristics and operating conditions where high levels of turbulence (energy dissipation) and kinetic energy exchange due to fluid compressibility may determine significant thermal effects. Furthermore, hydro-

static annular pressure seals are also under consideration as support elements for cryogenic turbopumps. These type of damping bearings (Von Prageneu, 1982, 1990) require particularly rough stator (bearing) surfaces and increased axial lengths to provide the necessary load support. These conditions then lead to the need of a thermohydrodynamic (THD) analysis in order to predict accurately the static and dynamic force performance characteristics of highly turbulent cryogenic liquid HJBs and seals.

As stated earlier, cryogenic liquids present material properties strongly dependent on their local state of pressure and temperature. In some cryogenic turbopump applications, annular hydrostatic annular seals may be subjected to axial pressure drops as large as 45MPa, and therefore, the working fluid presents a wide spectrum of property changes across the seal. Pressure variations are most important on the viscosity and density changes of liquid hydrogen, while temperature has a pronounced influence on the material properties of liquid oxygen. The viscosity of liquid oxygen is an order of magnitude larger than in liquid hydrogen, but the kinematic viscosity is about the same for both fluids for the range of conditions applicable in cryogenic environments. Mechanical energy dissipation in turbulent flows is a non-linear increasing function of the fluid viscosity and the flow Reynolds number; and thus, thermal effects in liquid oxygen seals are expected to be of importance. This consideration becomes fundamental when it is further known that the heat capacity of liquid oxygen is relatively small.

The understanding of thermohydrodynamic (THD) phenomena in hydrodynamic bearings has advanced steadily in recent years. A well documented review of the related literature relevant to THD lubrication theory and experiments is given by Khonsari (1987). The monumental work of Pinkus (1990) offers a comprehensive review and insight of the current problems and describes the needs for

future work. The interested reader should refer to these publications for complete information. The conventional THD theory of hydrodynamic bearings considers incompressible fluids of large viscosity (like oils), and thus, shows dominance of circumferential flow effects. Most analyses consider the flow as laminar and inertialess, and the axial variation of temperature is usually neglected. On the other hand, the THD analysis of externally pressurized bearings such as HJBs and damper seals needs to account for flow turbulence, fluid inertia and the transport of energy in the direction of the pressure flow.

Isothermal-variable properties bulk-flow fluid film models for the analysis of annular seals in cryogenic environments have been adopted by Simon and Frene (1989) and San Andres (1991c, 1993b-c). These models still account for the material properties variation and have been shown to be accurate for design of liquid hydrogen seals as described latter. Yang et al. (1993a,b) have presented the most advanced THD analysis for the turbulent bulk-flow of a real properties liquid in an annular pressure seal of arbitrary non-uniform clearance. The thermal model considers conservation of bulk-flow momentum and energy transport while an adiabatic heat flow process is assumed for simplicity. The bulk-flow equations for the zeroth-order flow variables are solved numerically to determine leakage, fluid film forces and restoring moments. Dynamic force and moment coefficients due to small amplitude perturbations in shaft center displacements and shaft axis rotations are calculated from the solution of first-order flow field equations. The material properties used for cryogenic liquids are determined from the 32-term Benedict-Webb-Rubin equation of state as given in the standard computer program of McCarty (1986).

Numerical results from the THD model correlate well with measured temperatures for the Preburner Impeller Rear Wear-Ring Seal of the SSME high pres-

sure oxidizer turbopump. Calculations performed with the analysis of Yang et al. (1993a) for a high speed, rough surface LO_2 seal predicted a large temperature rise and the onset of two-phase flow conditions (liquid boiling) at moderate shaft eccentricities despite the large pressure differentials impossed across the seal. It is imperative to note that large temperature rises in a cryogenic seal can lead to thermal solid distortions affecting the operating clearance and possibly causing a significant reduction on the direct stiffness of the hydrostatic seal.

Two-phase (liquid-gas) flows are not desirable in cryogenic liquid fluid film bearings and seals. A quote from Pinkus (1990) is the more explicit since "difficulties attendant to the phenomenon of change of phase includes a negative stiffness over certain ranges of operation, leading to unstable equilibrium and collapse of the fluid film. Even when operation is possible, self-sustained oscillations may lead to chatter, ultimately causing destruction of the seal". Pinkus also states that the analysis of two-phase lubrication with cryogenic liquids is extremely complex due to the "inadequate state of knowledge of certain branches of fluid dynamics in general and the lack of basic experiments". Beatty and Hughes (1987, 1990) have introduced fundamental studies on two-phase flow phenomena for steady state, centered operation, annular seals with adiabatic surface considerations. The analyses showed that viscous heat generation is the mechanism for limiting seal leakage as the operating conditions are near two-phase regions.

Research is needed to develop a thermohydrodynamic model for the analysis of turbulent single-phase and two-phase flows in hydrostatic bearings and annular seals for cryogenic applications. Advanced analytical and numerical tools are needed to predict accurately the steay-state and dynamic force response of rough surface, fluid film bearings with significant levels of energy dissipation. Typical hydrostatic bearings and annular seals in a cryogenic environment operate with

large pressure differentials and, in some circumstances, the inlet temperature to the bearing/seal is just a few degrees below the liquid saturation temperature. For example, hydrostatic annular seals control effectively leakage and could also (in the near future) replace conventional rolling element bearings as load support devices in high speed turbopumps. Thus, the design of these seals (damper bearings) calls for operation at moderate to large eccentric rotor positions in order to generate adequate load support. On the other hand, these operating characteristics generate the conversion to heat of mechanical energy due to the hydrodynamic effects as well as that due to the macroscopic roughness of the stator surfaces used. Recent experimental evidence from tests beds at both Rockwell and NASA Marshall Research Center (Nolan et al., 1993) have shown that prototype damper seals present a two-phase flow condition (flashing) of the liquid at the discharge plane of the damper seal. Operation of actual turbopumps under these conditions may be potentially catastrophic.

SCOPE OF THE WORK IN 1993 (PHASE I)

The research progress presented in this report concentrates on the thermohydrodynamic analysis of real properties, fluid film bearings for cryogenic applications. The bearing geometries of interest include hydrostatic bearings of arbitrary recess geometry, hydrostatic annular seals and cylindrical rigid–pad bearings. The motion of a cryogenic fluid on the thin film flow region is governed by a closed set of mass and momentum conservation, and energy transport equations for the primitive bulk-flow variables and, accompanied by thermophysical state equations for evaluation of the fluid material properties. The turbulent bulk-flow in the thin film land regions is modeled with simple friction coefficient laws including the effect of macroscopic surface roughness. Zeroth-order equations describe the fluid flow field for a journal static equilibrium position, while first-order linear equations govern the fluid flow for small amplitude journal center translational motions and journal axis conical motions. Solution to the zeroth-order flow field equations provides the bearing flow rate, load capacity, restoring moments and torque, and the temperature field within the flow field. Solution to the first-order equations determines the linearized force and moment coefficients due to journal lateral and angular motions.

On 1993 (Phase I), the analysis of single-row and side-to-side parallel row, rectangular recess hydrostatic bearings, annular pressure seals, and fixed geometry journal pad bearings has been completed. Thermal effects (energy transport) are considered in the fluid film bearing with thermally adiabatic solid surfaces bounding the annular flow region, or isothermal journal and bearing surfaces.

The computer program developed named as *hydrosealt* calculates:

1) bearing flowrate (seal leakage),
2) friction torque and temperature rise,
3) load capacity (fluid film forces) and restoring moments,

4) rotordynamic force coefficients due to journal center displacements,
5) rotordynamic force coefficients due to journal axis rotations,
6) rotordynamic moment coefficients due to journal center displacements,
7) rotordynamic moment coefficients due to journal axis rotations,
8) Complete pressure and temperature fields on the bearing surface, as well as density and viscosity field variations, with ranges of fluid flow Reynolds numbers and Mach numbers.

for isothermal or adiabatic journal and bearing surface conditions.

as a function of:

a) journal (rotor) center eccentricity and journal axis misalignment.
b) inlet specified circumferential pre-swirl velocity distribution.
c) general clearance function as defined below
d) mean surface roughness on bearing and journal film lands.

The fluid properties (density, viscosity and specific heat) are calculated from the 32 term Benedict-Webb-Rubin equations of state as given by NBS Standard Reference Database 12 (McCarty, 1986) for the following cryogenic liquids: LO_2, LH_2, LN_2, and methane. Other fluids included in the program are water, mineral oils and air.

The program *hydrosealt* handles the following boundary conditions at the bearing discharge (exit) planes:

1) periodic pressure asymmetry in the circumferential direction.
2) local discharge end seal effects via an orifice like model to simulate end wear-rings in hydrostatic bearings or annular seals.

The axial clearance functions included are of the type:

a) uniform,
b) tapered,
c) stepped, or,
d) arbitrary via spline interpolation, and,
e) tilted about any arbitrary axis for journal misalignment conditions.

The present computational research program needs support from a complimentary experimental research effort directed to measure the dynamic force performance of high speed, externally pressurized fluid film bearings with flow conditions similar to those found in cryogenic environments. Some empirical flow

parameters should also be identified from the test data. These coefficients, like orifice discharge coefficients, recess edge entrance loss factors, shear friction coefficients, and thermal mixing groove parameters are of fundamental importance for the accurate prediction of the flow and force dynamics in high-speed, turbulent flow fluid film bearings.

ANALYSIS

Fluid Film Bearing Geometries

The following bearing geometries are considered in the analysis:

(1) Orifice–compensated hydrostatic journal/pad bearings (Fig.1).

The type of bearing being considered for use in the LH_2 and LO_2 turbopumps is a full, 360° hydrostatic journal bearing, orifice compensated, with a variable number of feeding recesses or pockets machined in the surface of the bearing. Axial grooves may be designed in the bearing surface to improve the bearing dynamic stability. The bearing surface may also be intentionally roughened to reduce the cross-coupled stiffnesses and improve the bearing stability.

The bearing recesses have a depth larger than the radial clearance under the film lands. Fluid flows from a high-pressure supply, passes through an orifice in route to the recess and leaves the bearing sides by flowing through the thin film gap. The surfaces of the journal and bushing are separated by a film of fluid forced under external pressurization. When the center of the shaft is displaced from the center of the bearing, on one side of the bearing the film gap is reduced, while the gap is increased on the other side. On the reduced-gap side, the flow from the recess to film lands is more restricted and the recess pressure rises. On the opposite side, however, the flow from the recess is increased and the recess pressure decreases. The difference between the pressures on the two sides results in a net bearing film force which is equal and opposite to the externally applied load on the journal. The hydrodynamic effect due to journal rotation increases the fluid film forces but also introduces the potential of a self-excited whirl instability at rotor speeds twice above the system first critical speed.

(2) Annular pressure (damper) seals or hydrostatic annular bearings (Fig.2).

Annular pressure seals are used in turbomachinery to limit the leakage

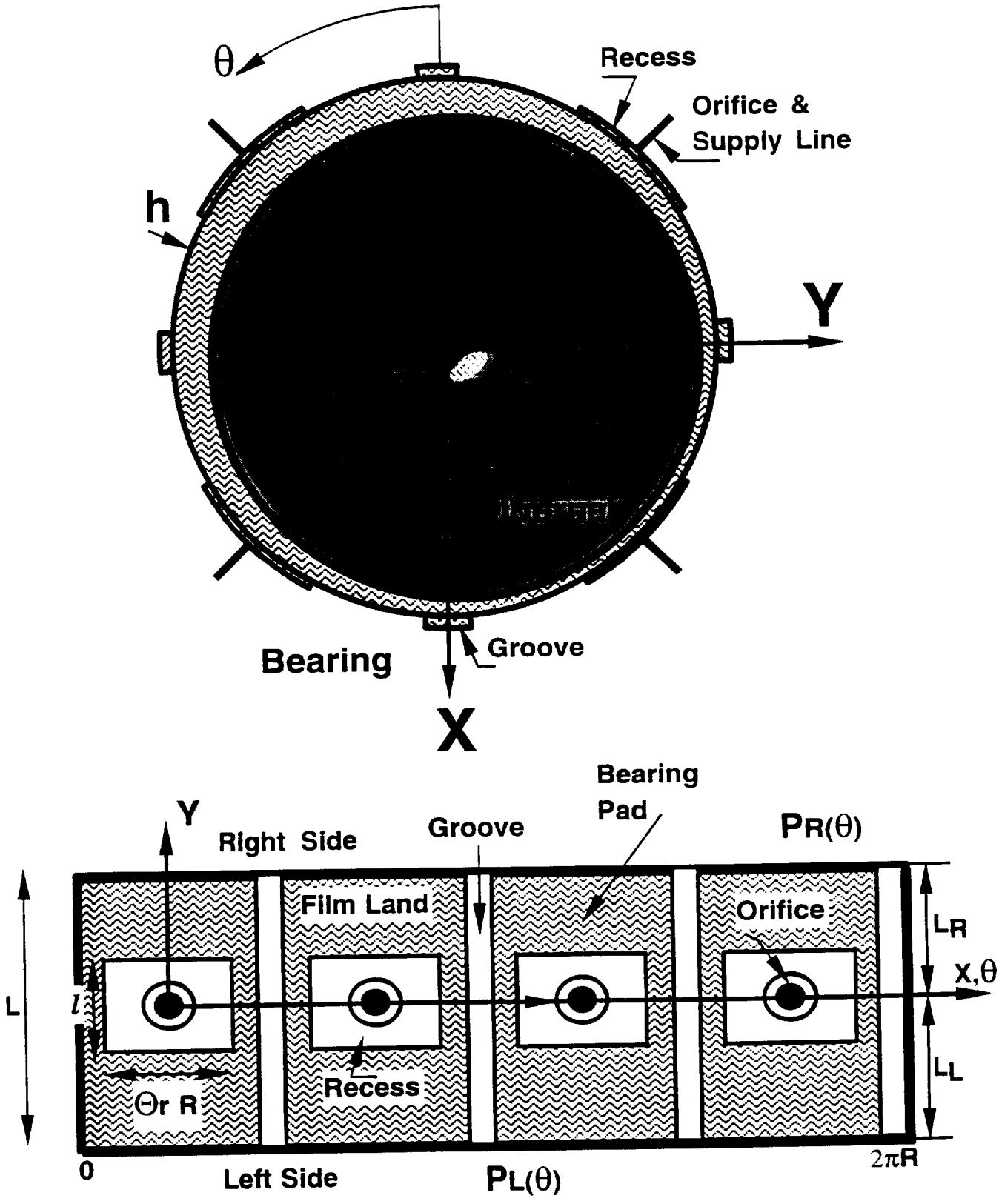

Fig.1 Geometry of Hydrostatic Pad Bearing

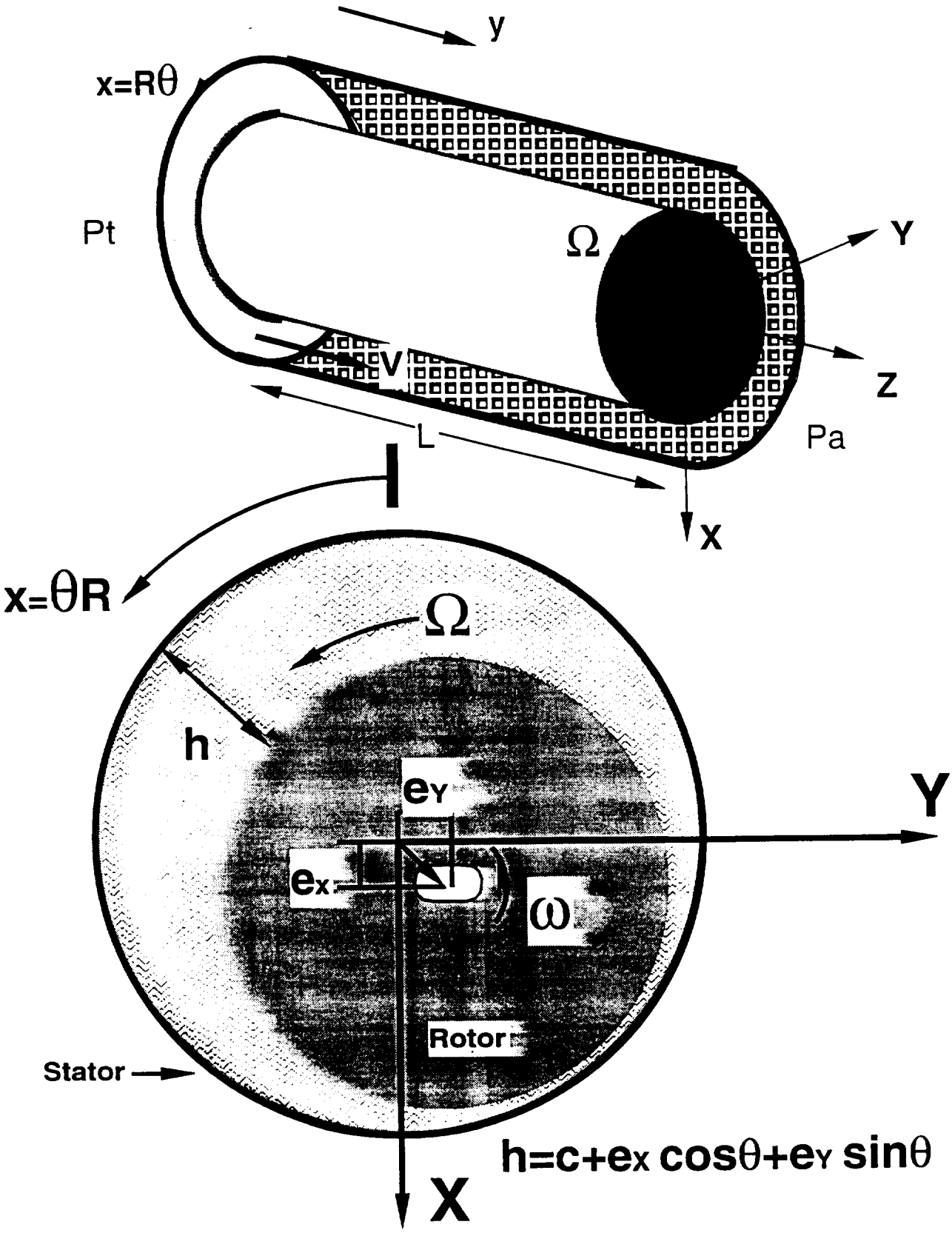

Fig. 2. Geometrical Description of Annular Pressure Seal

of fluid from stages of high pressure to those of lower pressure. Like fluid film journal bearings, annular pressure seals have a significant influence on the rotordynamic stability of high-performance turbomachinery. Von Pragenau (1982, 1990) proposed damping seals, i.e., annular seals using rough stators and smooth rotors, to improve rotordynamic stability. In a damping seal, the average tangential velocity induced by journal rotation and the cross-coupled stiffnesses decrease. Scharrer et al.(1992a) showed that a damper seal (called a hydrostatic annular bearing there) can also be used as a supporting element to replace a current rolling-element bearing in cryogenic turbopumps.

(3) Cylindrical pad journal bearings (Fig.3).

The working mechanism of a hydrodynamic journal bearing is different from a HJB. The pressure generation in a hydrodynamic bearing is provided by journal rotation and fluid viscosity. External pressurization serves only to provide enough lubricant to the fluid film region. Therefore, a hydrodynamic journal bearing is also called a self-acting bearing. Unlike a hydrostatic bearing, a hydrodynamic bearing has no load capacity unless the journal rotates at an off-center position (a wedge like hydrodynamic effect). The lack of hydrodynamics may lead to wear damage during startup and shutdown transients.

For fixed pad journal bearings, feeding axial grooves are located at circumferential locations away from the maximum pressure (minimum film thickness) region. Feeding grooves supply fresh (cold) fluid to the bearing, i.e., provide the required lubricant flow to the fluid film region and are critical in avoiding journal-bearing overheating at high speed operation. Due to the low level of external pressurization (relative to ambient conditions), the mass flow rate in a hydrodynamic journal bearing is much smaller than in a HJB or an annular pressure seal, and consequently thermal effects may be of great importance for fluids with low

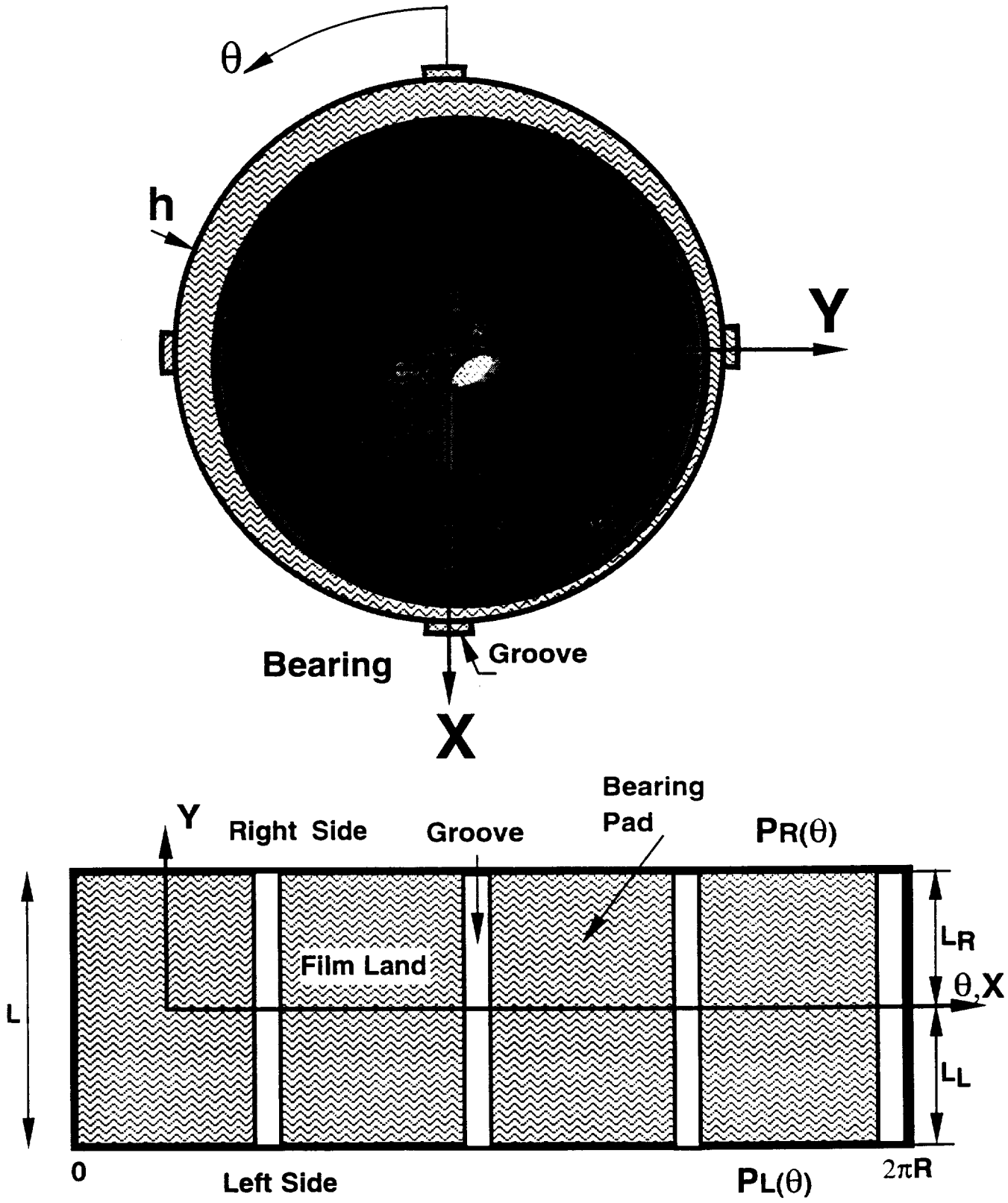

Fig. 3 Geometry of Fixed Arc Pad Bearing

heat capacity. A too large temperature rise in the fluid film affects pronouncedly the fluid properties, and hence the bearing performance characteristics. More importantly, unequal thermal growth of bearing components can modify the fluid film clearance and induce seizure. Bearings with **compliant** surfaces (foil bearings) exhibit advantages over rigid surface bearings by accommodating thermal distortion or mechanical deformation of bearing components and journal misalignments. NASA currently sponsors the development of fluid-film foil bearings for use in space shuttles and military missiles (O'Connor, 1993).

For all the three fluid film bearing configurations considered above, the flow is confined to the thin film annular region between an inner rotating journal and a non-rotating bushing. The fluid flow is characterized by high levels of turbulence due to the high journal surface speed and/or the externally imposed large axial pressure drop across the bearing/seal. Two different flow patterns are defined in the analysis.

Flow On Film Lands

Fully developed, single–phase (liquid or gas), turbulent bulk–flow model;

Governing Equations:

Mass conservation equation

Momentum Bulk-Flow equations

Energy Transport equation

Turbulence Closure Model:

Bulk flow with friction parameters based on Moody's
friction-factor equation for physically sound characterization
of roughened surfaces.

Liquid of variable properties as functions of pressure and temperature with realistic thermophysical equations of state

(for cryogenic fluids, see McCarty, 1986).

Flow On Bearing Recesses and Grooves

Global mass conservation equation with liquid compressibility at recess-volumes.

Pressure rise/drop at edge of bearing recesses with a simplified

1-D Rayleigh **step** bearing model.

Global energy balance equations at bearing recesses and grooves to determine entrance temperature conditions at the recess and boundaries.

Governing Equations for Turbulent Bulk-Flows

The motion of a fluid in thin film geometries is described by a set of mass, momentum conservation, and energy transport equations for the primitive flow variables, and accompanied by thermophysical state equations for evaluation of the fluid material properties. The smallness of the clearance to radius ratio (c_*/R) allows the reduction of the general governing equations to the simplified forms given on the film lands (Yang et al., 1993a): (Note: the **nomenclature** of this report is provided in Appendix A)

Continuity Equation

$$\frac{\partial \rho}{\partial t} + \frac{\partial \rho \tilde{U}}{\partial x} + \frac{\partial \rho \tilde{V}}{\partial y} + \frac{\partial \rho \tilde{W}}{\partial z} = 0 \tag{1}$$

Circumferential-Momentum Equation

$$\rho \frac{D\tilde{U}}{Dt} = -\frac{\partial \tilde{P}}{\partial x} + \frac{\partial \tau_{xz}}{\partial z} \tag{2}$$

Axial-Momentum Equation

$$\rho \frac{D\tilde{V}}{Dt} = -\frac{\partial \tilde{P}}{\partial y} + \frac{\partial \tau_{yz}}{\partial z} \tag{3}$$

Cross-Film-Momentum Equation

$$\frac{\partial \tilde{P}}{\partial z} = 0 \tag{4}$$

Energy-Transport Equation (Bird et al.,1960, Whitaker,1977)

$$\begin{aligned} \rho C_p \frac{D\tilde{T}}{Dt} + \frac{\rho}{2}\frac{D}{Dt}(\tilde{U}^2 + \tilde{V}^2) = \frac{\partial}{\partial z}\Big(K\frac{\partial \tilde{T}}{\partial z}\Big) + \tilde{T}\beta_t \frac{D\tilde{P}}{Dt} \\ - \Big(\tilde{U}\frac{\partial \tilde{P}}{\partial x} + \tilde{V}\frac{\partial \tilde{P}}{\partial y}\Big) + \frac{\partial}{\partial z}(\tilde{U}\tau_{xz} + \tilde{V}\tau_{yz}) \end{aligned} \tag{5}$$

on the flow region $\{x \in (0, \pi D), y \in (-L_L, L_R), z \in (0, H(x,y,t))$, for journal bearings and hydrostatic bearings, while $y \in (0, L)$ for annular pressure seals$\}$; and where

$$\frac{D}{Dt} = \frac{\partial}{\partial t} + \tilde{U}\frac{\partial}{\partial x} + \tilde{V}\frac{\partial}{\partial y} + \tilde{W}\frac{\partial}{\partial z} \tag{6}$$

is the material derivative.

To undertake a study of the general equations (1)—(5) in their full three-dimensional complexity is a difficult task, perhaps unnecessary to obtain meaningful solutions in a reasonable time and at an affordable cost. Large pressure gradients, typical of externally pressurized cryogenic bearings and seals, and high rotational speeds generate large flow Reynolds numbers, and consequently, the effect of turbulent mixing far outweighs molecular diffusivity. Thus, the temperature rise produced by viscous dissipation tends to be distributed uniformly across the film thickness and hence temperature gradients in the cross-film coordinate (z) are confined to turbulent flow boundary layers adjacent to the bounding (bearing and journal) surfaces (Suganami and Szeri, 1979; Di Pasquantonio and Sala, 1984). Furthermore, in the absence of regions of reversed flow or recirculation, the fluid velocity field presents the same characteristics as discussed above.

Let bulk-flow primitive variables be defined as average quantities across the

film thickness, i.e.

$$U = \frac{1}{H}\int_0^H \tilde{U}\,dz\,; \quad V = \frac{1}{H}\int_0^H \tilde{V}\,dz\,; \quad T = \frac{1}{H}\int_0^H \tilde{T}\,dz \tag{7}$$

Then, the considerations presented allow the governing equations (1) to (5) to be integrated across the film thickness to determine turbulent bulk-flow equations at each bearing pad configuration (Yang et al., 1993a):

Continuity Equation

$$\frac{\partial(\rho H)}{\partial t} + \frac{\partial(\rho HU)}{\partial x} + \frac{\partial(\rho HV)}{\partial y} = 0 \tag{8}$$

Circumferential-Momentum Equation

$$\frac{\partial(\rho HU)}{\partial t} + \frac{\partial(\rho HU^2)}{\partial x} + \frac{\partial(\rho HUV)}{\partial y} = -H\frac{\partial P}{\partial x} + \tau_{xz}|_0^H \tag{9}$$

Axial-Momentum Equation

$$\frac{\partial(\rho HV)}{\partial t} + \frac{\partial(\rho HUV)}{\partial x} + \frac{\partial(\rho HV^2)}{\partial y} = -H\frac{\partial P}{\partial y} + \tau_{yz}|_0^H \tag{10}$$

Energy-Transport Equation

$$\begin{aligned} &C_p\Big[\frac{\partial(\rho HT)}{\partial t} + \frac{\partial(\rho HUT)}{\partial x} + \frac{\partial(\rho HVT)}{\partial y}\Big] \\ &\quad + \frac{1}{2}\Big[\frac{\partial(\rho HV_t^2)}{\partial t} + \frac{\partial(\rho HUV_t^2)}{\partial x} + \frac{\partial(\rho HVV_t^2)}{\partial y}\Big] + Q_s \\ &\quad = T\beta_t H\frac{\partial P}{\partial t} + (T\beta_t - 1)H\big(U\frac{\partial P}{\partial x} + V\frac{\partial P}{\partial y}\big) + R\Omega\tau_{xz}|^H. \end{aligned} \tag{11}$$

Note that Eqs.(9) to (11) imply "flat" bulk flow profiles characteristic of turbulent film flows at high Reynolds numbers. By Neglecting the fluid-inertia terms on the left hand sides of Eqs.(9) and (10), Eqs.(8) to (10) reduce to a single lubrication equation—namely, the turbulent flow Reynolds equation.

In the above equations, $V_t = \sqrt{U^2 + V^2}$ is the bulk-flow speed, $\tau_{xz}|_0^H$ and $\tau_{yz}|_0^H$ are the wall shear stress differences in the circumferential and axial directions, $\tau_{xz}|^H$ is the shear stress on the journal surface in the circumferential direction, and

$$Q_s = h_B(T - T_B) + h_J(T - T_J) \tag{12}$$

is the heat flux from the film to the bounding (bearing and journal) surfaces. Further, h_B and h_J denote the bulk-flow heat transfer coefficients to the bearing and journal surfaces (Appendix B). If the fluid-film temperature (T) is higher than the bounding-surface temperatures (T_B,T_J), heat flows from the film to the bounding solids, and vice versa. For an adiabatic flow process, $Q_s = 0$.

The fluid properties for a cryogenic liquid (density, viscosity, specific heat, and volumetric expansion coefficient, etc.):

$$\rho = \rho(P,T), \quad \mu = \mu(P,T), \quad C_p = C_p(P,T), \quad \beta_t = \beta_t(P,T) \tag{13}$$

are determined from general 32-term thermophysical state equations as given by McCarty (1986).

The wall shear stresses are calculated according to the bulk-flow theory for turbulence in thin film flows (Hirs, 1973, Launder and Leschziner, 1978):

$$\begin{aligned}
\tau_{xz}|_0^H &= -\frac{\mu}{H}\left(k_x U - k_J \frac{R\Omega}{2}\right); \\
\tau_{yz}|_0^H &= -\frac{\mu}{H}(k_y V); \\
\tau_{xz}|^H &= \frac{H}{2}\frac{\partial P}{\partial x} + \frac{\mu}{4H}[U k_B - (U - R\Omega)k_J]
\end{aligned} \tag{14}$$

where the turbulent shear parameters (k_x,k_y) and (k_J,k_B) are local functions of the Reynolds numbers and friction factors based on Moody's formulae (Massey, 1983).

Substitution of the bulk-flow momentum equations (9), (10) into the energy equation (11), and invoking the mass conservation principle given by equation (8) allows the energy transport equation to be expressed as:

$$C_p[\frac{\partial(\rho HT)}{\partial t} + \frac{\partial(\rho HUT)}{\partial x} + \frac{\partial(\rho HVT)}{\partial y}] + Q_s$$
$$= T\beta_t H(\frac{\partial P}{\partial t} + U\frac{\partial P}{\partial x} + V\frac{\partial P}{\partial y}) + R\Omega\tau_{xz}|^H - U\tau_{xz}|_0^H - V\tau_{yz}|_0^H \quad (15)$$

which reflects the energy balance in the fluid film as:

CONVECTION + DIFFUSION = COMPRESSION WORK + DISSIPATION

(Energy Disposed) = (Energy Generated)

The variation of temperature in the axial direction and the energy generated by compression work are retained in the analysis due to the strong influence of the large pressure drop across the length of a HJB or an annular pressure seal. These conditions differentiate the present problem from conventional THD analyses of viscous, incompressible fluids in journal bearings where the volumetric expansion coefficient β_t is zero and temperature variations along the bearing axial direction are usually considered negligible.

Governing Equations for Bearing Recess and Groove Flows

The analysis of turbulent flows in a HJB recess is complicated and not yet fully understood. To date, only two-dimensional laminar flow numerical solutions are available for rectangular recesses (See, for example, San Andres and Velthuis, 1992, Hill et al., 1993, Braun et al. 1993). While the actual prediction of flow fields in the recess may give a better description of the recess-film edge boundary conditions, the global mass and energy conservation principles at the recess are shown to be both efficient and accurate in HJB analysis. The study of the flow field in a bearing recess is a subject which requires detailed experimental results since

analytical or full 3-D numerical solutions can not model efficiently the complexity of this flow field dominated by both surface shear (rotation) and induced external pressure flows of strong turbulence character.

- Mass Conservation at a Recess

The continuity equation at the recess is defined by the global balance between the supply mass flow rate (Q_{in}), the outflow into the film lands (Q_r) and the temporal change of fluid mass within the recess volume ($\forall_r$). The recess flow continuity equation is expressed as:

$$Q_{in} = Q_r + \rho_r \frac{\partial \forall_r}{\partial t} + \rho_r \forall_r \Big(\beta_p \frac{\partial P}{\partial t} - \beta_t \frac{\partial T}{\partial t} \Big)_r \tag{16}$$

where the flow through the orifice restrictor is

$$Q_{in} = A_0 \sqrt{2\rho_r (P_s - P_r)}, \tag{17}$$

and

$$Q_r = \int_{\Gamma_r} \rho H (\vec{\mathbf{U}} \cdot \vec{\mathbf{n}})\, d\Gamma \tag{18}$$

is the mass flow rate across the recess boundary (Γ_r) and entering the film lands.

$$\beta_p = \frac{1}{\rho}\Big(\frac{\partial \rho}{\partial P}\Big)_T, \quad \beta_t = -\frac{1}{\rho}\Big(\frac{\partial \rho}{\partial T}\Big)_P \tag{19}$$

are the liquid compressibility factor and volumetric expansion coefficient, respectively. In general,

$$\beta_p, \beta_t \begin{cases} = 0 & \text{for incompressible liquids;} \\ = \frac{1}{P}, \frac{1}{T} & \text{for ideal gases;} \\ > 0 & \text{for cryogenic liquids.} \end{cases} \tag{20}$$

In HJBs, the compressibility of cryogenic liquids has been shown to promote pneumatic hammer, a class of self-excited instability mechanism as described by San Andres (1991).

- Global Energy Balance Equation at a Recess

The energy transport phenomenon in a HJB recess is controlled by the following three mechanisms: the carry-over of hot fluid from upstream to downstream of the recess, the mixing of fresh fluid from the supply source into the recess volume, and the heat generation in the recess volume due to shear dissipation by journal rotation. Energy transport produced by pressure gradients, kinetic energy changes, and heat conduction are considered negligible due to the uniformity of pressure and the large mass flow rate through the recess. Based on these considerations, the general three-dimensional energy equation (5) reduces to

$$\rho C_p \frac{D\tilde{T}}{Dt} = \frac{\partial}{\partial z}(\tilde{U}\tau_{xz} + \tilde{V}\tau_{yz}) \tag{21}$$

Invoking the continuity equation (1), Eq.(21) can be written as

$$C_p\Big[\frac{\partial \rho\tilde{T}}{\partial t} + \vec{\nabla}\cdot(\rho\vec{\mathbf{V}}\tilde{T})\Big] = \frac{\partial}{\partial z}(\tilde{U}\tau_{xz} + \tilde{V}\tau_{yz}) \tag{22}$$

where

$$\vec{\mathbf{V}} = \{\tilde{U}, \tilde{V}, \tilde{W}\} \tag{23}$$

Integration of Eq.(22) over the recess volume gives the global energy balance equation which reflects the heat carry-over (advection) and mixing effects, and the friction heat generation (dissipation) in the recess (Fig. 4) (C_p is regarded as constant for simplicity in this part of the analysis):

$$\begin{aligned} C_p\frac{\partial(\rho T)}{\partial t}\forall_r + C_p\Big(\sum \dot{m}_d T_d + \sum \dot{m}_{side} T_{side}\Big) \\ = C_p\Big(\sum \dot{m}_u T_u + Q_{in} T_s\Big) + T^r_{or}\Omega \end{aligned} \tag{24}$$

where

$$\dot{m}_{d,u} = (\rho U H \delta y)_{d,u} \quad \text{and} \quad \dot{m}_{side} = (\rho V H \delta x)_{side} \tag{25}$$

are the mass flow rates over edge differential segments. The summation ($\sum$) is over each recess edge, and the subscripts "u", "d" and "side" refer to the upstream,

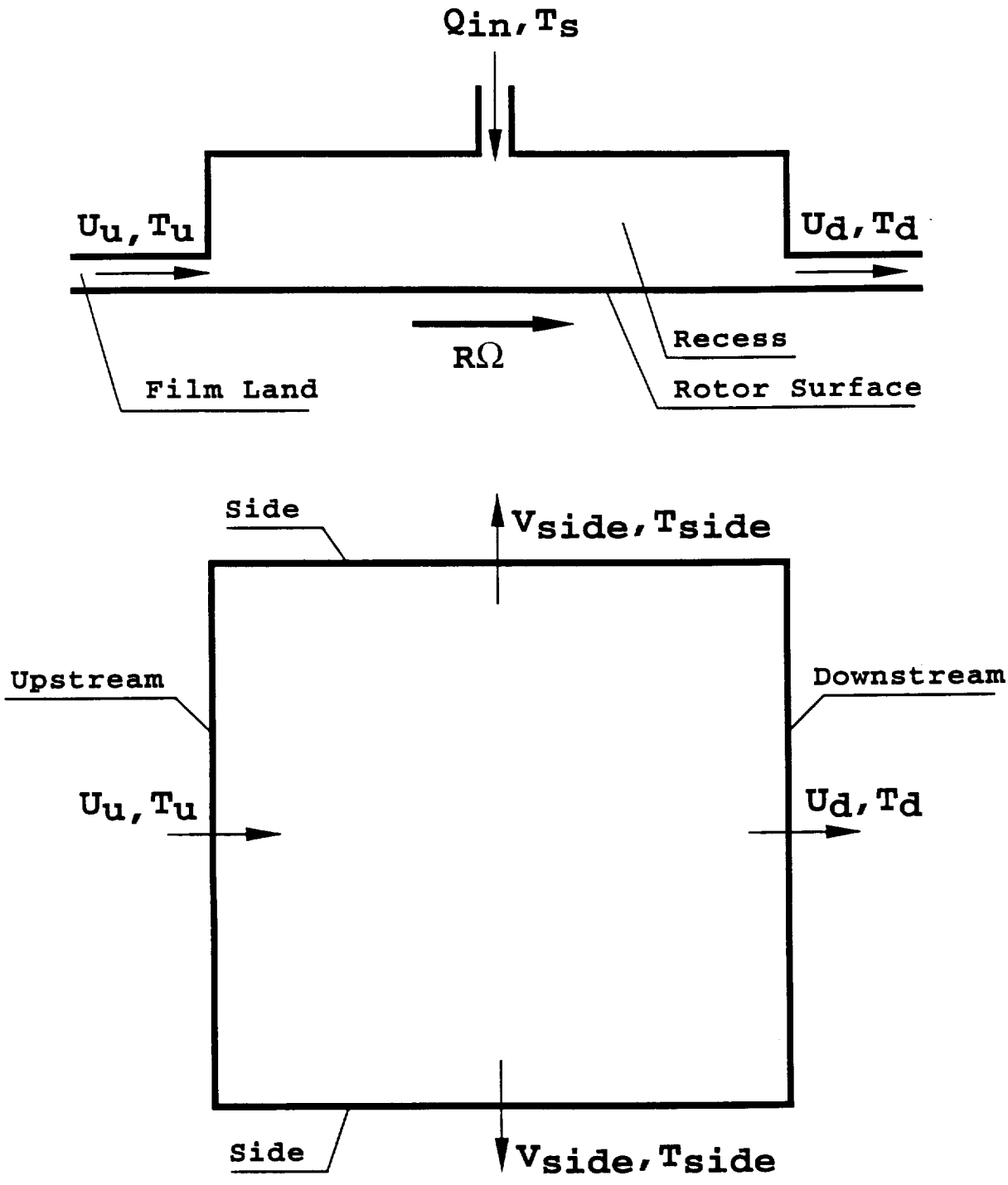

Fig. 4 Conceptual description of global energy balance at a recess

downstream, and side (axial) edges of a rectangular recess, respectively. Q_{in} is the total mass flow rate through the supply orifice, and

$$T_{or}^{r} = \tau_{xz}^{H} A_r R \tag{26}$$

is the drag torque over the recess with volume $\forall_r$. The left hand side of Eq.(24) represents the temporal variation of energy in the recess volume and the energy flow rate out of the recess, while the right hand side denotes the energy influx and the dissipation of mechanical energy.

Our purpose here is to obtain the recess-edge temperatures which serve as boundary conditions for solution of the thermal field on the film lands. The temperatures at all the recess edges and within the recess can be obtained from the global energy equation for different recess flow conditions. Since the global energy equation involves the time (t) as a parameter, different treatments are needed for the zeroth- and first-order temperatures produced by the perturbation analysis. Appendix C provides the formulas for calculation of the zeroth- and first-order recess/edge temperatures.

- Global Energy/Flow Balance Equation at a Groove

Axial bearing grooves (Figs.1 or 3) are used for different purposes, such as to feed the bearing, to improve stability of a HJB by providing bearing asymmetry, or to remove foreign particles in the lubricant. A groove is usually narrow (small circumferential width) and deep (depth much larger than the film thickness). Therefore, the grooves are treated separately from the film lands.

At an axial groove, the flow mixes and energy transfer occurs with cooling of the pad leading edge flow if the bearing is properly designed. The problem is complicated and subject to empiricism. Here a global model using averaged flow variables along the groove edges is implemented.

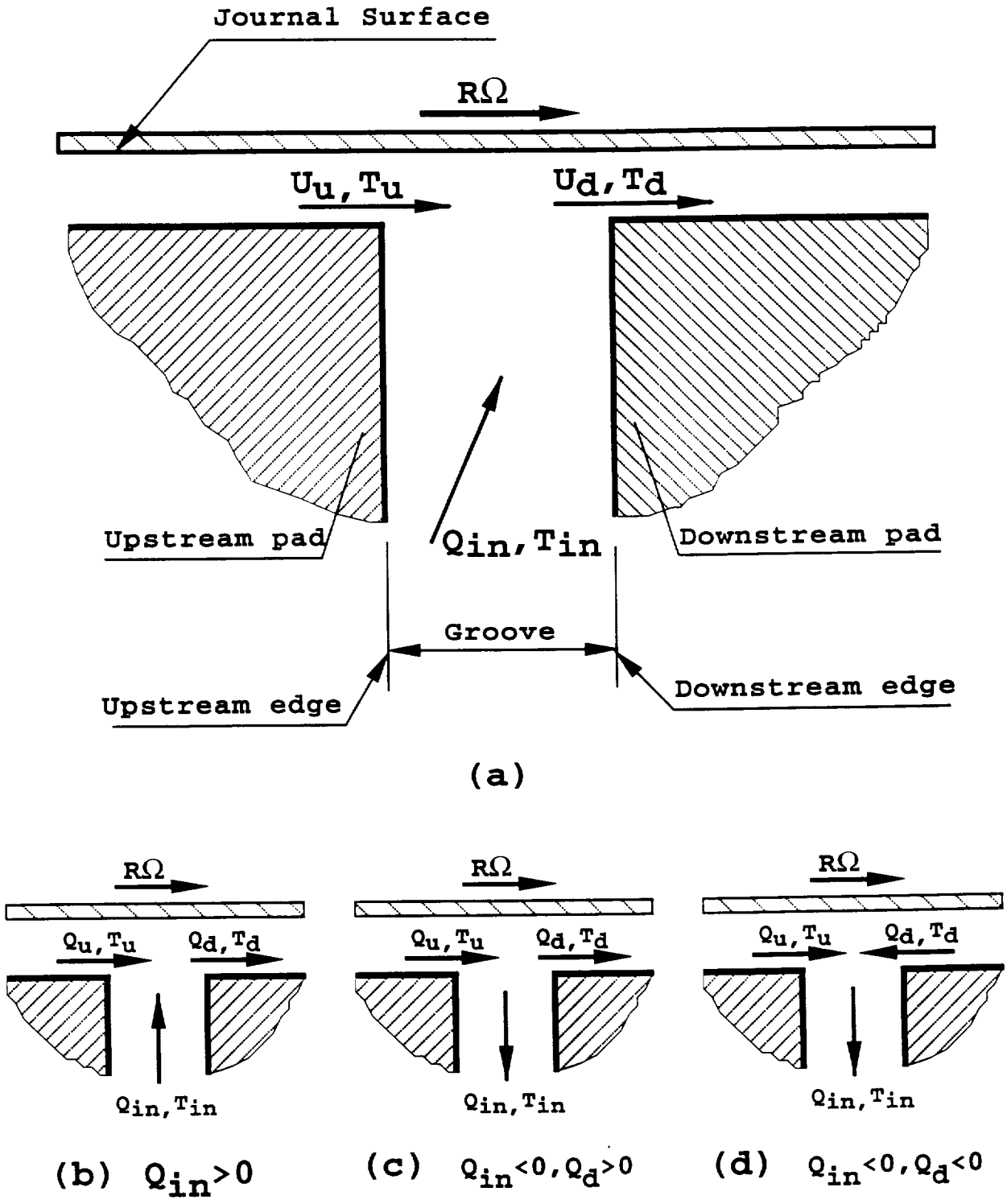

Fig. 5 Conceptual description of global energy balance at a groove

Fig. 5 presents the conceptual description of global energy balance at a groove. The energy transport phenomenon in a groove is controlled by the carry-over of hot fluid from the upstream pad to the downstream one, and the mixing of fresh fluid from the supply source into the groove. The global energy conservation equation at a groove is given as (C_p is regarded as constant here):

$$C_p \sum \dot{m}_d T_d = C_p \sum \dot{m}_u T_u + C_p Q_{in} T_{in} \tag{27}$$

where $\dot{m}_d$ and $\dot{m}_u$ are the mass flow rates over edge differential segments as given by Eq.(25), and the summation ($\sum$) is over the downstream (leading) and upstream (trailing) groove edges. Also,

$$Q_{in} = \sum \dot{m}_d - \sum \dot{m}_u = Q_d - Q_u \tag{28}$$

represents the net mass flow rate through the groove, providing the minimum flow rate required to prevent starved lubrication for a journal bearing with a single feeding groove. T_d and T_u represent the temperatures at the downstream and upstream groove edges, and T_{in} is the temperature flowing with mass flow Q_{in}.

If the mass flow rate leaving the trailing edge of the upstream (relative to the journal rotation) pad to the groove is greater than zero, i.e.,

$$Q_u = \sum \dot{m}_u > 0, \tag{29}$$

then, the fluid temperature at the trailing edge can be found by their upstream values given by the solution on film lands (upstream pad):

$$T_u = \text{Upstream Film Values on Upstream Pad} \tag{30}$$

Temperatures at the downstream edge (leading edge of the downstream pad) can be obtained for different flow conditions in the groove:

(a) If $Q_d = \sum \dot{m}_d > Q_u$, i.e., $Q_{in} > 0$ and flow is supplied into the groove, then the flow entering the downstream edge of the groove is the combination of the upsteam (Q_u) and the groove supply (Q_{in}) flows (Fig.5b), and an averaged uniform downstream-edge temperature (T_d) can be obtained from the mixing of upstream and inlet temperatures:

$$T_d = \frac{\lambda \sum \dot{m}_u T_u}{Q_d} + \left(1 - \lambda \frac{Q_u}{Q_d}\right) T_{in} \tag{31}$$

where $0.4 < \lambda < 1.0$ is the mixing coefficient, a participation ratio of the hot lubricant (recirculating fluid) in the mixing process (Mitsui et al., 1983).

$$T_{in} = T_s \tag{32}$$

that is, all make-up flow in the groove is at the fluid supply temperature.

(b) If $Q_d < Q_u$, i.e., $Q_{in} < 0$ and flow is discharged out of the groove, then two cases may occur. First, a fraction of the upstream flow enters the downstream pad ($Q_d > 0$)(Fig.5c). Then, the leading edge temperatures(T_d) are equal to the trailing edge ones (T_u). Second, both edge flows enter the groove ($Q_u > 0$ and $Q_d < 0$) (Fig.5d) and the temperatures on both edges can be obtained from thermal solutions on their respective pads. These two cases are typical of HJBs and represented by:

$$T_d = \begin{cases} \lambda T_u, & \text{if } Q_d \geq 0 \text{ (Fig.5c);} \\ \text{Upstream Film Values on Downstream Pad,} & \text{if } Q_d < 0 \text{ (Fig.5d).} \end{cases} \tag{33}$$

- Recess/Film Entrance Pressure Rise/Drop at HJBs

For purely hydrostatic operations, a uniform recess pressure is desirable not only to simplify the HJB design (and analysis) but also to increase the load capacity. A uniform recess pressure can be achieved by deepening the recess. However, a minimum recess volume is required to avoid the characteristic

pneumatic hammer instability problem in HJBs. Design criteria for uniformity of recess pressure and pneumatic hammer instability are given by Redecliff and Vohr (1969), and San Andres (1991a, 1992b).

For hybrid operation of a HJB, a pressure rise due to the journal rotation is produced in the downstream portion of the recess (Ho and Chen, 1984, Chaomleffel and Nicholas, 1986). San Andres (1992a) considered this region as a one-dimensional step bearing and evaluated the pressure rise just in front of the downstream recess edge (P_e^-) as (Fig. 6):

$$P_e^- = \begin{cases} P_r - \frac{b\eta^2 \mu k_r}{2H^2(1-M_r^2)} \left[\vec{\mathbf{U}} \eta (\frac{\rho_e}{\rho_r}) - \frac{\vec{\mathbf{V}}_r}{2} \right] \cdot \vec{\mathbf{n}}, \; for \quad (\vec{\mathbf{U}} \cdot \vec{\mathbf{n}}) > 0, & \text{in x direction;} \\ P_r, & \text{in y direction} \end{cases} \tag{34}$$

where

$$\vec{\mathbf{U}} = U\vec{i} + V\vec{j}, \qquad \vec{\mathbf{V}}_\mathbf{r} = R\Omega\vec{i} + 0\vec{j}, \tag{35}$$

$k_r = Re_r^{0.681}/7.753$ is a turbulent shear factor at the bearing recesses, $\eta = H/(H_r + H)$ is the ratio of thicknesses at film land and recess depth, and $M_r = \alpha R\Omega\sqrt{\beta\rho_r}$ is the recess flow Mach number for hybrid operation.

The local acceleration of fluid from the deep recess to the film lands causes a sudden pressure drop at the recess edges (Fig. 6). The pressure at the entrance to the film lands is modeled by simple Bernoulli type relations based on the turbulent flow theory developed by Constantinescu and Galetuse (1975):

$$P_e^+ = P_e^- - \frac{\rho_e}{2}(1+\zeta_i)(1+\xi_i)\left[1 - \eta^2(\frac{\rho_e}{\rho_r})\right](\vec{\mathbf{U}} \cdot \vec{\mathbf{n}})^2 \; ; \quad (\vec{\mathbf{U}} \cdot \vec{\mathbf{n}}) > 0 \tag{36}$$

where

$$\zeta_i = \{\zeta_x, \zeta_y\} = \{1.95/Re_H^{0.43}, 0\}, \tag{37}$$

$$\xi_i = \{\xi_x, \xi_y\} \tag{38}$$

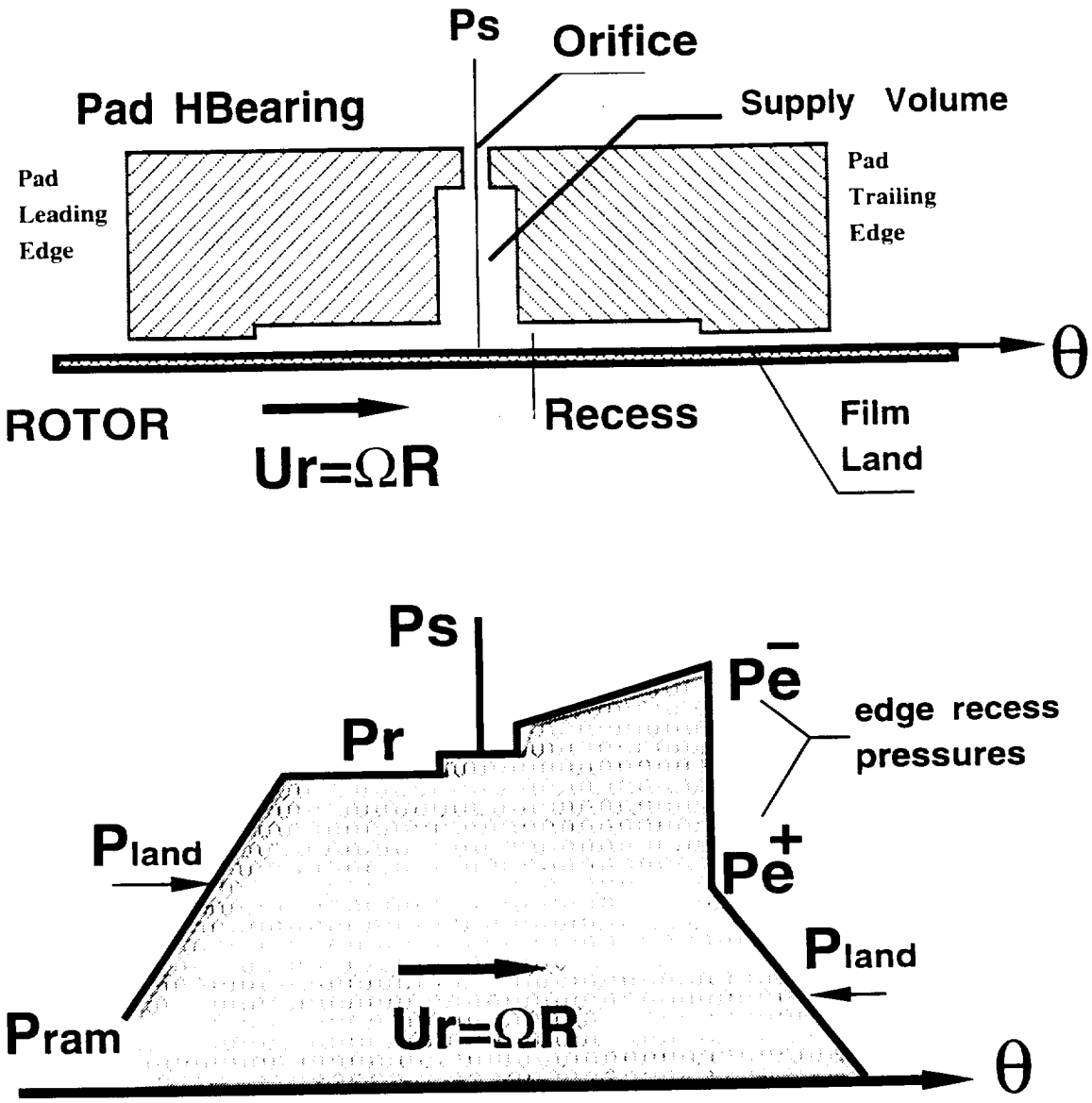

Fig. 6 Conceptual description of pressure rise and drop at recess edge of a hydrostatic pad bearing, and pressure ram effect at leading edge of bearing pad.

are the empirical entrance loss coefficients and $\vec{n}$ is the normal vector to the recess boundary (Γ_r).

The pressure at the entrance of an annular pressure seal can be obtained similarly by using a Bernoulli type relation. The corresponding expression is given latter in the boundary-conditions section.

Dimensionless Governing Equations at Film Lands

Dimensionless coordinates and variables are defined as follows

$$\bar{x} = \frac{x}{R}; \quad \bar{y} = \frac{y}{R}; \quad h = \frac{H}{c_*}; \quad \tau = \omega t;$$

$$u = \frac{U}{U_*}; \quad v = \frac{V}{U_*}; \quad p = \frac{P - P_a}{\Delta P}; \quad \bar{T} = \frac{T}{T_*}; \tag{39}$$

$$\bar{\rho} = \frac{\rho}{\rho_*}; \quad \bar{\mu} = \frac{\mu}{\mu_*}; \quad \bar{C}_p = \frac{C_p}{C_{p*}}; \quad \bar{\beta}_t = \beta_t T_*;$$

and

$$U_* = \frac{c_*^2 \Delta P}{\mu_* R}$$

is a characteristic speed due to pressure induced flow with $\Delta P = P_s - P_a$ for externally pressurized bearings (HJBs and annular pressure seals). If $P_s = P_a$, like in a pure hydrodynamic bearing, the characteristic speed is set equal to the journal surface speed

$$U_* = R\Omega \tag{40},$$

and

$$\Delta P = \mu_* \Omega \left(\frac{R}{c_*}\right)^2. \tag{41}$$

In dimensionless form, the governing flow equations at the film lands are written as:

Continuity Equation

$$\frac{\partial}{\partial \bar{x}}(\bar{\rho} h u) + \frac{\partial}{\partial \bar{y}}(\bar{\rho} h v) + \sigma \frac{\partial(\bar{\rho} h)}{\partial \tau} = 0; \tag{42}$$

Circumferential-Momentum Equation

$$-h\frac{\partial p}{\partial \bar{x}} = \frac{\bar{\mu}}{h}(k_x u - k_j \frac{\Lambda}{2}) + Re_s \frac{\partial}{\partial \tau}(\bar{\rho} h u) + Re_p^*[\frac{\partial}{\partial \bar{x}}(\bar{\rho} h u^2) + \frac{\partial}{\partial \bar{y}}(\bar{\rho} h u v)]\,; \quad (43)$$

Axial-Momentum Equation

$$-h\frac{\partial p}{\partial \bar{y}} = \frac{\bar{\mu}}{h}(k_y v) + Re_s \frac{\partial}{\partial \tau}(\bar{\rho} h v) + Re_p^*[\frac{\partial}{\partial \bar{x}}(\bar{\rho} h u v) + \frac{\partial}{\partial \bar{y}}(\bar{\rho} h v^2)]\,; \quad (44)$$

Energy-Transport Equation

$$\begin{aligned} &\bar{C}_p Re_s \frac{\partial}{\partial \tau}(\bar{\rho} h \bar{T}) + \bar{C}_p Re_p^*[\frac{\partial}{\partial \bar{x}}(\bar{\rho} h u \bar{T}) + \frac{\partial}{\partial \bar{y}}(\bar{\rho} h v \bar{T})] + Re_p^* \bar{Q}_s \\ &= E_c \Big\{ \bar{\beta}_t h (\sigma \frac{\partial p}{\partial \tau} + u \frac{\partial p}{\partial \bar{x}} + v \frac{\partial p}{\partial \bar{y}}) \bar{T} + h \frac{\Lambda}{2} \frac{\partial p}{\partial \bar{x}} \\ &\quad + \frac{\bar{\mu}}{h}[k_x (v_t^2 + \frac{1}{2} u \Lambda) + k_j (\frac{1}{4}\Lambda^2 - u\Lambda)] \Big\} \end{aligned} \quad (45)$$

The dimensionless flow parameters are defined as

$$\sigma = \frac{R\omega}{U_*}\,; \quad \Lambda = \frac{R\Omega}{U_*}\,; \quad E_c = \frac{U_*^2}{T_* C_{p*}}\,;$$

$$Re_s = \frac{\rho_* \omega c_*^2}{\mu_*} = \sigma Re_p^*\,; \quad Re_p = \frac{\rho_* U_* c_*}{\mu_*}\,; \quad Re_p^* = Re_p(\frac{c_*}{R})$$

In externally pressurized bearings the frequency (σ) and speed (Λ) numbers denote the importance of squeeze film and hydrodynamic flow effects relative to the pressure induced flow, respectively. The reference Reynold numbers (Re_p) denotes the ratio of fluid advection forces to viscous flow induced forces. In most HJBs, flow turbulence is produced by the Poiseuille flow due to the high pressure drop across the bearing length. The ratio of (Re_p/E_c) or (Re_s/E_c) may be interpreted as the effect of heat convection relative to shear dissipation. The Eckert number (E_c) denotes the ratio of kinetic energy to heat convection in the fluid film.

Dimensionless Governing Equations at Recesses

In dimensionless form, the governing equations at recesses are written as:

- Mass Conservation at a Recess

$$q_{in} = q_r + \sigma \bar{\rho}_r \frac{\partial \bar{\forall}_r}{\partial \tau} + \lambda_1 \bar{\rho}_r \left(\bar{\beta}_{pr} \frac{\partial p_r}{\partial \tau} - \bar{\beta}_{tr} \frac{\partial \bar{T}_r}{\partial \tau} \right) \tag{46}$$

where

$$q_{in} = \delta_* \sqrt{\bar{\rho}_r (1 - p_r)} \qquad \text{for orifice flow} \tag{47}$$

$$q_r = \int \bar{\rho} h (\vec{u} \cdot \vec{n}) \, d\Gamma_r, \tag{48}$$

$$\delta_* = A_o \mu_* \sqrt{2} / [c_*^3 \sqrt{\rho_* \Delta P}], \tag{49}$$

$$\lambda_1 = \sigma \bar{\forall}_r \ , \tag{50}$$

$$\bar{\beta}_{pr} = \beta_{pr} \Delta P \ , \tag{51}$$

$$\bar{\beta}_{tr} = \beta_{tr} T_* \ , \tag{52}$$

$$\bar{\forall}_r = \forall_r / (c_* R^2) \tag{53}$$

The orifice parameter δ_* is a design variable to determine a certain recess pressure ratio at the desired operating condition, and thus determines the size of the orifice restrictor. The major uncertain factor in the orifice parameter δ_* is the value of the orifice discharge coefficient C_d which is highly dependent on the local Reynolds number in the orifice feeding hole as well as on downstream flow conditions. In general, C_d takes values ranging from 0.6 for sharp edged orifice configurations and highly compressible fluids, to 1.0 for highly turbulent flows and reduced orifice length–to–diameter ratios (Redecliff and Vohr, 1969). However, the experimental measurements performed by Scharrer and Hibbs (1990) show that the discharge coefficients can be as low as 0.3 for large pressure drops in hydrostatic bearing geometries handling cryogenic fluids. Extensive experiments show that the discharge coefficient (C_d) takes values between 0.75 and 0.95 for

water HJBs with different clearance, orifice diameters, and operating conditions (Kurtin et al., 1993, Franchek and Childs., 1993, and Mosher, 1993).

The frequency parameter at a recess volume (λ_1), like σ, denotes the ratio of squeeze film flow to the pressure induced flow. $\bar{\beta}_{pr}$ is the dimensionless recess volume-liquid compressibility factor, which should be small to avoid pneumatic hammer instability at low frequencies (Reddecliff and Vohr, 1969, San Andres, 1991). A combination of large compressibility and frequency parameters, $\bar{\beta}_{pr}$ and λ_1, could bring undesirable hardening stiffness and substantial loss of damping at high excitation frequencies (Rohde and Ezzat, 1976, Ghosh et al., 1979,1987). Note that the introduction of temperature variation in the recess may mitigate or deteriorate the pneumatic instability problem depending on the sign of $\frac{\partial \bar{T}_r}{\partial \tau}$ (see Eq.(46)).

- Global Energy Balance Equation at a Recess

$$\begin{aligned} \sigma \bar{C}_p \bar{\forall}_r \frac{\partial(\bar{\rho}\bar{T})}{\partial \tau} + \bar{C}_p\Big(\sum \bar{\dot{m}}_d \bar{T}_d + \sum \bar{\dot{m}}_{side} \bar{T}_{side}\Big) \\ = \bar{C}_p\Big(\sum \bar{\dot{m}}_u \bar{T}_u + q_{in}\Big) + (\bar{T}^r_{or}\Lambda) E_c / Re^*_p \end{aligned} \tag{54}$$

where

$$\bar{T}^r_{or} = \frac{T^r_{or}}{c_* \Delta P R^2}, \tag{55}$$

is the dimensionless torque over the recess area.

- Global Energy Balance Equation at a Groove

$$\sum \bar{\dot{m}}_d \bar{T}_d = \sum \bar{\dot{m}}_u \bar{T}_u + q_{in} \bar{T}_{in} \tag{56}$$

where

$$q_{in} = \sum \bar{\dot{m}}_d - \sum \bar{\dot{m}}_u = q_d - q_u \tag{57}$$

If flow leaves the traling edge of a pad then

$$q_u = \sum \bar{\dot{m}}_u > 0, \tag{58}$$

so that

$$\bar{T}_u = \text{Upstream Film Values on Upstream Pad} \tag{59}$$

and the dimensionless temperatures at the downstream edge of a feeding groove are given by:

(a) If $q_d = \sum \bar{\dot{m}}_d > q_u$, then

$$\bar{T}_d = \frac{\lambda \sum \bar{\dot{m}}_u \bar{T}_u}{q_d} + \left(1 - \lambda \frac{q_u}{q_d}\right) \bar{T}_{in} \tag{60}$$

where

$$\bar{T}_{in} = 1.0; \tag{61}$$

(b) If $q_d < q_u$, then

$$\bar{T}_d = \begin{cases} \lambda \bar{T}_u \text{ or } \bar{T}_{in}, & \text{if } q_d \geq 0; \\ \text{Upstream Film Values on Downstream Pad}, & \text{if } q_d < 0. \end{cases} \tag{62}$$

- Recess/Film Entrance Pressure Rise/Drop

$$p_e^- = \begin{cases} p_r - \bar{\mu}_r \phi_r \left[\vec{\mathbf{u}} \eta \left(\frac{\bar{\rho}_e}{\bar{\rho}_r} \right) - \frac{\vec{\mathbf{\Lambda}}}{2} \right] \cdot \vec{\mathbf{n}}, & (\vec{\mathbf{u}} \cdot \vec{\mathbf{n}}) > 0, \quad \text{in x direction} \\ p_r, & \text{in y direction;} \end{cases} \tag{63}$$

$$p_e^+ = p_e^- - \frac{\phi_i \bar{\rho}_e}{2} (\vec{\mathbf{u}} \cdot \vec{\mathbf{n}})^2 ; \quad (\vec{\mathbf{u}} \cdot \vec{\mathbf{n}}) > 0 \tag{64}$$

where

$$\vec{\mathbf{u}} = u\vec{i} + v\vec{j}, \qquad \vec{\mathbf{\Lambda}} = \Lambda \vec{i} + 0\vec{j}, \tag{65}$$

$$\phi_r = k_r (b/D)(\eta/h)^2 / (1 - M_r^2) \tag{66}$$

$$\phi_i = \phi_{x,y} = Re_p^* (1 + \zeta_{x,y})(1 + \xi_{x,y})[1 - (\eta \bar{\rho}_e / \bar{\rho}_r)^2] \tag{67}$$

Perturbation Analysis

A perturbation analysis separates the governing equations into zeroth- and first-order equations. The zeroth-order equations describe the fluid flow field for a journal static equilibrium position, while the first-order linear equations govern the fluid flow for small amplitude journal center translational motions and journal axis conical motions. Solution to the zeroth-order flow field equations provides the bearing flow rate, film forces and load capacity, restoring moments and torque. Solution to the first-order equations determines the rotor dynamic force and moment coefficients due to journal lateral and angular motions.

Fig. 7 illustrates the journal translational and rotational motions in an annular seal. The inertial coordinate system $\{X,Y,Z\}$ helps to define the position of the spinning journal. For steady state operating conditions, the journal is at an equilibrium position given by two journal center displacements (e_{X0}, e_{Y0}), and by two angular rotations (δ_{X0}, δ_{Y0}) about $\{X,Y\}$ axes and centered at the axial coordinate Z_0, as shown in Fig. 7. Note that the origin of the inertial coordinate system in a HJB is different from that of a seal. For HJBs, the Z axis starts at the mid-plane of bearing recesses (San Andres, 1993a). The angles δ_{X0} or δ_{Y0} define a misalignment condition for the journal axes relative to the stator. Superimposed on the static equilibrium position, the journal describes motions of small amplitude (Δe_X, Δe_Y, Fig.7a) as well as angular rotations of amplitude ($\Delta\delta_X$, $\Delta\delta_Y$, Fig.7b) with center at Z_0. The film thickness is given by the superposition of steady-state (h_0) and dynamic (h_1) components, and represented in dimensionless form by the real part of the following expression:

$$h = h_0 + h_1 \tag{68}$$

$$h_0 = \bar{c}_0 + [\varepsilon_{X0} + \delta_{Y0}(Z - Z_0)/c_*]\cos\theta + [\varepsilon_{Y0} - \delta_{X0}(Z - Z_0)/c_*]\sin\theta \tag{69}$$

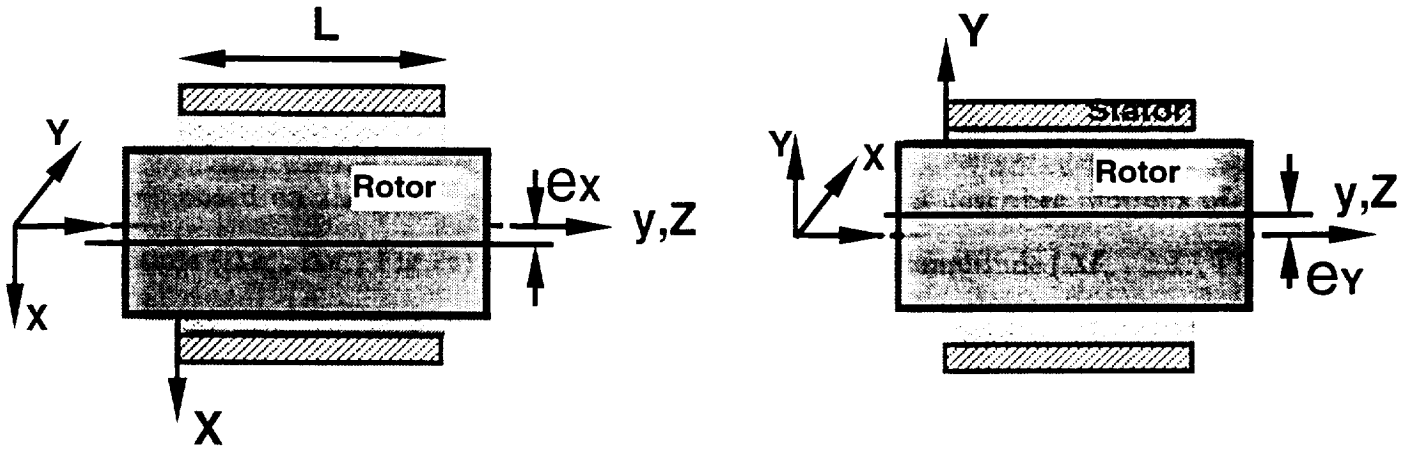

(a) Journal translational motions

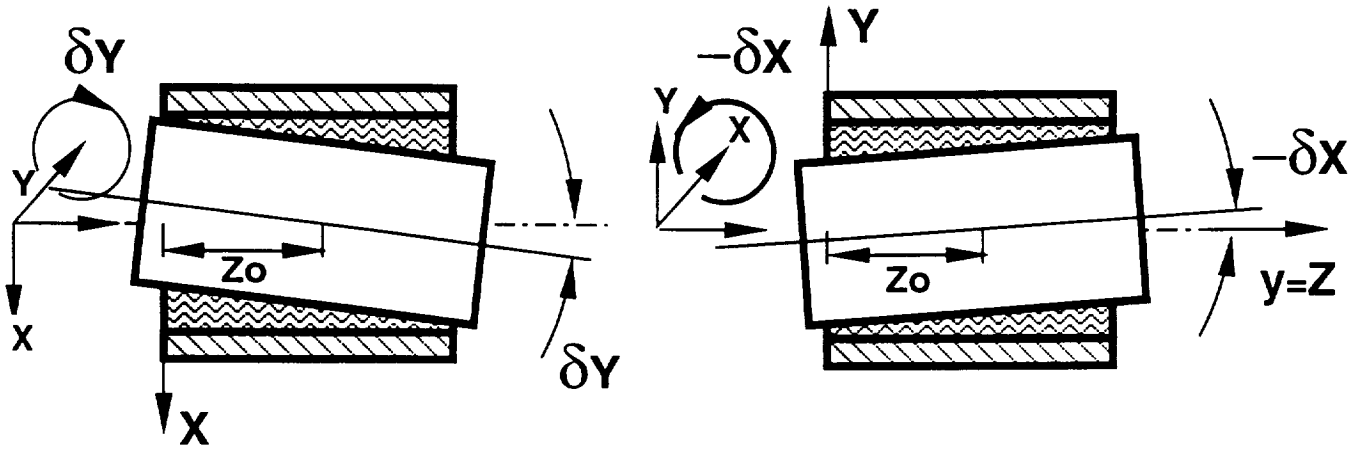

Zo: Axial Distance to Center of Rotations

(b) Journal rotational motions

Figure 7. Description of journal motions in an annular seal

$$h_1 = e^{i\tau}[(\Delta\xi_X \cos\theta + \Delta\xi_Y \sin\theta - \frac{R\Delta\delta_X}{c_*}(\bar{Z} - \bar{Z}_0)\sin\theta + \frac{R\Delta\delta_Y}{c_*}(\bar{Z} - \bar{Z}_0)\cos\theta] \quad (70)$$

and

$$\bar{Z}_0 = Z_0/R, \qquad \tau = \omega t, \quad \mathrm{i} = \sqrt{-1} \quad (71)$$

where $\theta = \bar{x} = x/R$ is the dimensionless circumferential coordinate in the unwrapped fluid film plane (refer to Figs. 1 to 3), $\bar{Z} = Z/R$ the dimensionless inertial axial coordinate, and $\bar{c}_0(y)$ is a general function that describes the clearance variations in the axial coordinate.

For small amplitude motions, all the dependent variables $(p, u, v, \bar{T})$ as well as the fluid properties ($\bar{\rho}$,$\bar{\mu}$,$\bar{\beta}$,etc.) are expressed as the superposition of zeroth- and first-order fields representing the steady state and dynamic motion conditions, respectively. In general, we let

$$\phi = \phi_0 + e^{i\tau}(\Delta\xi_X\phi_X + \Delta\xi_Y\phi_Y + \frac{R\Delta\delta_X}{c_*}\phi_{\delta_X} + \frac{R\Delta\delta_Y}{c_*}\phi_{\delta_Y}) = \phi_0 + e^{i\tau}\Delta\varepsilon_j\phi_{\delta_j} \quad (72)$$

where

$$\phi = u, v, p, \bar{T}, \bar{\rho}, \bar{\mu}, \bar{\beta}_t, k_x, k_y, ..., etc. \quad \text{and} \quad j = X, Y, \delta_X, \delta_Y \quad (73)$$

Expansion of the governing equations in the perturbation variables yields the dimensionless zeroth- and first-order flow equations presented in Appendix C.

Boundary Conditions for the Flow

The boundary conditions for both the zeroth-order and the first-order flow variables are given and discussed for the three different configurations. The first set refers to a circular (360°) bearing, the second one to a characteristic bearing pad, and the third set to an annular pressure seal.

Boundary Conditions for a circular (360°) bearing

(a) On the 360-degree extended film land, the pressure, velocity, and temperature fields are continuous and single-valued in the circumferential direction:

$$u_0, v_0, p_0, \bar{T}_0(\bar{x}, \bar{y}) = u_0, v_0, p_0, \bar{T}_0(\bar{x} + 2\pi, \bar{y}) \quad (74)$$

$$u_j, v_j, p_j, \bar{T}_j(\bar{x}, \bar{y}) = u_j, v_j, p_j, \bar{T}_j(\bar{x} + 2\pi, \bar{y}) \tag{75}$$

(b) At the bearing side discharge planes, the fluid pressure is equal to specified values of discharge or sump pressures if no end restrictions are present, i.e.,

$$p_0(\bar{x}, l_R) = p_R(\bar{x}) \tag{76}$$

$$p_0(\bar{x}, -l_L) = p_L(\bar{x}) \tag{77}$$

In general the discharge pressures are uniform and constant. However, in some cryogenic turbopump applications the bearing may be located close to the pump-impeller discharge. In this case, the sump pressures are non-uniform but rotationally symmetric. The model expresses the discharge pressures in a series form given as:

$$p_R = p_{R0} + \sum_{n=1} p^n_{Rc} \cos(n\theta) + p^n_{Rs} \sin(n\theta) \tag{78}$$

$$p_L = p_{L0} + \sum_{n=1} p^n_{Lc} \cos(n\theta) + p^n_{Ls} \sin(n\theta) \tag{79}$$

where the p^n_L, p^n_R terms correspond to the Fourier coefficients of a series expansion of the non-uniform discharge (sump) pressures.

A value of dynamic pressure (p_j, $j = X, Y, \delta_X, \delta_Y$) equal to zero is imposed at all locations where time invariant pressures are specified, i.e.

$$p_j(\bar{x}, l_R) = 0 \tag{80}$$

$$p_j(\bar{x}, -l_L) = 0. \tag{81}$$

On the other hand, if end seals or wear rings are present at the discharge sides of the bearings and the fluid flows out of the bearing to the sump conditions ($\vec{V} \cdot \vec{n} > 0$), then there is a pressure increase (ram pressure) at the discharge sides:

$$p_0(\bar{x}, l_R) = p_R(\bar{x}) + \frac{1}{2}\bar{\rho}_0 \mathcal{K}_R R^*_{e_p} v_0^2|_{l_R, \bar{x}}, \quad \text{if} \quad v_0|_{l_R, \bar{x}} > 0 \tag{82}$$

$$p_0(\bar{x}, -l_L) = p_L(\bar{x}) + \frac{1}{2}\bar{\rho}_0 \mathcal{K}_L R_{e_p}^* v_0^2|_{-l_L,\bar{x}}, \quad \text{if} \quad v_0|_{-l_L,\bar{x}} < 0 \tag{83}$$

$$p_j(\bar{x}, l_R) = \frac{1}{2}\mathcal{K}_R R_{e_p}^* v_0(2\bar{\rho}_0 v_j + \bar{\rho}_j v_0)|_{l_R,\bar{x}}, \quad \text{if} \quad v_0|_{l_R,\bar{x}} > 0 \tag{84}$$

$$p_j(\bar{x}, -l_L) = \frac{1}{2}\mathcal{K}_L R_{e_p}^* v_0(2\bar{\rho}_0 v_j + \bar{\rho}_j v_0)|_{-l_L,\bar{x}}, \quad \text{if} \quad v_0|_{-l_L,\bar{x}} < 0 \tag{85}$$

where $\mathcal{K}_R$,$\mathcal{K}_L$ are the end seal discharge coefficients at the right and left sides of the bearing, respectively. Typical values for $\mathcal{K}$ range from 1.0 to 4.0 (Childs, 1989). However, applications such as those with wear end rings of tight clearances present larger values of $\mathcal{K}$'s (Scharrer et al., 1992b).

The temperatures at the discharge planes can be obtained from their upwind values on the film lands (Roach, 1976).

Boundary Conditions for a Bearing Pad

At low rotational speeds, the pressures at the side boundaries of the pad ($\bar{y} = -l_L$ & l_R) are essentially constant and equal to specified values of ambient or sump pressures, similar to those for a circular (360°) bearing. A linear pressure distribution is assumed along the leading and trailing edges of the pads (downstream and upstream edges of the grooves).

On the other hand, significant momentum changes occur at the pad leading edge at high journal surface speeds. The fluid entering the film lands at the leading edge is assumed to have a dynamic head equal to some fraction of a reference dynamic pressure based on the bearing surface speed (Burton and Carper, 1967; Smalley et al., 1974; Mori et al., 1991; Ettles and Cameron, 1968), i.e.,

$$\Delta p_0(\bar{x}_{inlet}, \bar{y}) = \frac{1}{2}\mathcal{K}_P \bar{\rho}_0 R_{e_p}^* \left(\frac{\Lambda}{2}\right)^2 \tag{86}$$

$$p_j(\bar{x}_{inlet}, \bar{y}) = 0 \tag{87}$$

The coefficient ($\mathcal{K}_P$) is an empirical (experimental) ram pressure factor. Burton and Carper (1967) suggest a value of $\mathcal{K}_P = 0.64$ for high speed flows with large turbulent levels.

Across the line, $-l_L < \bar{y} < l_R$, at the pad leading edge the flow is regarded as parallel to the bearing pad, i.e., the axial velocity is null:

$$v_0(\bar{x}_{inlet}, \bar{y}) = 0 \tag{88}$$

$$v_j(\bar{x}_{inlet}, \bar{y}) = 0 \tag{89}$$

Temperatures at the leading and trailing edges of the pads are given by the global energy balance equation at a groove for different flow conditions as shown before.

Boundary Conditions for an Annular Pressure Seal

The periodic boundary condition in the circumferential direction also holds for an annular pressure seal (see Eqs.(74) and (75)). Boundary conditions at the seal inlet and exit planes follow:

(a) Due to fluid inertia, the local acceleration of fluid from relatively stagnant conditions at the upstream seal region to a high velocity at the seal inlet causes a sudden pressure drop. The entrance pressure at the seal inlet plane ($\bar{y}$=0) is modeled by a simple Bernoulli equation:

$$p_{01} = p_0(\bar{x}, 0) = 1 - \alpha_y \bar{\rho}_{01} v_{01}^2 \quad \text{if} \quad v_{01} > 0\,; \qquad \alpha_y = \frac{1}{2}(1+\xi) Re_p^* \tag{90}$$

$$p_{j1} = p_j(\bar{x}, 0) = -\alpha_y v_{01}(2\bar{\rho}_{01} v_{j1} + v_{01}\bar{\rho}_{j1}) \qquad \text{if} \quad v_{01} > 0 \tag{91}$$

The inlet circumferential velocities are given by

$$u_{01} = u_0(\bar{x}, 0) = \alpha\Lambda\,; \qquad u_{j1} = u_j(\bar{x}, 0) = 0 \tag{92}$$

where α is a pre-swirl factor, and "1" denotes the seal entrance location.

The entrance bulk-flow temperatures are equal to (Yang et al., 1993a)

$$\bar{T}_{01} = \bar{T}_0(\bar{x}, 0) = 1 - \frac{v_{01}^2}{2}(1+\xi)[1-(1-\bar{\beta}_t)\bar{\rho}_{01}]E_c, \tag{93}$$

$$\bar{T}_{j1} = -(1+\xi)E_c v_{01}[v_{j1} - (1-\bar{\beta}_t)(\bar{\rho}_{01}v_{j1} + \bar{\rho}_{j1}v_{01}/2)] \quad \text{if} \quad v_{01} > 0. \tag{94}$$

For incompressible liquids, $\bar{\beta}_t = 0$ and $\bar{\rho}_{01} = 1$, therefore,

$$\bar{T}_{01} = 1 \quad \text{and} \quad \bar{T}_{j1} = 0. \tag{95}$$

For ideal gases, $1 - \bar{\beta}_t = 0$, therefore,

$$\bar{T}_{01} = \bar{T}_0(\bar{x}, 0) = 1 - \frac{v_{01}^2}{2}(1+\xi)E_c \quad \text{and} \quad \bar{T}_{j1} = -(1+\xi)E_c v_{01} v_{j1} \quad \text{if} \quad v_{01} > 0. \tag{96}$$

(b) At the seal exit plane ($\bar{y} = L/R$), the discharge pressure for subsonic conditions is:

$$p_0(\bar{x}, L/R) = p_R\,; \qquad p_j(\bar{x}, L/R) = 0 \tag{97}$$

If an end seal or wear ring is present, the discharge pressure can be treated in the same way as for end seals in a HJB.

Other Boundary Conditions

If the bearing is symmetric both in geometry and operating conditions, then, the axial velocity and the axial gradients of all the primitive variables are zero at the circumferential central plane ($\bar{y} = 0$) of the bearing:

$$v_0(\bar{x}, 0) = 0 \tag{98}$$

$$v_j(\bar{x}, 0) = 0 \tag{99}$$

$$\frac{du_0}{d\bar{y}}, \frac{dp_0}{d\bar{y}}, \frac{d\bar{T}_0}{d\bar{y}}(\bar{x}, 0) = 0 \tag{100}$$

$$\frac{du_j}{d\bar{y}}, \frac{dp_j}{d\bar{y}}, \frac{d\bar{T}_j}{d\bar{y}}(\bar{x}, 0) = 0 \tag{101}$$

Heat Transfer Between Fluid Film and Bounding Solids

Temperature boundary conditions at the fluid-journal and fluid-bushing interfaces are modeled by heat transfer to the journal and the bearing (Q_s by Eq.(12)) and *directly* incorporated into the energy equation (11) (Constantinescu, 1973).

An adiabatic flow process ($Q_s = 0$) is shown to be a reasonable approximation for turbulent flow HJBs and annular seals with large pressure drops across the seal/bearing length. In such conditions, the heat generated in the fluid is carried away mainly by fluid advection while heat conduction through the bushing/stator is relatively small. The adiabatic flow assumption greatly simplifies the analysis, and numerical predictions based on this assumption correlate well with experimental data (Yang et al., 1993a,b).

Regarding pad journal bearings without external pressurization, the adiabatic flow assumption is highly conservative. Without significant supply flow of fresh fluid into the fluid film, hot lubricant recirculates in the journal bearing and causes a much larger temperature increase than in a HJB or an annular pressure seal. Heat convection by the side (axial) flow is greatly reduced and heat transfer between the fluid film and the bounding solids is significant for this bearing configuration.

Different THD models exist to address the heat transfer from the fluid film to the bounding solids. In a full THD analysis, the solution of the Reynolds equation (or the continuity and the Navier-Stokes equations) is coupled to the energy equation in the fluid film and the heat conduction equations in the solids. This coupling leads to a nonlinear iterative problem which is costly and may be

sensitive and prone to numerical instabilities. Another shortcoming of the full THD treatment is that the bearing pad is never an isolated, single component but part of an assembly that includes bearing liner, housing, pedestals, and seals, often made of different materials (Pinkus, 1990). Therefore, a full THD solution is strongly machine dependent and not considered necessary in the context of the current analysis.

More simplified heat conduction models have been used to treat the heat flow in the journal and bushing. Safar and Szeri (1974) considered the journal to be isothermal at the mean temperature of the bushing inner surface. Radial heat flow into the bushing of a hydrodynamic journal bearing was considered as a reasonable approximation ut this might lead to error in the calculated maximum temperature in the fluid film. This over-simplification allows calculation of the global heat flow from the heat source (fluid film) to the heat sink (ambient) even for composite bearing assemblies. Suganami and Szeri (1979) found that at high rotational speeds an adiabatic journal surface assumption might be more appropriate than the isothermal surface since heat generation in the fluid film is large in comparison with the heat capacity of the journal and the time available to absorb this energy is short.

In this analysis and the computer code being developed, different simplified THD models are adapted (Fig. 8). Options included are:

(a) Adiabatic journal and bearing surfaces $Q_s = 0$,

(b) Adiabatic bearing and isothermal journal surfaces, $Q_s = h_J(T - T_J)$,

(c) Adiabatic journal and isothermal bearing surfaces, $Q_s = h_B(T - T_B)$, and

(d) Isothermal journal and bearing surfaces ($T = T_{supply}$).

A more detailed model including radial heat transfer through the sleeve or stator will be a subject of investigation on Phase II (1994) of the present work.

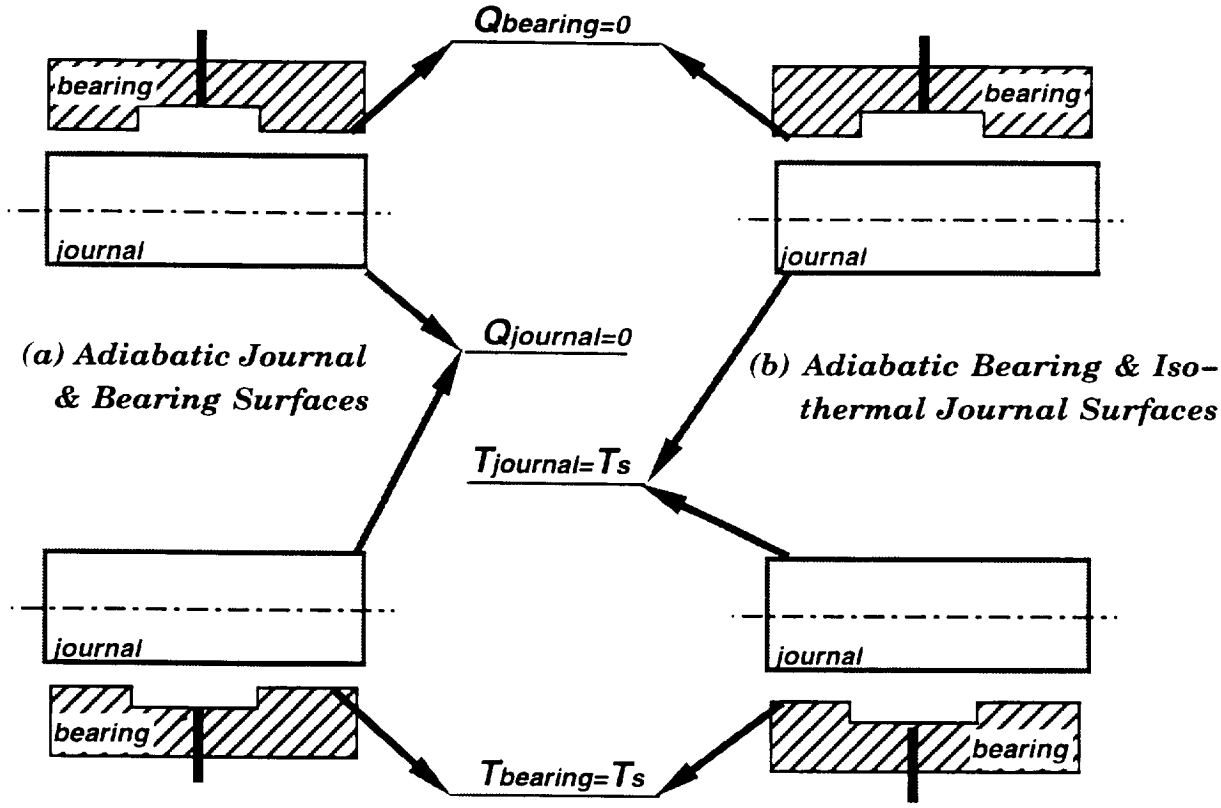

Fig. 8 Thermal Models of Heat Transfer with Different Surface Boundary Conditions

Film Forces, Torque, and Dynamic Force Coefficients

Once the zeroth-order and the first-order equations are solved, the static and dynamic performance characteristics of the bearing can be evaluated. Fluid film forces and moments are calculated by integration of the pressure field over the pad surfaces. The components of the static equilibrium force and moment are given by:

$$\begin{bmatrix} F_{X0} \\ F_{Y0} \end{bmatrix} = \Delta P R^2 \sum_{k=1}^{N_{pad}} \int_{-l_L}^{l_R} \int_0^{\theta_{pad}} p_0^k \begin{bmatrix} \cos\theta \\ \sin\theta \end{bmatrix} d\theta d\bar{y} \tag{102}$$

and

$$\begin{bmatrix} M_{X0} \\ M_{Y0} \end{bmatrix} = \Delta P R^3 \sum_{k=1}^{N_{pad}} \int_{-l_L}^{l_R} \int_0^{\theta_{pad}} p_0^k (\bar{Z} - \bar{Z}_0) \begin{bmatrix} -\sin\theta \\ \cos\theta \end{bmatrix} d\theta d\bar{y} \tag{103}$$

where p_0^k corresponds to the zeroth-order pressure field for the k-th pad.

The perturbation analysis allows the dynamic force and moment coefficients due to journal center displacements and journal axis rotations to be obtained from the general expression for dynamic force given as:

$$\begin{aligned} \begin{bmatrix} F_X \\ F_Y \\ M_X \\ M_Y \end{bmatrix} = \begin{bmatrix} F_{X0} \\ F_{Y0} \\ M_{X0} \\ M_{Y0} \end{bmatrix} &- \begin{bmatrix} K_{XX} & K_{XY} & K_{X\delta_X} & K_{X\delta_Y} \\ K_{YX} & K_{YY} & K_{Y\delta_X} & K_{Y\delta_Y} \\ K_{\delta_{XX}} & K_{\delta_{XY}} & K_{\delta_X\delta_X} & K_{\delta_X\delta_Y} \\ K_{\delta_{YX}} & K_{\delta_{YY}} & K_{\delta_Y\delta_X} & K_{\delta_Y\delta_Y} \end{bmatrix} \begin{bmatrix} \Delta e_X \\ \Delta e_Y \\ \Delta \delta_X \\ \Delta \delta_Y \end{bmatrix} \\ &- \begin{bmatrix} C_{XX} & C_{XY} & C_{X\delta_X} & C_{X\delta_Y} \\ C_{YX} & C_{YY} & C_{Y\delta_X} & C_{Y\delta_Y} \\ C_{\delta_{XX}} & C_{\delta_{XY}} & C_{\delta_X\delta_X} & C_{\delta_X\delta_Y} \\ C_{\delta_{YX}} & C_{\delta_{YY}} & C_{\delta_Y\delta_X} & C_{\delta_Y\delta_Y} \end{bmatrix} \begin{bmatrix} \Delta \dot{e}_X \\ \Delta \dot{e}_Y \\ \Delta \dot{\delta}_X \\ \Delta \dot{\delta}_Y \end{bmatrix} \\ &- \begin{bmatrix} M_{XX} & M_{XY} & M_{X\delta_X} & M_{X\delta_Y} \\ M_{YX} & M_{YY} & M_{Y\delta_X} & M_{Y\delta_Y} \\ M_{\delta_{XX}} & M_{\delta_{XY}} & M_{\delta_X\delta_X} & M_{\delta_X\delta_Y} \\ M_{\delta_{YX}} & M_{\delta_{YY}} & M_{\delta_Y\delta_X} & M_{\delta_Y\delta_Y} \end{bmatrix} \begin{bmatrix} \Delta \ddot{e}_X \\ \Delta \ddot{e}_Y \\ \Delta \ddot{\delta}_X \\ \Delta \ddot{\delta}_Y \end{bmatrix} \end{aligned} \tag{104}$$

The dynamic–force coefficients defined by Eq.(104) are important measures of dynamic bearing performance since they influence the critical speeds, the resonant amplitude response, and rotordynamic stability of the rotor-bearing system.

The above expression (Eq.(104)) allows the dynamic force coefficients to be calculated from integration of the first-order complex pressure field (p_j) over the pad surfaces. The force coefficients due to journal center displacements are defined by the following relationships (San Andres, 1993a):

$$K_{ij} - \omega^2 M_{ij} + \mathrm{i}\omega C_{ij} = -\Delta P \frac{R^2}{c_*} \sum_{k=1}^{N_{pad}} \int_{-l_L}^{l_R} \int_{0}^{\theta_{pad}} p_j^k h_i \, d\theta d\bar{y}; \quad i,j = X,Y \quad (105)$$

The force coefficients due to journal axis rotations are equal to

$$K_{i\delta_j} - \omega^2 M_{i\delta_j} + \mathrm{i}\omega C_{i\delta_j} = -\Delta P \frac{R^3}{c_*} \sum_{k=1}^{N_{pad}} \int_{-l_L}^{l_R} \int_{0}^{\theta_{pad}} p_{\delta_j}^k h_i \, d\theta d\bar{y}; \quad i,j = X,Y \quad (106)$$

The moment coefficients about Z_0 due to journal center displacements are given by:

$$K_{\delta_i j} - \omega^2 M_{\delta_i j} + \mathrm{i}\omega C_{\delta_i j} = -\Delta P \frac{R^3}{c_*} \sum_{k=1}^{N_{pad}} \int_{-l_L}^{l_R} \int_{0}^{\theta_{pad}} p_j^k (\bar{Z} - \bar{Z}_0) h_{\delta_i} \, d\theta d\bar{y}; \quad i,j = X,Y \quad (107)$$

and, the moment coefficients due to rotor axis rotations about Z_0 are equal to

$$K_{\delta_i \delta_j} - \omega^2 M_{\delta_i \delta_j} + \mathrm{i}\omega C_{\delta_i \delta_j} = -\Delta P \frac{R^4}{c_*} \sum_{k=1}^{N_{pad}} \int_{-l_L}^{l_R} \int_{0}^{\theta_{pad}} p_{\delta_j}^k (\bar{Z} - \bar{Z}_0) h_{\delta_i} \, d\theta d\bar{y}; \quad i,j = X,Y \quad (108)$$

where

$$h_X = h_{\delta_Y} = \cos\theta, \quad h_Y = -h_{\delta_X} = \sin\theta \quad (109)$$

It is noted that the characterization of force coefficients in terms of stiffness, damping and inertia parameters is appropriate for incompressible fluids only. For highly compressible liquids and gases, the force coefficients are themselves functions of frequency.

The friction torque is given by integration of the wall shear stress at the journal surface over the pads as

$$T_{or} = R \sum_{k=1}^{N_{pad}} \int_{-L_L}^{L_R} \int_{0}^{R\theta_{pad}} \tau_{xz}^{H,k} \, dx dy \tag{110}$$

NUMERICAL SOLUTION PROCEDURE

The governing equations presented above are nonlinear, and therefore, difficult to solve analytically. Numerical methods are then needed to obtain meaningful solutions. A finite-difference scheme has been implemented to solve the coupled, non-linear PDES of mass and momentum conservation and energy transport. The procedure is based on the forward marching scheme presented by Launder and Leschziner (1978) and uses the SIMPLEC algorithm of Van Doormaal and Raithby (1984). The algorithm has been adopted by San Andres (1992a) and Yang et al.(1993a) to solve the barotropic and THD fluid-film-flow problems in HJBs and annular pressure seals. Appendix D presents the discretized algebraic set of equations used for solution of the flow field in fluid film bearings.

The computer program *hydrosealt* was completed on 1993 for the analysis of turbulent flow cryogenic liquid bearings. *hydrosealt* handles iosthermal and adiabatic flow models with variable properties for cryogenic liquids. In general, the analytical bearing model and computer code calculate:

(a) bearing leakage,

(b) friction torque and temperature rise,

(c) load capacity (fluid film forces)and restoring moments,

(d) rotordynamic force coefficients due to journal center displacements and journal axis rotations,

(e) rotordynamic moment coefficients due to journal center displacements and journal axis rotations,

(f) stability indicators such as whirl frequency ratios for lateral and conical journal motions, and equivalent bearing stiffness,

(g) complete pressure, velocity, and temperature fields on the flow region, as well as density and viscosity distributions.

The *hydrosealt* has been developed in standard Fortran 77 in a SGI 4D-35 computer. A detailed User's Manual and Tutorial accompany the *hydrosealt* program (San Andres, 1993d) A great number of cases has been run to test the *hydrosealt* code. Comparisons show that for LO_2 damper seals, results from *hydrosealt* code are the same as those from a especialized seal code (Yang et al., 1993a). For the single-row, five-recess water HJBs tested at Texas A&M University, predictions from the *hydrosealt* code show good agreement with the results from experiments. Refer to the Examples Manual of *hydrosealt* for a description and discussion of the examples presented (San Andres, 1993e).

RESULTS AND DISCUSSION

The analysis presents a general thermal flow model for the static and dynamic force and moment response in fully developed, variable properties, turbulent flow fluid film bearings. The bearing geometries of interest correspond to hydrostatic journal pad bearings (HJBs), annular pressure seals or damper bearing seals, and fixed arc pad journal bearings.

Numerical predictions from the present THD model and prior analytical developments have been presented in several earlier publications. The analytical effort has always stressed in presenting comparisons with experimental results when these have been available in the open literature. San Andres et al.(1991c, 1993b) and Yang et al.(1993a,b) present results for the effects of journal misalignment and thermal effects in annular pressure seals, respectively. Kurtin et al.(1993), Mosher (1993) and Franchek et al.(1993) present a direct comparison between experimental measurements of the static and dynamic force response of a 5 recess, water hydrostatic bearing with numerical predictions from the present model. Yang et al. (1993c, d) also present comparisons between the THD adiabatic and isothermal models predictions with experimental results for turbulent flow liquid hydrogen and water HJBs, respectively. In all cases the correlations with the experimental measurements are reported to be good and provide validity for the analysis.

This section presents results for several relevant fluid film bearing applications. Many more examples are discussed in the *hydrosealt* Examples Manual (San Andres, 1993e). The first example studied refers to a direct comparison between the load capacity and rotordynamic force coefficients for a hydrostatic bearing and a damper bearing seal operating in liquid oxygen. The HJB and damper seal have been designed to replace the duplex ball bearings next to the left inducer in the liquid oxygen high pressure turbopump (LO_x HPOTP). The fluid operating

conditions (pressure and temperature) as well as the actual bearing clearance, and most importantly, the load supported by the bearings are a function of the rotating speed of the pump. Information relevant to the load characteristics in the HOPTP were obtained from Shoup (1993) and the fluid operating conditions directly extracted from the technical report of Heshmat (1991). The hydrostatic bearing has 6 recesses of rectangular shape and orifice restrictors, while the damper seal consists of two parallel annular seals of convergent tapered clearance and separated by a deep feeding central groove (Von Prageneu, 1990). The damper seal has a rough stator surface of the knurled type while the hydrostatic bearing and journal surfaces are perfectly smooth. This type of damper seal geometry is also known as an annular hydrostatic bearing (Scharrer et al., 1992c). Table 1 shows a description of the bearing geometries, and it also presents the actual clearances, supply and discharge pressures and supply temperature for liquid oxygen, and the nominal load acting on the bearings as the operating speed increases from 14,035 cpm to 30,367 cpm. Note that the load and pressures are proportional to the second power of the rotational speed. At the nominal operating conditions, here taken as 26,000 cpm, the nominal clearance in the HJB is equal to 0.175 mm, while the inlet and exit clearances in the damper seal are equal to 0.221 mm and 0.129 mm (ratio = 1.715) with an average clearance identical to that of the hydrostatic journal bearing.

The hydrostatic bearing is designed for operation at the nominal speed with a concentric pressure ratio equal to 0.60 to provide maximum direct stiffness coefficients. On the other hand, the ratio of inlet to discharge clearance in the damper seal has been optimized to also obtain the largest direct stiffness coefficients. The maximum specific load (load divided by bearing projected area) is equal to 6.55 MPa (950 psi) and 7.22 MPa (1048 psi) for the hydrostatic bearing

Table 1. Geometry and operating characteristics of hydrostatic bearing and parallel damper seals for load support in LOx HPOTP.

Hydrostatic Bearing: Number of recesses **Nrec** = 6

Diameter (D)	Length (L)	Clearance (C*)	Recess Depth	Axial Length(ℓ)	Recess Arc
85.1 mm (3.35 in)	48.85 mm (1.92 in)	175.2μm (6.9 mils)	508μm (20 mils)	24.42 mm (0.96 in)	30 deg

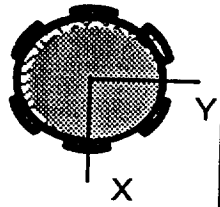

journal and bearing surface conditions: smooth.
L/D=0.57; **Hr/C**=2.9, **ℓ/L**=0.5, Recess area ratio=0.25, **C/R** =0.0041
Orifice C_d=0.90; diameter **do** = 4.44 mm
Recess edge coefficients ξ_{xu}=0.0; ξ_{xd}=0.50; ξ_y=0.0

Damper Seal: Two parallel seal land (2 x L) (groove width unspecified)

Diameter (D)	Length (L)	Inlet Clearance	Exit Clearance	Ratio	Average Clearance
85.1 mm (3.35 in)	22.2 mm (0.874 in)	221.3μm (8.7 mils)	129.1μm (5.08 mils)	1.71	175.2μm (6.9 mils)

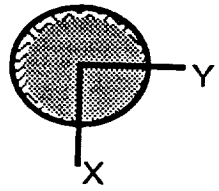

journal smooth, bearing rough, r/h = 0.044 (Knurled)
Entrance coefficient ξ_y=0.25

Operating Conditions:

Speed cpm	Psupply MPa	Pa	Tsupply K	Tsat K	Load N	Reynolds# Rec	Average Clearance* (μm)
14,035	16.00	1.654	102.77	128.9	5,828	72,816	180
19,732	29.59	1.792	107.22	130.5	11,519	100,700	177.7
26,000	39.60	2.089	110.55	133.7	20,000	130,130	175.2
28,340	43.60	2.434	111.33	137.0	23,762	143,720	174.3
30,367	55.69	2.551	115.00	138.0	27,282	147,600	173.2

Inlet swirl ratio α= 0.50

Fluid: **LO_2 (liquid oxygen)** at 110.6 K (200R)

P (MPa)	ρ (kg/m3)	μ (E-3 Pa.s)	Cp(J/kg-K)
39.60	1134.4	0.177	1,606.4
2.09	1038.1	0.124	1,827.2

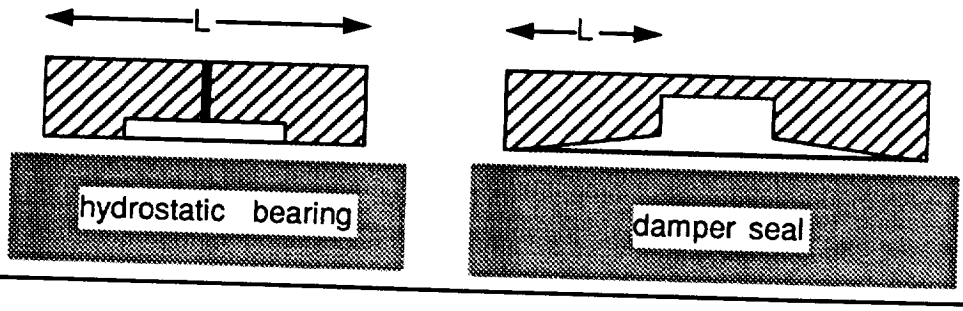

and damper seal, respectively. These specific loads are very large considering the nature of the bearing application with a fluid of very low viscosity such as liquid oxygen. The calculations for the static and dynamic performance characterictics of the HJB and seal are performed using the adiabatic journal (rotor) and bearing (stator) thermal model. Numerical calculations for the damper seal are performed only for the thin land portion and then multiplied by two. The central groove and its effect on load capacity and dynamic force coefficients are altogether neglected. This oversimplification seems appropriate as a first attempt to correlate the performance of the HJB and seal. However, it is now known that central feeding grooves do have a pronounced effect on the dynamic force response of fluid film bearings, in particular with regard to inertia and cross-coupled damping force coefficients (Arauz et al., 1993, Lindsey, 1993).

Figure 9 depicts the fluid supply temperature, bearing load and pressure drop across the HJB and seals as the rotational speed of the pump increases. The largest load of 27,282 N (6,137 lbs) corresponds to the highest operating speed. The Figure also shows the values of the nominal circumfererential flow Reynolds number $Re_c = \rho_* R\Omega c_* / \mu_*$ to range from approximately 70,000 to 150,000 as the rotor speed rises. The flow in the bearings is then turbulent. Figure 10 presents the HJB and damper seal flow rate and drag torque as the journal speed increases. The hydrostatic bearing (h) shows approximately 14 percent more flow rate than the damper seal (s), while it produces approximately 27 percent less drag torque than the seal at the largest operating speed. These results are a direct consequence of the rough stator surface in the damper seal.

Figure 11 presents the journal operating eccentricity and attitude angle as well as the maximum temperature rise in the HJB and damper seal as the operating speed increases. Note that as the speed rises so does the applied load

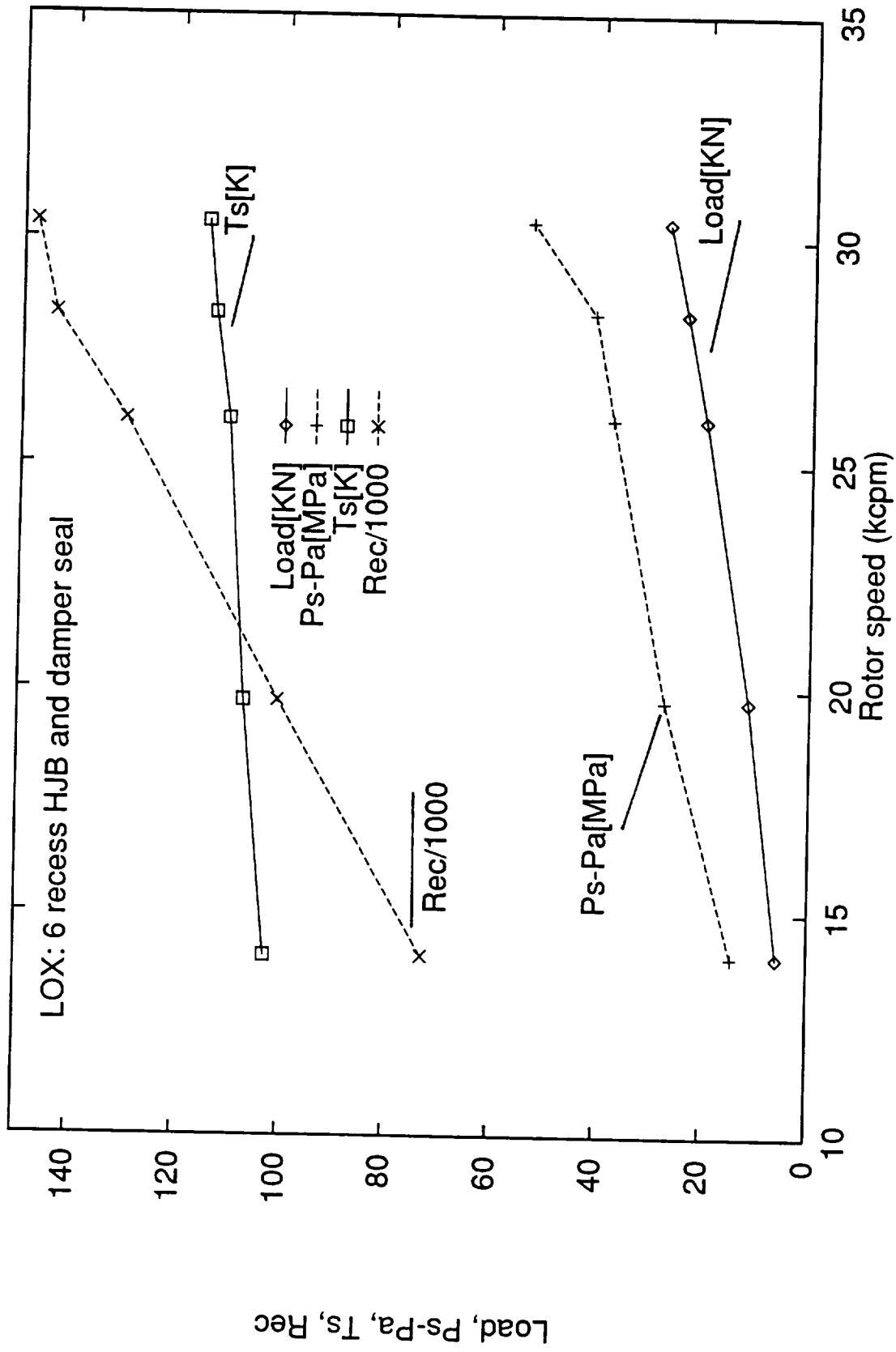

Fig. 9. Supply temperature, pressure drop, Reynolds number and load vs. rotational speed for LOx 6 recess HJB and damper seal.

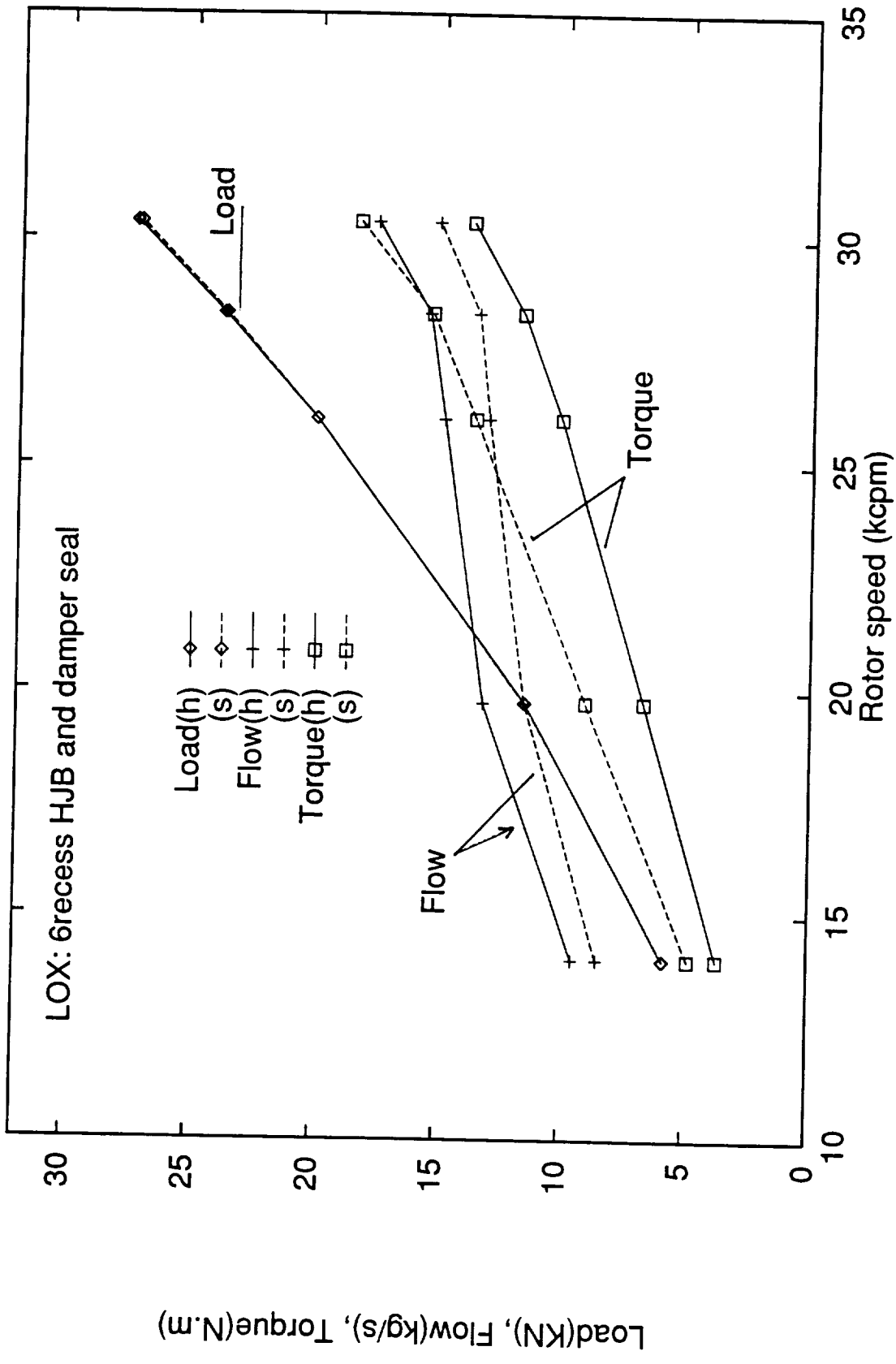

Fig.10. Flow rate and drag torque vs. rotational speed for LOx (h) 6 recess HJB and (s) parallel damper seal.

at a rate proportional to the journal speed squared. The load for the HJB is directed towards the bottom of a bearing recess (X direction). The dimensionless journal eccentricity has been determined as the ratio between the journal offcenter displacement divided by the nominal clearance at 26,000 cpm, i.e. 0.175 mm. Note that the attitude angle is less than 10° for both bearings and the journal eccentric displacement is rather moderate considering the magnitude of the loads applied. The low value in the attitude angle indicates dominance of hydrostatic effects over hydrodynamic effects. The maximum temperature in the film lands of the hydrostatic bearing and seals increases rapidly with journal speed. The HJB shows a larger thermal differential between the bearing supply condition and discharge planes. The results also indicate that both HJB and damper seal operate well below the critical LO_2 temperature of $T_c = 154.6°K$ (278 $°R$)

Figures 12 to 14 present the synchronous stiffness, damping and inertia force coefficients versus the rotational speed for the HJB and damper seals, respectively. Note the similar values between all direct coefficients (say K_{XX} and K_{YY}) and cross coupled coefficients (say K_{XY} and -K_{YX}) which denote that the HJB and damper bearing seal have very uniform force coefficients as the operating eccentricity (and load) increases with the operating speed. Figure 12 shows a HJB with slightly smaller direct stiffness coefficients (K_{XX} and K_{YY}) than the damper seal, while its cross-coupled stiffness (K_{XY}) is larger. Note the dominance of hydrostatic (direct) coefficients over the cross-coupled coefficients induced solely by journal rotation.

Figure 13 shows the HJB to have larger direct damping coefficients (C_{XX} and C_{YY}) than the damper seals (approximately 47 percent higher). These results produce at the largest journal speed a whirl frequency ratio (WFR) equal to 0.39 and 0.45 for the HJB and damper seal, respectively. Thus, in this example when the inlet swirl ratio is equal to 0.50, the HJB offers slightly better dynamic stability

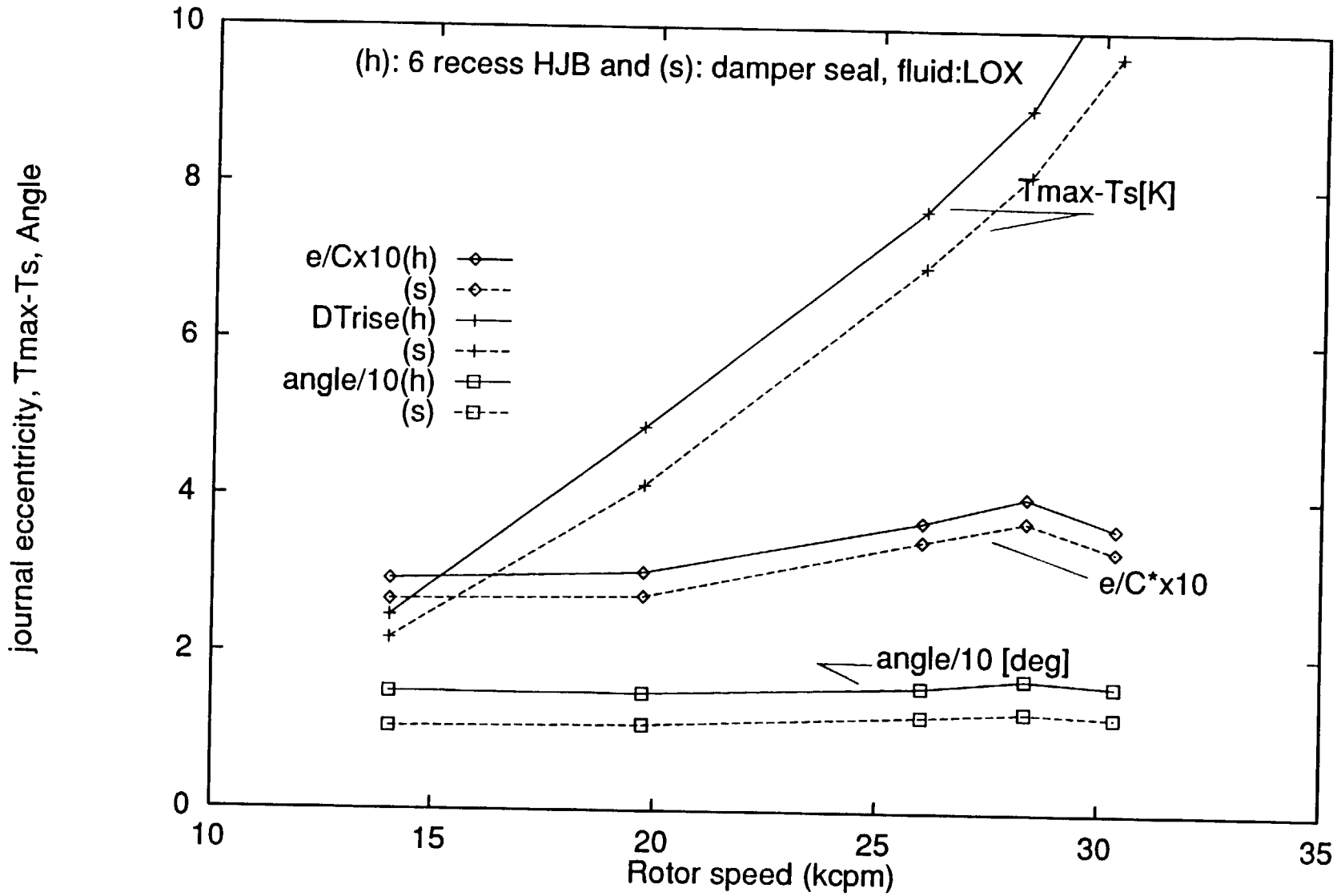

Fig.11. Journal eccentricity and attitude angle and maximum temperature rise vs. rotational speed for LOx (h) 6 recess HJB and (s) parallel damper seal.

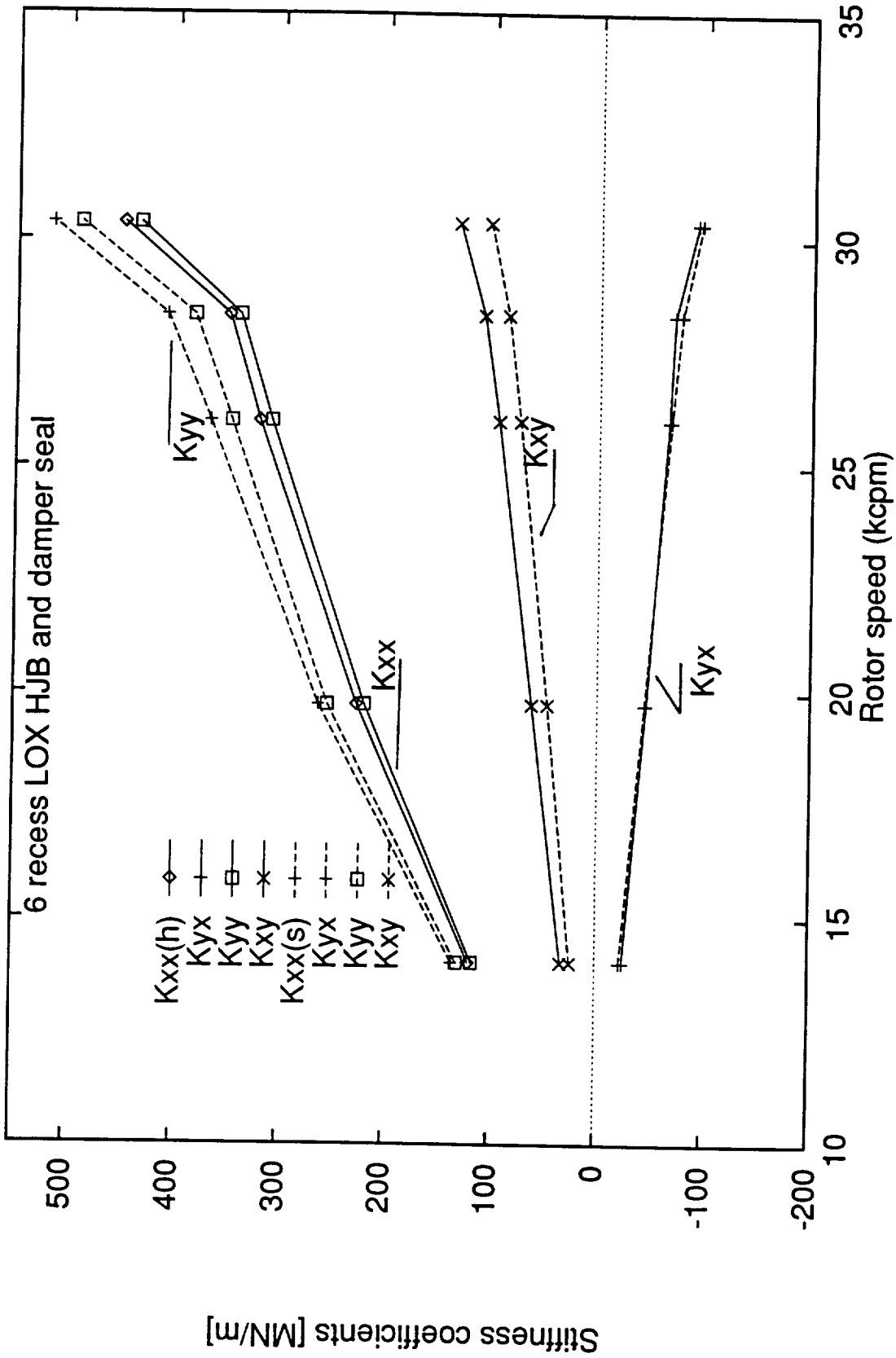

Fig.12. Stiffness Coefficients vs. rotational speed for LOx (h) 6 recess HJB and (s) parallel damper seal.

characteristics than the parallel lands damper seal.

Figure 14 shows the damper seal direct inertia force coefficients (M_{XX} and M_{YY}) to be the on the order of 1.5 kg and large in relationship to the HJB direct inertia coefficients. The reason for this lies on the tapered geometry of the damper bearing seal with a small clearance at the exit plane. The cross-coupled inertia coefficients (M_{XY} and M_{YX}) are small in nature. Here it is noted that in practice the direct inertia coefficients for the damper seal will be much larger than the ones predicted. The central feeding groove will act as a parallel inertia and compliance to the seal lands, it will increase the value of the inertia coefficients, and reduce substantially the direct dynamic stiffness of the damper seal. Experimental results showing this behavior have been given recently by Lindsey (1993).

The example demonstrates that a properly designed HJB or a parallel damper bearing seal can support easily the loads expected in the LO_x HP turbopump. The results show that the HJB and seal will operate at low eccentricity ratios with uniform force coefficients. The case studied shows an important application of the hydrostatic principle where good engineering practice utilizes the available pressure differential in a cryogenic turbopump to provide a reliable fluid film bearing support. It is worth noting that the original test case included a three pad journal bearing with a clearance similar to that of the HJB but with a bearing preload of 0.076 mm. The results are not reproduced here because the journal bearing offered a very low load capacity in comparison with the HJB and damper seal, and it also produced a rather large temperature rise. Details of these calculations can be found elsewhere (San Andres, 1993e).

Adams et al. (1992) presented experimental results for the force coefficients of a four pad, one recess/pad, hydrostatic bearing operating at low speeds and using motor oil SAE 30 at ($T = 38°C$) as the working fluid. Table 2 shows the

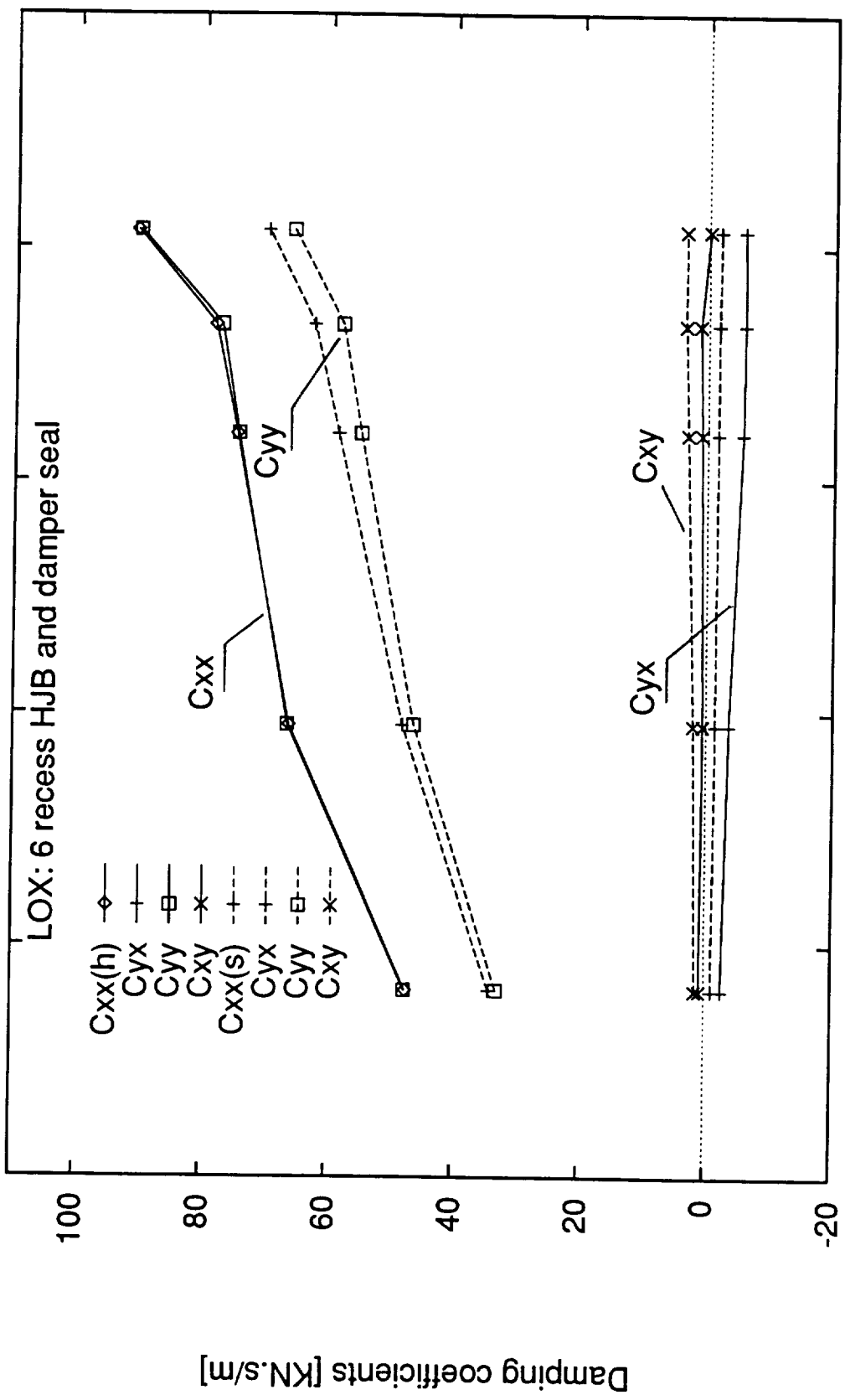

Fig.13. Damping Coefficients vs. rotational speed for LOx (h) 6 recess HJB and (s) parallel damper seal.

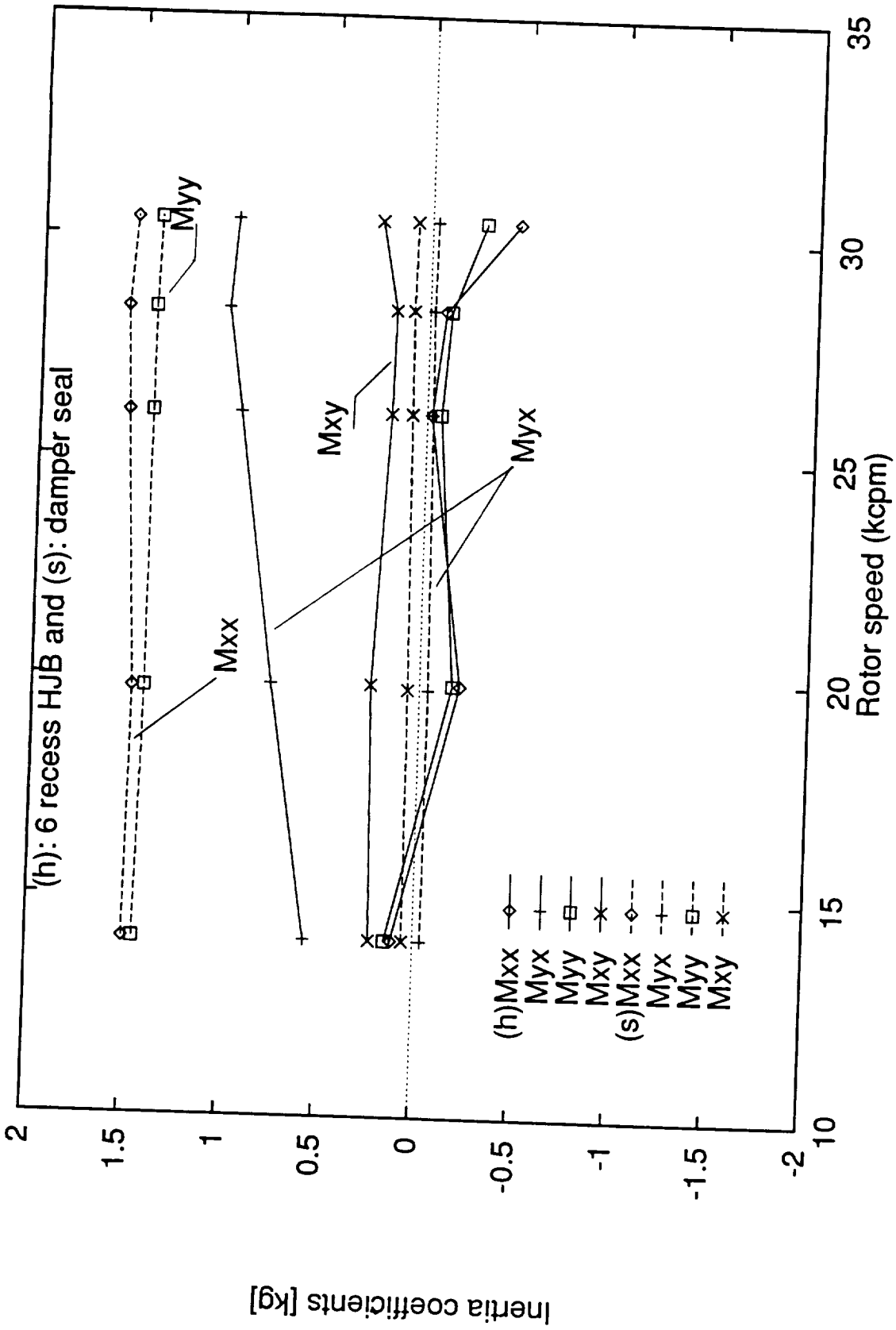

Fig.14. Inertia Coefficients vs. rotational speed for LOx (h) 6 recess HJB and (s) parallel damper seal.

geometry and operating characteristics of the HJB test article with four recesses of large area and depth. The maximum operating speed is equal to 2,000 cpm and the circumferential flow Reynolds number is equal to 23.0. The flow conditions clearly specify a laminar flow regime without significant fluid inertia effects at film lands and recess edge on the forced response of the bearing. Adams et al.'s tests derive from an experimental research program whose results may be used for extrapolation of the dynamic force performance in high-speed, turbulent flow hydrostatic bearings in cryogenic turbopumps. Adams et al. present the force coefficients in graphical form versus the amplitude of a dynamic eccentricity used in the experimental procedure. The numerical predictions are based on the adiabatic thermal model with the journal center operating at the concentric position.

Table 3 presents a comparison between the predicted values and the experimental force coefficients determined by Adams et al. The values for the measurements correspond to average values along with the largest positive and negative deviations from the average number. The numerical predictions show a good agreement with the experimental results although the latter show very wide variations. Very similar numerical results were obtained for a flow model with isothermal characteristics. The hydrostatic bearing of Adams et al. (1992) demonstrates that the bearing flow rate and direct stiffness coefficients are not affected by rotational speed. On the other hand, the cross-coupled stiffness coefficients are directly proportional to journal speed. The results are representative of **laminar** flow hydrostatic bearings and can not be extended to turbulent flow operating conditions. Inertia coefficients are not reported here. Added mass coefficients are difficult to calculate (and measure) accurately for small values of the squeeze film Reynolds number (Re_s). The experimental results for inertia force coefficients

Table 2. Geometry and Operating Conditions of Four Pad Hydrostatic Bearing from Adams et al. (1992).

Number of Pads: **Npad** = 4, Number recesses/pad **Nrec** = 1

Diameter, **D**	Length, **L**	clearance, **C**	length, l	depth, **Hr**
114.7 mm	53.98 mm	210.8μm	35.56 mm	4.763 mm
(4.51 in)	(2.12 in)	(8.3 mils)	(1.40 in)	(0.187 in)

Pads: circumferential length Θ_p=80.50 deg, groove width = 9.50deg.

Recess: circumferential length Θ_r=56.deg.

L/D=0.47, l/**L**=0.659, $\Theta r/\Theta p$=0.696 , **Area Ratio**=0.459, **C/R**=0.0037, **Hr/C**=22.6

journal and bearing surface conditions: smooth.

Orifice C_d=1.00, diameter **do=1.592mm** for concentric recess presure ratio **pr=0.40,**

Recess edge coefficients ξ_{xu}=0.0; ξ_{xd}=0.00; ξ_y=0.0,

Pad leading edge coefficient, κ=0.64

Operating Parameters:

Rotational speed: 1,000 and 2,000 cpm

Pressure supply, Ps=1.206 MPa (175psig), 2.586 MPa (375psig)

exit, Pa= 0.00 MPa (0 psig)

Recess Pressure, Pr=0.483 MPa (70psig), 1.034 MPa (150psig)

Fluid: SAE 30oil at 310K (100F), μ_s=0.09787Pa-s, $\rho s=\rho a$=890.00 Kg/m3

TYP Reynolds numbers:

$Re_{circ}=\rho\Omega Rc/\mu_s$=11.5 (1kcpm) , 23.0 (at 2kcpm)

$Re_{axial}=m/(2\pi D_R\ \mu_a)$=4.03 (Pr=70psig), 8.64 (Pr=150psig) *LAMINAR FLOW*

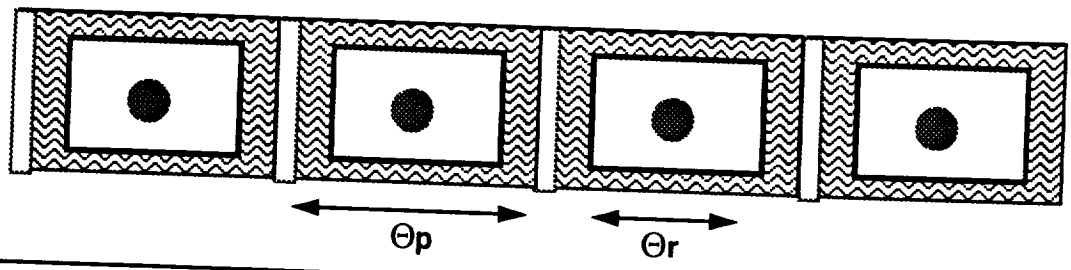

seem to be erroneous with identified magnitudes as large as 100 kg. Figure 15 shows the calculated pressure field at the concentric position for the four pad hydrostatic bearing studied. The figure depicts a pressure field typical of a pure hydrostatic bearing without fluid inertia effects.

Hydrodynamic journal bearings, in particular those of a compliant bearing surface nature, are currently a subject of attention for cryogenic applications (Heshmat, 1991). Experimental results for static and dynamic force performance characteristics in pure hydrodynamic journal bearings with cryogenic liquids have not been reported in the open literature. The interested reader needs to refer to the literature review provided by San Andres (1993f) on the subject of foil bearings.

The present THD model for journal bearings is used to analyze an axially grooved journal bearing as tested by Tonnesen and Hansen (1981). The published experimental measurements are very complete and detailed. This test bearing has then become an ideal example to validate THD models by several researchers (see Knight and Niewiarowski, 1990). Details of the bearing geometry and operating conditions are given in Table 4. The calculations are performed at a journal speed of 3,600 cpm with external loads directed towards the bottom pad and equal to 5,600 N and 8,600 N. The bearing analyzed handles a viscous lubricant and the smallness of the film clearance and rotational speed determine laminar flow conditions. For the calculations the adiabatic flow assumption was used although this is too crude since the measurements definitely show there is heat flow through the bearing surfaces and rotating journal. A groove mixing coefficient (λ) equal to 0.80 was used on the calculations as derived from the experimental results. Numerical predictions for the bearing centerline dimensionless pressure and temperature are shown in Figures 16 and 17, respectively. Table 4 also

Table 3. Performance Characteristics of Four Pad Hydrostatic Bearing at eccentricity ex=0.0. Comparison to test results from Adams et al.(1992)

Speed Kcpm	Precess MPa	Orifice do(mm)	Flow kg/s	Torque N·m	temperature rise(°C)	Reynolds # Min/Max	Squeeze Reynolds Res .
1.0	0.48	1.59	0.285	1.556	1.05	2.66/9.59	0.042
	1.03	1.93	0.616	1.543	4.26		
2.0	0.48		0.285	3.100	1.10	8.32/15.26	0.084
	1.03		0.612	3.102	1.10	5.10/19.51	

Stiifness Coefficients

Speed Kcpm	Precess Mpa	KXX	KYY	KXY	KYX	
			MN/m			
1.0	0.48	26.28	26.28	4.06	−4.07	predicted
		21.17+2.46	22.32+3.28	5.25+1.15	−3.05+1.28	experimental
		−1.97	−1.66	−0.82	−0.88	
	1.03	56.16	56.20	4.94	−4.78	predicted
		44.81+8.86	43.66+5.58	5.91+1.97	−4.27+3.28	experimental
		−5.42	−3.28	−2.95	−2.62	
2.0	0.48	26.00	26.00	8.19	−8.19	predicted
		19.17+1.84	22.76+2.45	7.88+1.57	−7.35+1.57	experimental
		−1.84	−2.80	−1.58	−2.10	
	1.03	55.76	55.76	7.99	−7.98	predicted
		41.50+8.40	45.34+9.28	9.80+3.85	−9.80+4.55	experimental
		−5.25	−5.95	−3.50	−4.90	

Damping Coefficients

Speed Kcpm	Precess Mpa	CXX	CYY	CXY	CYX	
			KNs/m			
1.0	0.48	78.08	79.07	0.30	−0.29	predicted
		65.65+10.10	70.70+10.00	2.81+12.3	−4.33+4.32	experimental
		−5.06	−10.10	−9.54	−8.65	
	1.03	77.76	78.00	−6.47	5.98	predicted
		48.91+24.25	64.74+31.00	−67.7+37.4	−30.25+20.80	experimental
		−27.03	−15.50	−48.0	−82.30	
2.0	0.48	78.38	78.37	0.41	−0.40	predicted
		76.30+6.63	75.62+25.85	13.78+10.54	−0.21+6.29	experimental
		−5.30	−15.92	−13.79	−3.43	
	1.03	78.14	78.12	0.58	−0.58	predicted
		67.34+1.68	87.54+53.90	−10.10+33.7	20.2+10.1	experimental
		−3.37	−30.30	−20.2	−3.36	

Experimental values obtained from graphical values shown by Adams et al. (1992).
Values refer to average quantities with maximum and minimum deviations from average.

Npads=4 1 recess/pad, L=114.71mm, D=53.97mm, l=35.56mm, θ_r R=56.134mm, c=210.8mm, H_r/c=22.5, groove width=9.525mm, recess Area ratio=0.4590

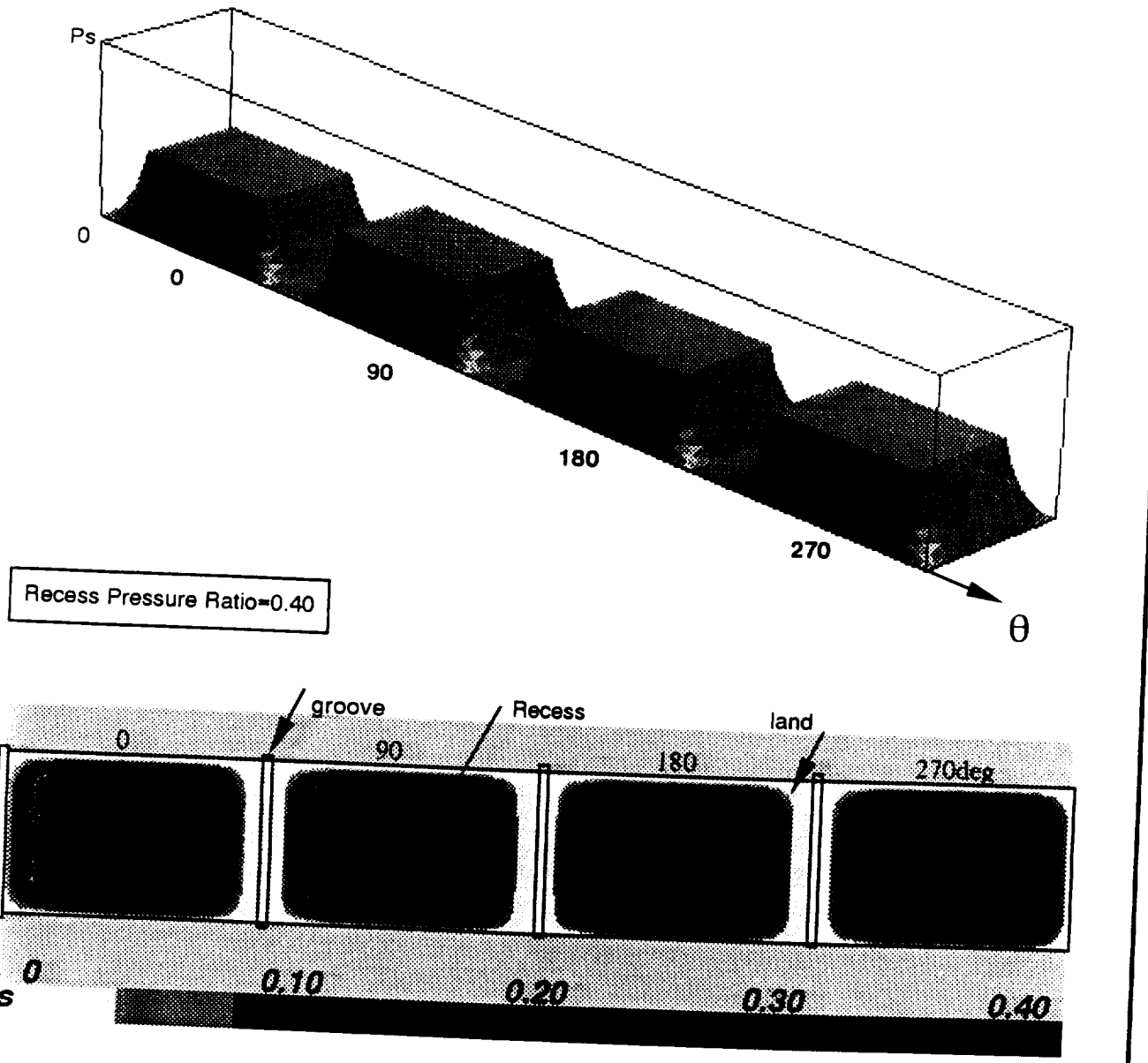

Ps=1.206MPa(175psig), PR=0.482MPa(70psig), 1000 rpm, fluid: oil SAE 30 , 37.5C (100F), μ=0.097Pa-s, ρ=890kg/m3

Re_c=11.50, Re_{max}=13.37, Q=0.286 kg/s, do=1.59mm, Cd=1.0

Figure 15. *Pressure Field in a 4 recess Hydrostatic Pad Bearing Concentric Position. Adams et al. (1992) bearing*

includes a comparison of the predicted values from the present adiabatic THD model with the experimental measurements. The pressure plot shows the top pad to be unloaded and the bottom pad carrying the applied load with a small fluid cavitation zone close to its trailing edge. The temperature plot shows the lubricant temperature to increase steadily on the loaded pad and then remaining uniform once fluid cavitation starts. The temperature remains uniform and larger than the groove supply temperature on the unloaded pad. The numerical predictions are very similar to those provided by the more advanced models of Lund and Tonnesen (1984) and Knight and Niewiarowski (1990). The correlation of present predictions with the experimental values is considered surprisingly good considering the crudness of the cavitation model used and the oversimplification in the thermal analysis. Dynamic for coefficients were not determined in the experimental work and also not reported here for brevity. However, the force coefficients for the case studied can be found elsewhere (San Andres, 1993e).

The last two examples have discussed predictions relevant to a laminar flow hydrostatic bearing and a laminar flow two–pad journal bearing, respectively. The present numerical model is able to predict with accuracy the experimental results for these laminar flow bearings. The examples demonstrate the generality of the analysis and also validate the computational model for applications to conventional (traditional) lubrication problems.

Braun et al. (1987b) introduced a comprehensive THD analysis for cryogenic liquid hydrodynamic journal bearings. A variable–properties Reynolds equation was coupled to a 2-D energy transport equation on the fluid film region. The heat transfer to the bounding solids (shaft and bush) was analyzed in its three dimensional complexity. Bulk-flow heat transfer coefficients were used to represent the boundary conditions at the fluid/solid interfaces. Braun et al.'s analysis

Table 4. Geometry and operating characteristics of axially grooved journal bearing from Tonnesen and Hansen (1981).

2 pad journal bearing:.

Diameter (D)	Length (L)	Clearance (C*)	Pad Arc	Groove width
100 mm (3.93 in)	55 mm (2.16 in)	69.0 μm (2.71 mils)	170 deg	10 deg

journal and bearing surface conditions: smooth.; **L/D**=0.55; **C/R**=0.0014

Thermal mixing groove coefficient λ= 0.80

Fluid: **oil** at inlet temperature 50 C (122 F) and Psupply=0.14MPa (20.3psig)

T (C)	ρ (kg/m3)	μ (Pa.s)	Cp(J/kg-K)
50	850	0.0182	2,000
90	850	0.0056	2,000

Operating Condition: journal speed 3,500 cpm

Load = 5,600 N

Case	e/c	Min T (C)	Max T (C)	Max P (MPa)	Pad
THD soln.	0.53	63.22	64.50	0.14	# 1 cavitated
		55.60	72.23	2.58	# 2 loaded
experimental	0.56	58.00	62.00	0.14	
		57.50	72.00	2.60	

Load = 8,600 N

Case	e/c	Min T (C)	Max T (C)	Max P (MPa)	Pad
THD soln.	0.63	63.10	64.70	0.14	# 1 cavitated
		55.50	75.10	4.31	# 2 loaded
experimental	0.66	58.00	not given	0.14	
		57.50	74.00	5.10	
				4.30	predicted by Lund & Tonnesen (1984)

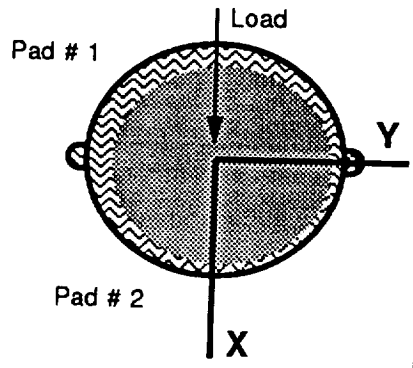

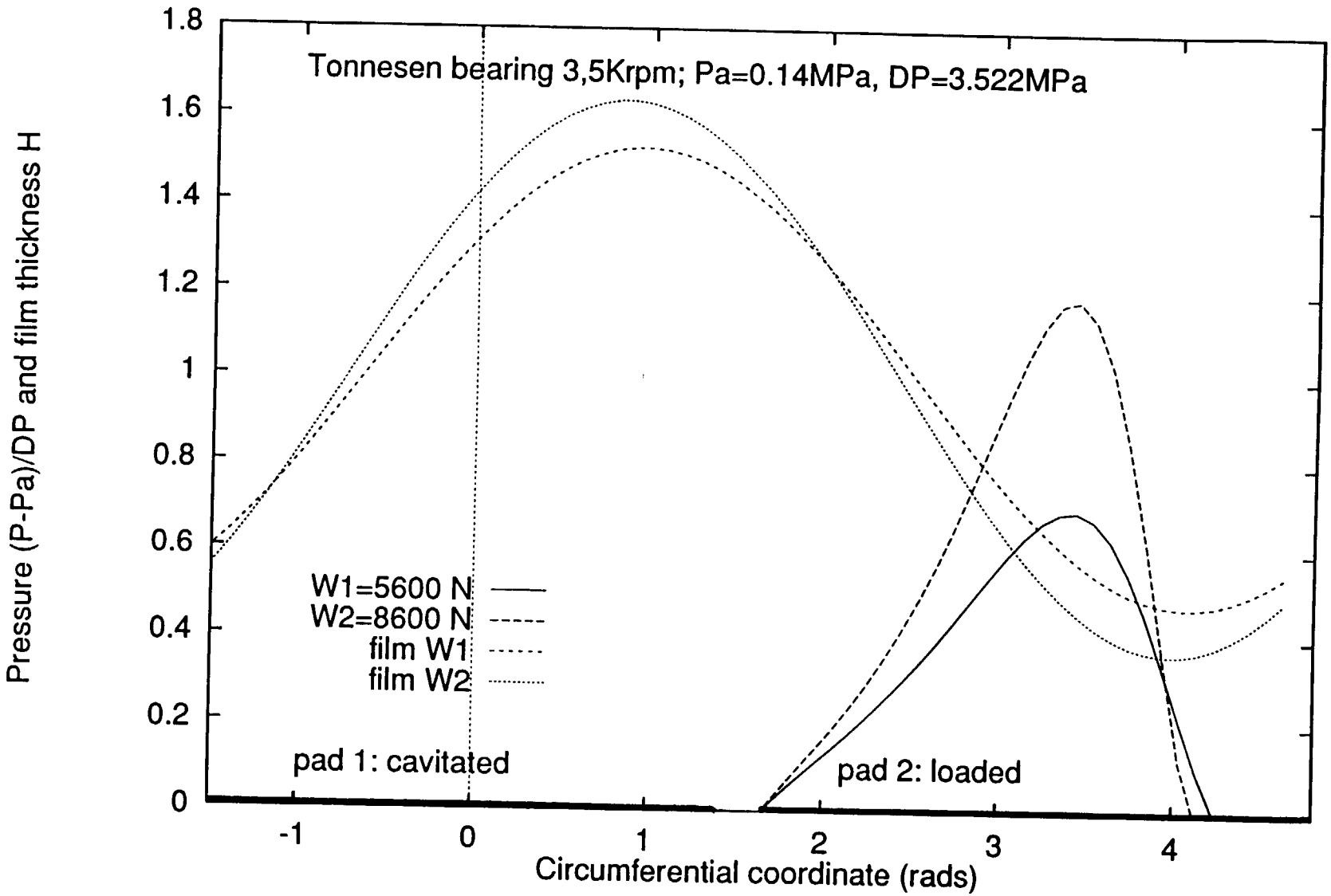

Fig.16. Centerline pressure for axially grooved journal bearing.
Bearing parameters as per Tonnesen et al. (1981). Loads 5.6 and 8.6 KN.

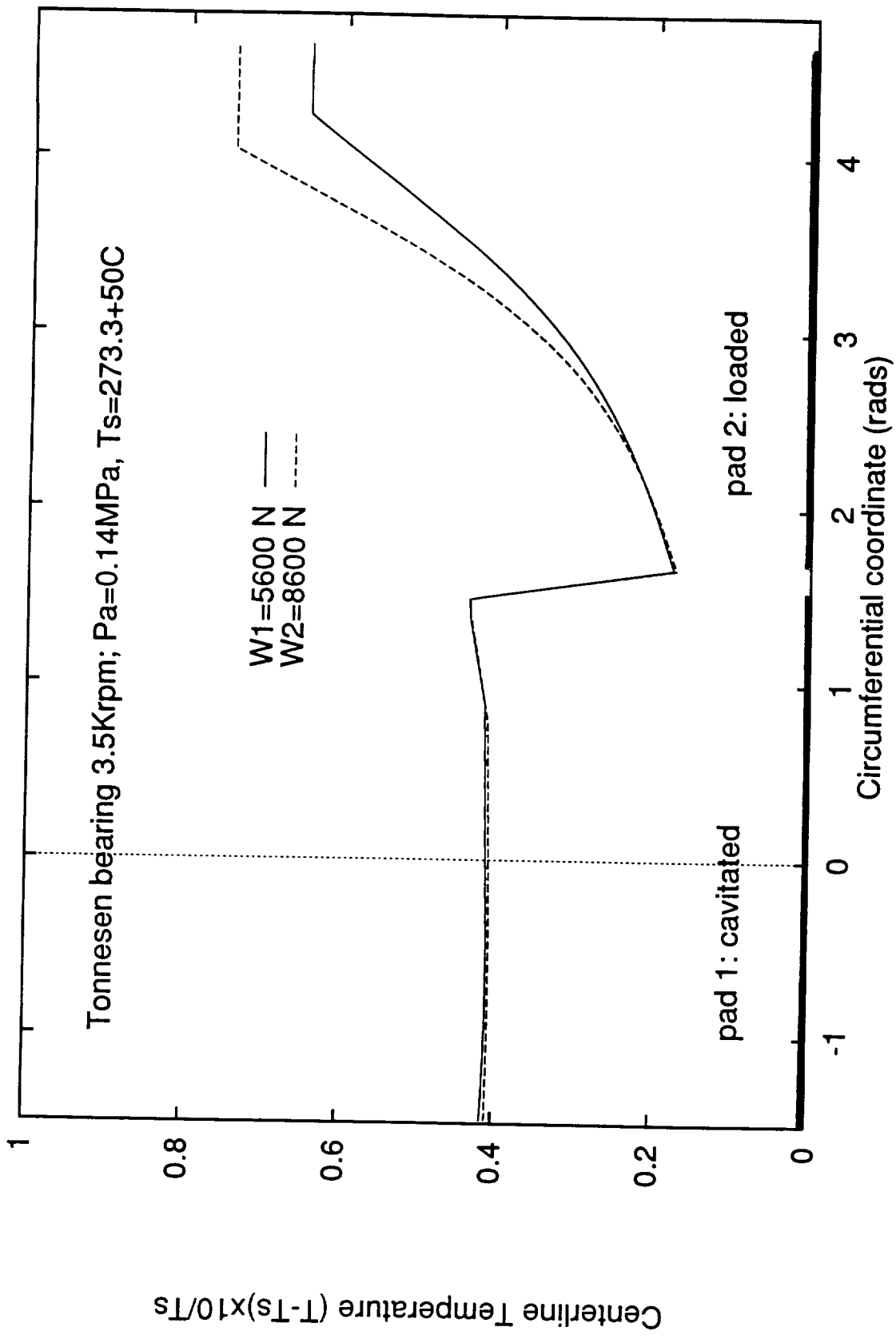

Fig.17. Centerline temperature for axially grooved journal bearing. Bearing parameters as per Tonnesen et al. (1981). Loads 5.6 and 8.6 KN.

regards the fluid flow as **laminar**, although large journal rotational speeds were considered in the application studied. The bearing geometry and operating conditions for the bearing studied by Braun et al. are given in Table 5. The journal bearing has a very small clearance equal to 0.0254 mm (0.001 in). At the rotational speed of 14,000 cpm the circumferential flow Reynolds number is Re_c = 12,027 with fluid properties evaluated at a supply pressure and temperature equal to 1.72 Mpa (250 psi) and 111°K (200°R), respectively.

The results presented by Braun et al. are most peculiar since they show a temperature field (Fig. 5 of cited reference) which is a maximum at the bearing center line and **decreasing** towards the axial discharge planes. Also the temperature field does not show a zero temperature gradient at the bearing centerplane as theory requires. Another shortcoming for the referred THD analysis is related to the adiabatic (journal and bearing) model used for a full 360° journal bearing as the calculations suggest. In a continous journal bearing without any feeding grooves, the adiabatic model is physically incorrect since, as the flow equations also show, the fluid at the bearing circumferential middle plane is "trapped" because the axial pressure gradient is null at this location. For this flow condition, a fluid particle at the midplane rotates ad-infinitum around the bearing and its temperature should increase without bound. These statements are by no means trivial since they were discovered (and thought over) after a long and tedious unsuccesful attempt to reproduce the results given in the cited reference.

For the calculations presented here it was decided to keep the adiabatic model (insulated journal and bearing surfaces) but to have the journal bearing with a feeding groove of arc length 10° at an angular location equal to 70° as shown on Table 5. The thermal mixing groove coefficient (λ) used in the calculations is equal to zero, i.e. only fresh fluid at the supply temperature enters the bearing

Table 5. Geometry and operating characteristics of a hydrodynamic journal bearing operating with liquid oxygen. Data from an application presented by Braun et al. (1987b)

journal bearing with feeding groove:.

Diameter (D)	Length (L)	Clearance (C)	Pad Arc	Groove width
76.2 mm (3.0 in)	76.2 mm (3.0 in)	25.4 μm (1.0 mil)	350 deg	10 deg at θ=70 deg

journal and bearing surface conditions: smooth.; **L/D**=1.0; **C/R**=0.00067

Thermal mixing groove coefficient λ= 0.00

Fluid: **LO2** (liquid oxygen)

T (K)	P (MPa)	ρ (kg/m3)	μ (E−6 Pa.s)	Cp(J/kg−K)	
111.1 (200 R)	1.723 (250 psia)	1,033	121.9	1,836.8	at supply (inlet) conditions

LO2 critical temperature and pressure: 154.8 K (278.6 R), 5.083 MPa (737.4 psia)

Operating Condition: journal speed 6,000 and 14,000 cpm. Load varies

Nominal circumferential flow Reynolds # (**Rec**) = *12,027* at 14 kcpm

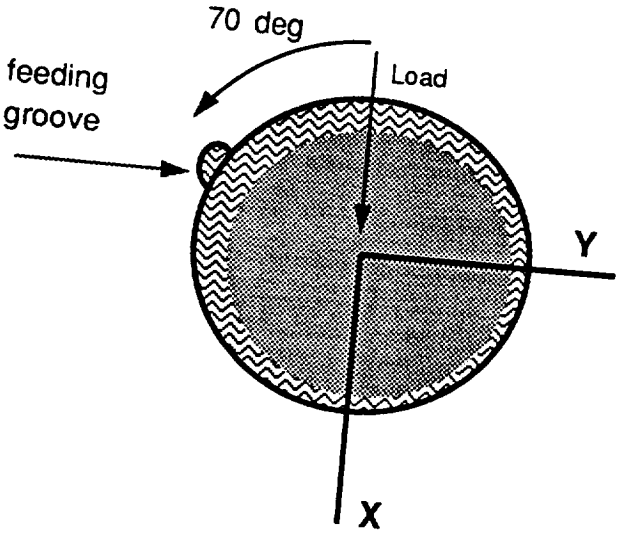

downstream of the feeding groove. The value used is rather conservative but highly recommended as it would become evident latter. Preliminary calculations with the *hydrosealt* program showed that the temperature within the fluid film region increased rapidly and this caused the saturation pressure of the liquid to drop sharply. For example, at a temperature of $111°K$ the liquid saturation pressure is equal to 0.582 MPa and much lower than the feeding groove pressure (1.723 MPa). However, at a film temperature of $126°K$ the saturation pressure is only 1.425 MPa and very close to the feeding pressure. It is well known that journal bearings are able to produce hydrodynamic pressures above (positive) and below (negative) the reference supply value. Liquid flashing (dispersion into a gaseous phase) is caused since these "negative" pressures can not be lower than the liquid saturation pressure. Here we will refer to this phenomena as some sort of cavitation since the computer model is unable to distinguish between liquid boiling (two-phase flow) and actual liquid cavitation. For the 14,000 cpm example, the cavitation pressure is set equal to the supply pressure (1.72 MPa) in the results that follow. On the other hand, for 6,000 cpm operation, the cavitation pressure is equal to 1.0 Mpa.

Table 6 provides a summary of the results calculated with the present analysis. Two models are considered (a) adiabatic journal and bearing surfaces, and (b) isothermal bearing without thermal effects. The calculations are performed for two loads equal to 2.5 KN and 5.0 KN. Figure 18 shows the centerline pressure field and temperature for the two loads considered. The pressure and temperature fields are symmetric about the bearing midplane with the temperature field varying very little in the axial direction. At the largest load considered (5.0 KN), the maximum temperature predicted within the fluid film is equal to $127.5°K$, i.e. $16.4°K$ above the supply value, and the operating journal eccentricity and attitude angle are equal to 0.371 and 77.2°, respectively. On the other hand, the results of Braun

Table 6. LOx hydrodynamic journal bearing. Comparison of results for two applied loads. Adiabatic and Isothermal models and calculations from Braun et al. (1987b).

Cases

B Predictions from Braun et al. (1987b), (*) denotes no values available
A Present model : adiabatic journal and bearing surfaces with variable fluid properties
I isothermal conditions with variable fluid properties
N artificial setting of laminar flow and no fluid inertia

Journal Speed: 14,000 cpm

Load N	Case	e/c	ϕ (°)	Torque N·m	Max P MPa	Max T °K	Reynolds # max / min
2,500	A	0.191	90.0	1.80	2.52	126.6	9,050 6,013
	I	0.213	86.2	2.03	2.55	111.1	7,290 4,733
5,000	A	0.371	77.2	1.84	3.44	127.5	10,613 4,919
	I	0.381	77.0	2.08	3.48	111.1	8,298 3,723
5,102	B	0.700	66.1	*	*	115.7	*

Load N	Case	Kxx	Kyx	Kyy	Kxy	Cxx	Cyx	Cyy	Cxy
		MN/m				KN/s			
2,500	A	50.1	−431.1	98.0	465.8	604.0	−32.9	625.2	205.6
	I	25.8	−401.8	109.5	504.7	658.1	5.0	587.2	255.5
5,000	A	158.9	−416.4	266.6	634.7	777.0	96.9	689.9	372.0
	I	156.8	−354.0	256.4	674.4	843.5	108.4	598.3	391.0
5,102	B	22.9	−255.1	533.6	522.8	*			

Load(N)	Case	Mxx	Myx	Mxy	Myy (kg)
2,500	A	58.1	−4.0	59.0	8.6
	I	59.5	0.9	48.6	4.1
5,000	A	59.0	−2.8	53.9	13.4
	I	60.3	0.2	40.3	3.4

Journal Speed: 6,000 cpm

Load N	Case	e/c	ϕ (°)	Torque N·m	Max P MPa	Max T °K	Reynolds # max / min
2,300	A	0.423	94.2	0.47	2.20	119.0	3,959 1,607
2,292	B	0.700	90.0	*	*	112.0	*

Load N	Case	Kxx	Kyx	Kyy	Kxy	Cxx	Cyx	Cyy	Cxy
		MN/m				KN/s			
2,300	A	9.3	−194.5	4.55	283.6	710.9	−106.6	878.3	33.4
2,292	B	0.0	−128.9	0.00	323.4	*			
	N	6.9	−134.9	8.40	329.6	436.4	50.4	1382.0	74.8

et al. analysis show an operating journal ecentricity equal to 0.7 and an attitude angle equal to 66.06 ° with a maximum film temperature equal to 115.8°K. The differences noted between the two THD analyses are easily explained since Braun et al's model considers the flow as laminar without fluid inertia effects. Dynamic force coefficients are given in Table 6, while Braun et al. only report values for the stiffness coefficients. It is also worth noticing that the results from the adiabatic and isothermal models are very similar although the thermal field is quite different for both models. A groove mixing coefficient (λ) larger than zero will cause the temperature rise in the fluid film region to be larger than the ones presented.

Results for operation at a journal speed equal to 6,000 cpm and a load equal to 2,300 N are also shown in Table 6. The maximum temperature predicted by the present adiabatic model within the fluid film is equal to 119°K, i.e. 7.9°K above the supply value, and the operating journal eccentricity ratio and attitude angle are equal to 0.423 and 94.2°, respectively. The bearing shows no cavitation and the attitude angle is larger than 90° due to the effect of fluid inertia. On the other hand, Braun et al. results present an operating journal ecentricity equal to 0.70 and an attitude angle equal to 90° with a maximum film temperature equal to 112°K for a load equal to 2,292 N. Again, the difference in results is explained by the absence of fluid inertia and turbulence flow effects in the cited reference of Braun et al. It is also noted that calculations were also performed for a journal bearing with laminar flow conditions by artificially reducing the density of the liquid. In this case, the numerical results render a load of 2,600 N at an eccentricity ratio equal to 0.70 with stiffness coefficients very similar to those reported by Braun et al. (Table 2, 1987b).

The last example presented refers to a three–pad journal bearing operating with liquid oxygen. The geometry and operating characteristics for the rigid

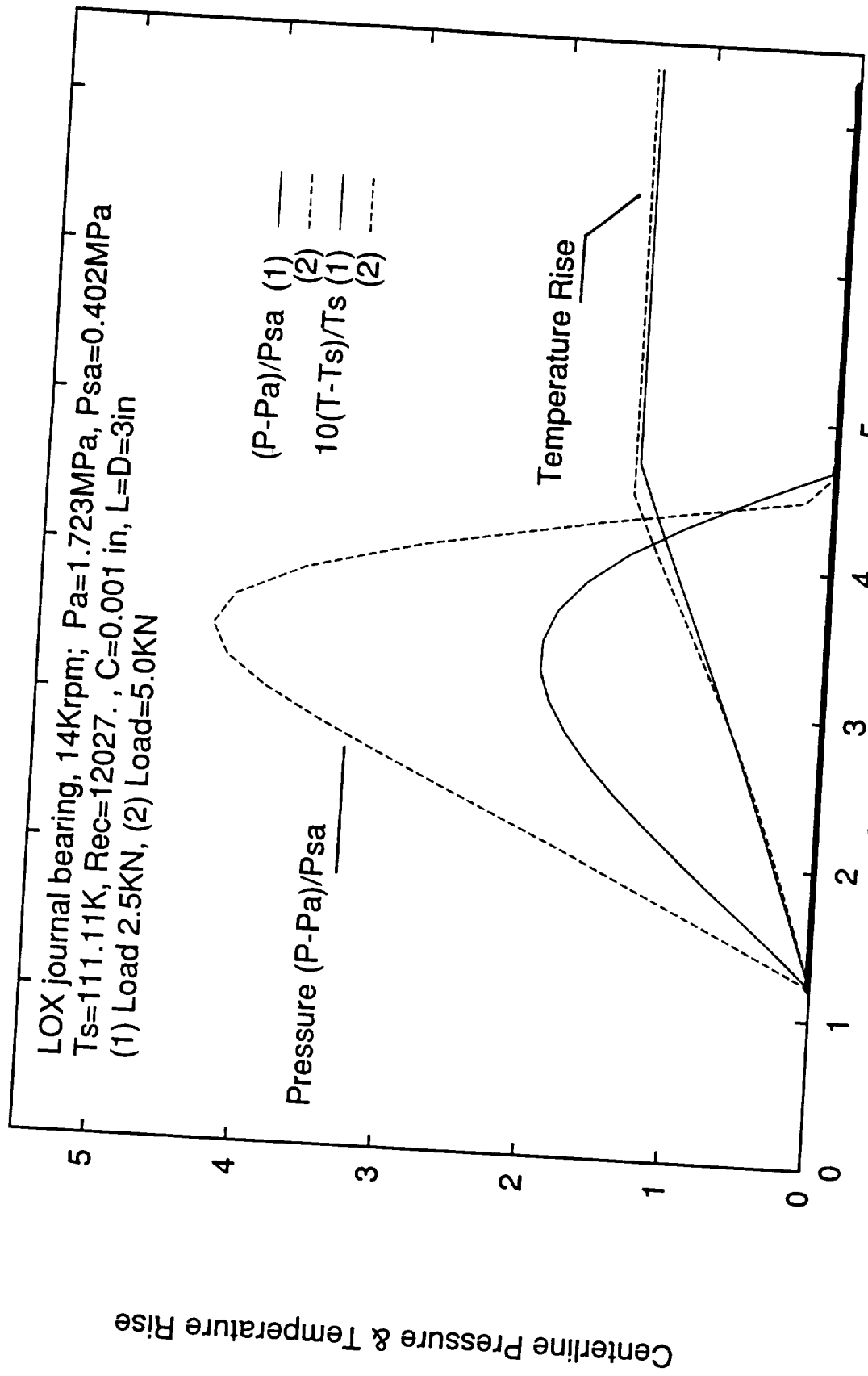

Fig.18. Centerline pressure and temperature for LOX journal bearing. Bearing parameters as per Braun et al. (1987a). Adiabatic THD model. Loads (1) 2.5 KN and (2) 5.0 KN along X direction.

pads bearing are given in Table 7. The data has been taken directly from Heshmat (1991). The example discusses the bearing load performance at a journal speed of 29,830 cpm for two different THD models, namely (a) adiabatic or insulated journal and bearing surfaces, and (b) isothermal bearing surface at the supply temperature and adiabatic journal. The bearing clearance is rather small (C=0.0381 mm) in order for the bearing to provide a substantial load capacity. Note that externally pressurized bearings such as HJBs or damper seals do not present this restriction. The largest load of 10,000 N determines a specific load in the bearing equal to 2.52 MPa (367 psi). The hydrodynamic 3–pad bearing test case intends to provide some benchmark data for comparisons with numerical predictions obtained for a bump-type foil bearing. Details on the static and dynamic force performance characteristics of the compliant surface bearing are given by San Andres (1993f).

A thermal mixing groove coefficient (λ) equal to zero is taken for all calculations. This value is very conservative but required to keep the fluid temperature within tolerable limits for the present application. In the numerical computations the fluid is not allowed to sustain subambient pressures, i.e. the mimimum pressures are equal to the supply groove pressure of 5.52 MPa (800 psi). This assumption is physically correct if the bearing pads are of a compliant nature. Note that the nominal value of the circumferential flow Reynolds number (Re_c) is equal to 32,216.

Figure 19 shows the bearing equilibrium journal eccentricity ratio and attitude angle as the bearing load increases from zero to a maximum value of 10,000 N (2,250 lbs). For small loads the attitude angle is larger than 90° denoting the effect of fluid inertia. The adiabatic bearing model shows a slightly smaller operating eccentricity and larger attitude angle than the isothermal bearing model.

Table 7. Liquid Oxygen, three pad hydrodynamic journal bearing. Geometry and operating conditions. Data from Heshmat (1991).

Number of bearing pads: 3

Diameter (D)	Length (L)	Clearance (C*)	Pad Arc	Groove width
88.9 mm (3.50 in)	44.45 mm (1.75 in)	38.1 μm (1.50 mils)	110 deg	10 deg

journal and bearing surfaces: smooth.; **L/D**=0.50; **C/R**=0.00086

Thermal mixing groove coefficient λ= 0.0

Fluid: LO_2 (liquid oxygen)

Ts (K)	P (MPa)	ρ (kg/m3)	μ (E−6 Pa.s)	Cp(J/kg−K)	
95 (171 R)	5.52 (800psia)	1,129.6	183.2	1,718.4	at supply (inlet) conditions

LO_2 critical temperature and pressure: 154.8 K (278.6 R), 5.083 MPa (737.4 psia)

Operating Condition: journal speed 29,830 cpm.
Load varies from 0 to 10,000 N (2,245 lbs)
Nominal circumferential flow Reynolds # (**Rec**) = *32,616*

Cases : **(A)** adiabatic journal and adiabatic bearing.
(I) adiabatic journal and isothermal bearing at Ts

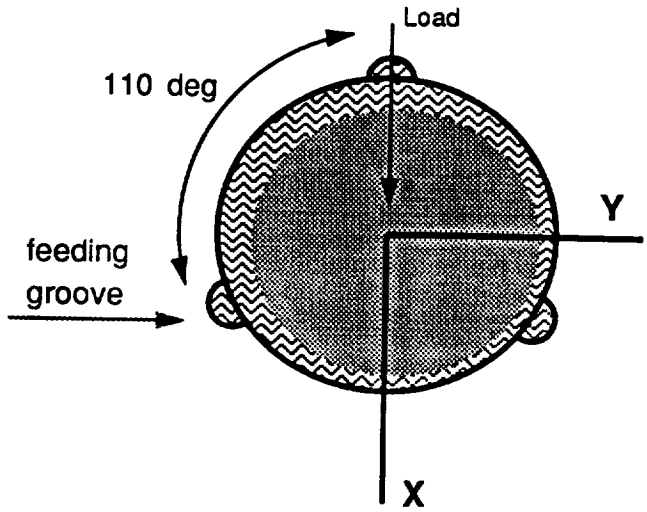

The journal eccentricity increases rapidly in a non-linear form with the applied load. Figure 20 depicts the centerline dimensionless pressure field and temperature rise for a bearing load equal to 7,000 N. Note that the pressure field is almost identical for both bearing models while the temperature curves show a different character. The results show the third bearing pad to be fully unloaded. Figure 21 presents the maximum temperature rise for both bearing models. The adiabatic model shows a dramatic increase in the bearing exit temperature even for the unloaded condition. The maximum temperature rise is over $50°K$ $(90°R)$ at the largest load. On the other hand, the isothermal bearing model offers a very moderate temperature rise which remains almost invariant for all loads applied. In the isothermal bearing case the pad surface acts as a sink for thermal energy and prevents the excessive rise of temperature within the film lands (see Figure 20).

Figure 22 shows the maximum pressure developed on the bearing and the drag torque as the bearing load increases. The peak pressure is proportional to the applied load, and with the isothermal model showing a larger pressure at the largest load. The drag torque is lower for the adiabatic model bearing since the larger film temperaturs reduce the liquid viscosity. On the other hand, this reduction in fluid viscosity due to temperature also causes an increment in the flow Reynolds number and enhances the turbulence flow effects. This may explain why the adiabatic bearing model produces a smaller bearing eccentricity than the isothermal model. Note that the present THD model assumes the bearing clearance not to be affected by thermal phenomena. This seems to be a rather poor consideration if the fluid temperature is to rise substantially.

Figures 23 to 25 present the synchronous stiffness (K_{ij}), damping (C_{ij}) and inertia (M_{ij}) force coefficients versus the applied load for the high speed

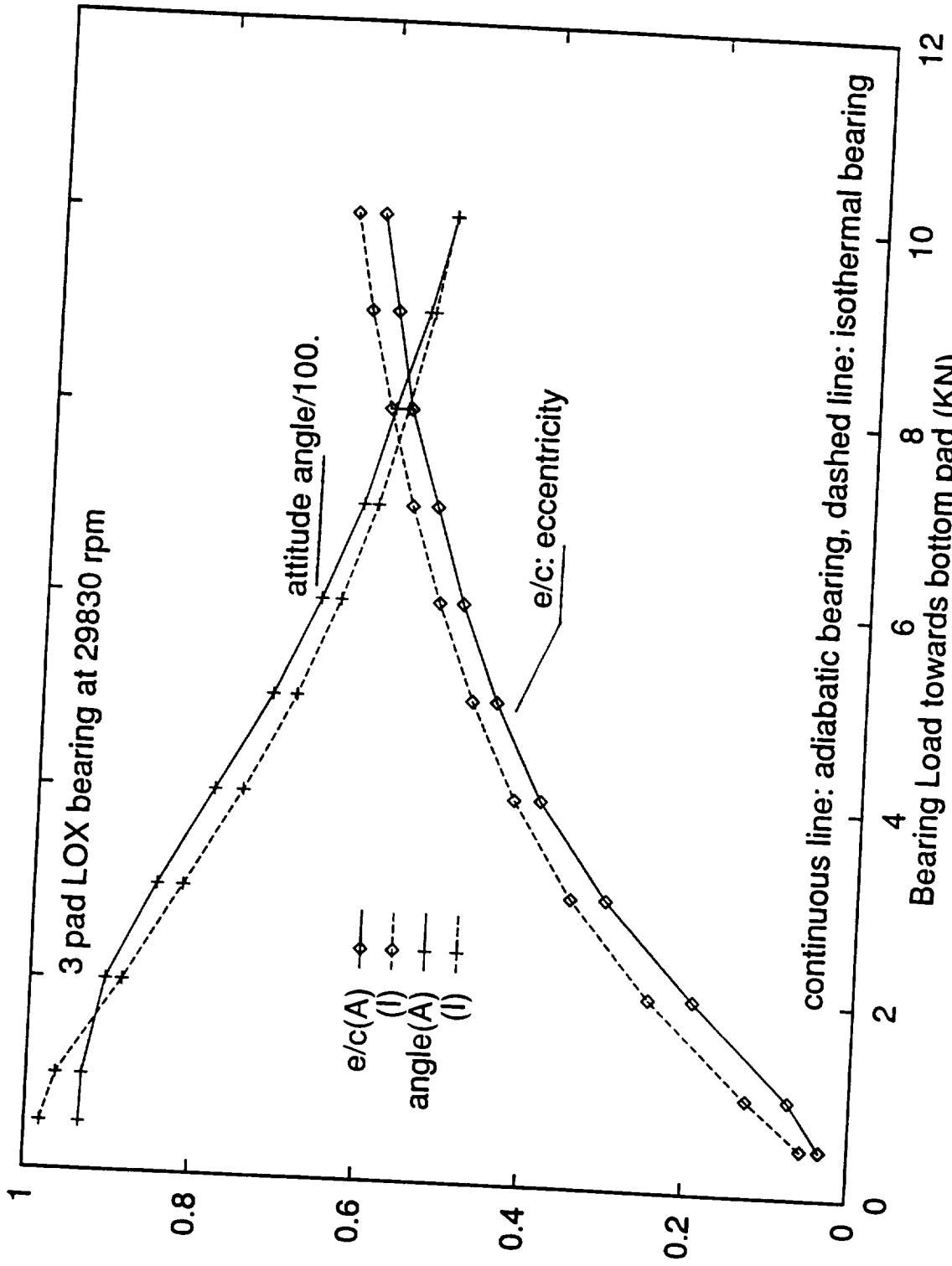

Fig 19. Equilibrium eccentricity and attitude angle vs. applied load for LOX 3-pad bearing. Journal speed 29,830 cpm. (A) adiabatic bearing, (I) isothermal bearing

C-2

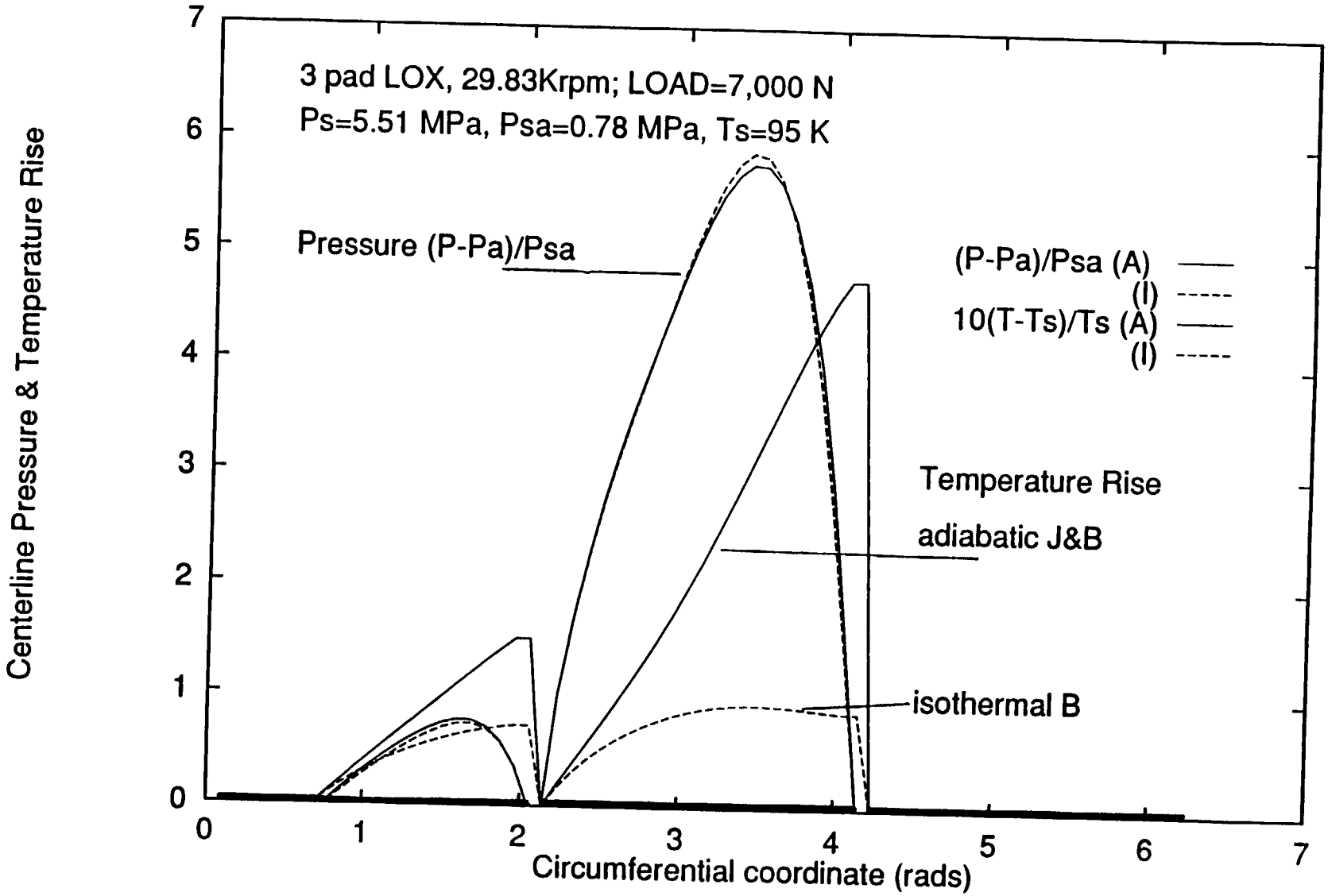

Fig 20. Centerline dimensionless pressure field and Temperature rise for LOX 3–pad bearing. Journal speed 29,830 cpm. (A) adiabatic bearing, (I) isothermal bearing

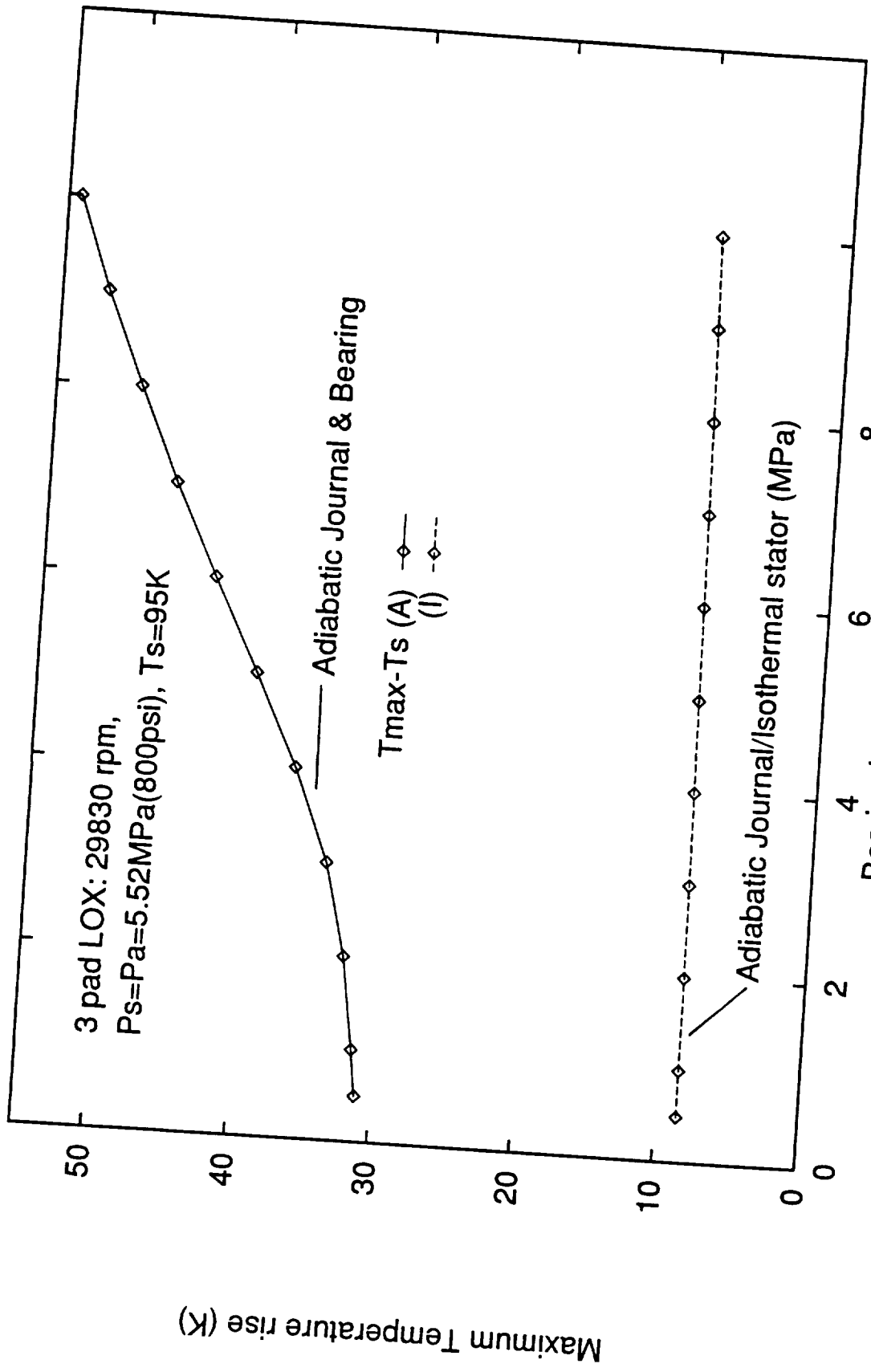

Fig 21. Maximum Temperature rise vs. applied load for LOX 3-pad bearing. Journal speed 29,830 cpm. (A) adiabatic bearing, (I) isothermal bearing

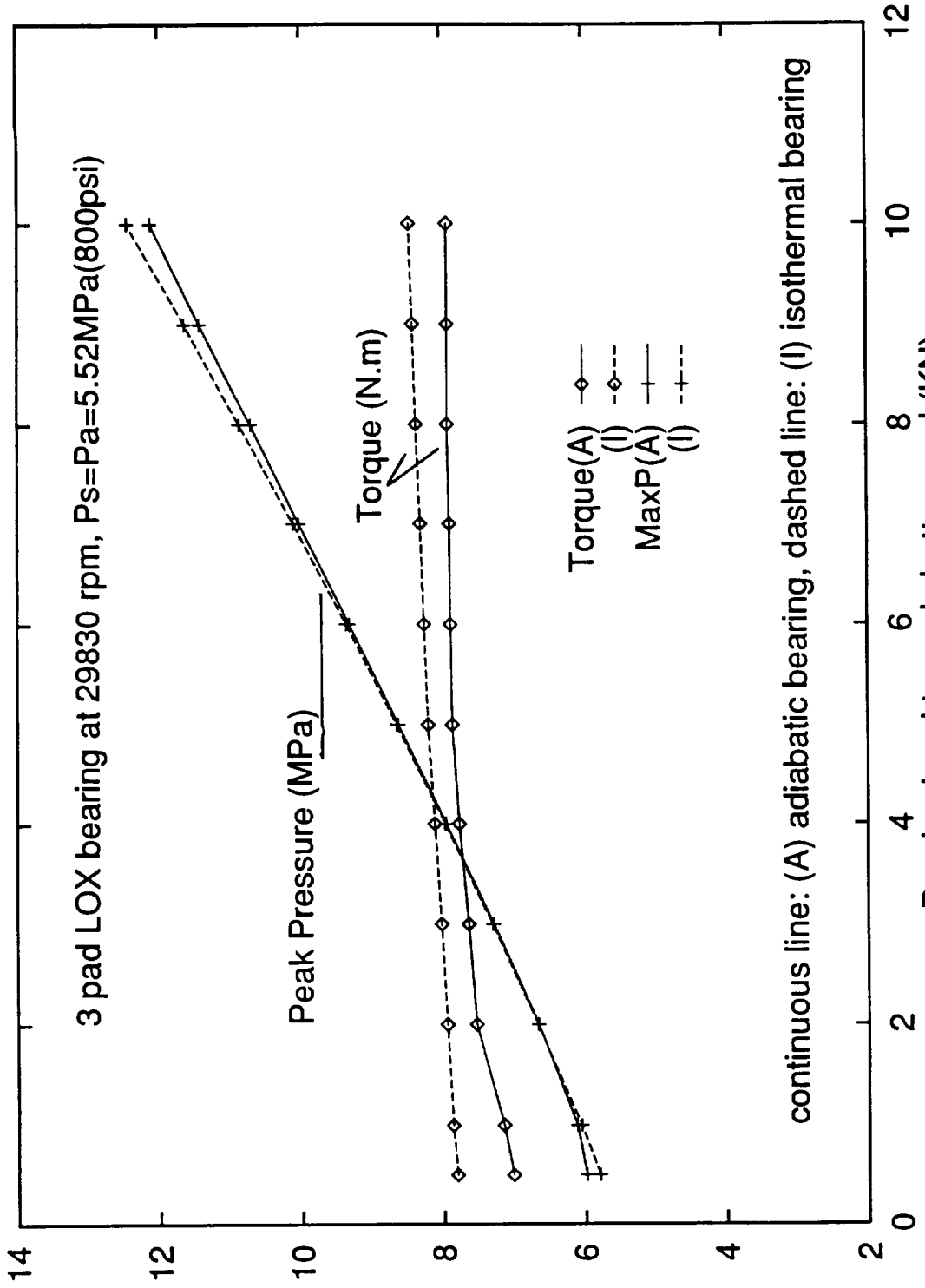

Fig 22. Bearing torque and maximum pressure vs. applied load for LOX 3-pad bearing. Journal speed 29,830 cpm. (A) adiabatic bearing, (I) isothermal bearing

three–pad LO_z hydrodynamic bearing. For low loads the force coefficients are very similar for both the adiabatic and isothermal bearing models. As the load increases (and so does the equilibrium journal eccentricity) the force coefficients show some differences. Most notably, the cross-coupled stiffness (K_{XY}) and direct stifness (K_{YY}) coefficients normal to the applied load are larger for the isothermal model. On the other hand, the direct damping coefficient (C_{XX}) for the adiabatic model is substantially smaller than that obtained from the isothermal model. The direct inertia force coefficients are large in magnitude due to the smallness of the clearance in the bearing.

Although the stiffness and damping force coefficients show very large magnitudes (for a liquid cryogen bearing) their impact on the bearing stability can only be determined by the study of the whirl frequency ratio (WFR) and the equivalent stiffness (K_{eq}). Figure 26 shows the WFR for the bearing to be equal to 0.50 for small loads and decreasing as the load increases. At the largest load, the adiabatic model offers better stability characteristics (lower WFR) than the isothermal model. Figure 27 shows the equivalent bearing stiffness (K_{eq}) as the bearing load increases. This (K_{eq}) is the stiffness of the bearing for a rigid rotor supported on fluid film bearings that will result in a system natural frequency equal to the operating speed times the WFR and with a threshold speed of instability equal to the operating journal speed (i.e. 29,830 cpm). For small loads K_{eq} is rather low and requires that the critical mass of the rotor-bearing system be also small. For example, for K_{eq}=121 MN/m and WFR=0.463 (at a load of 4 KN), the natural frequency of the system is equal to 1,446 rad/sec and the critical mass would be only 57.8 kg. On the other hand, at a load of 10 KN, K_{eq}=313.8 MN/m and WFR=0.304, the critical mass of the system would be rised to 348 kg. From Figure 26 and 27 it is inferred that although the isothermal bearing model

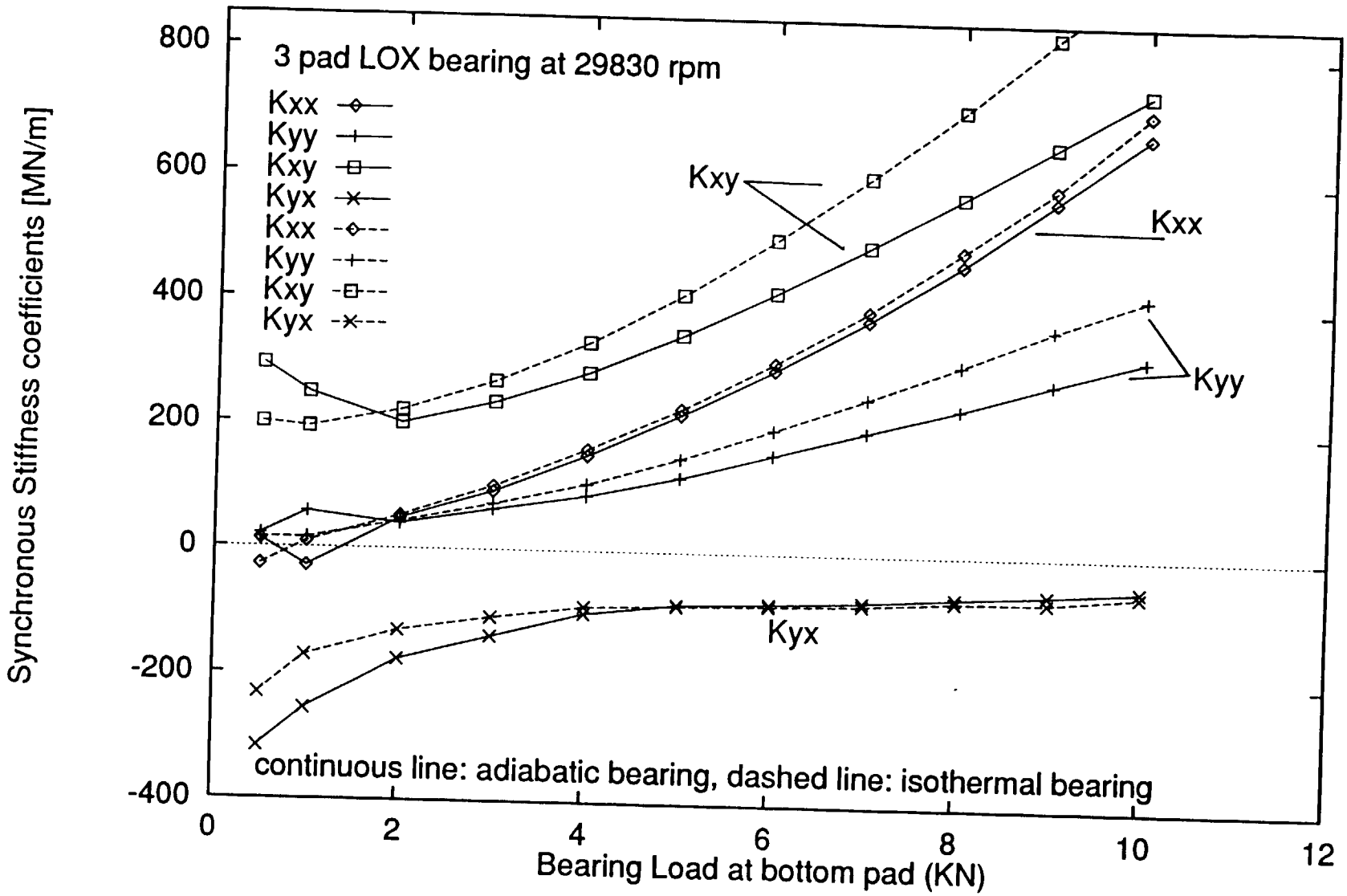

Fig 23. Synchronous stiffness coefficients vs. applied load for LOX 3-pad bearing. Journal speed 29,830 cpm. (A) adiabatic bearing, (I) isothermal bearing

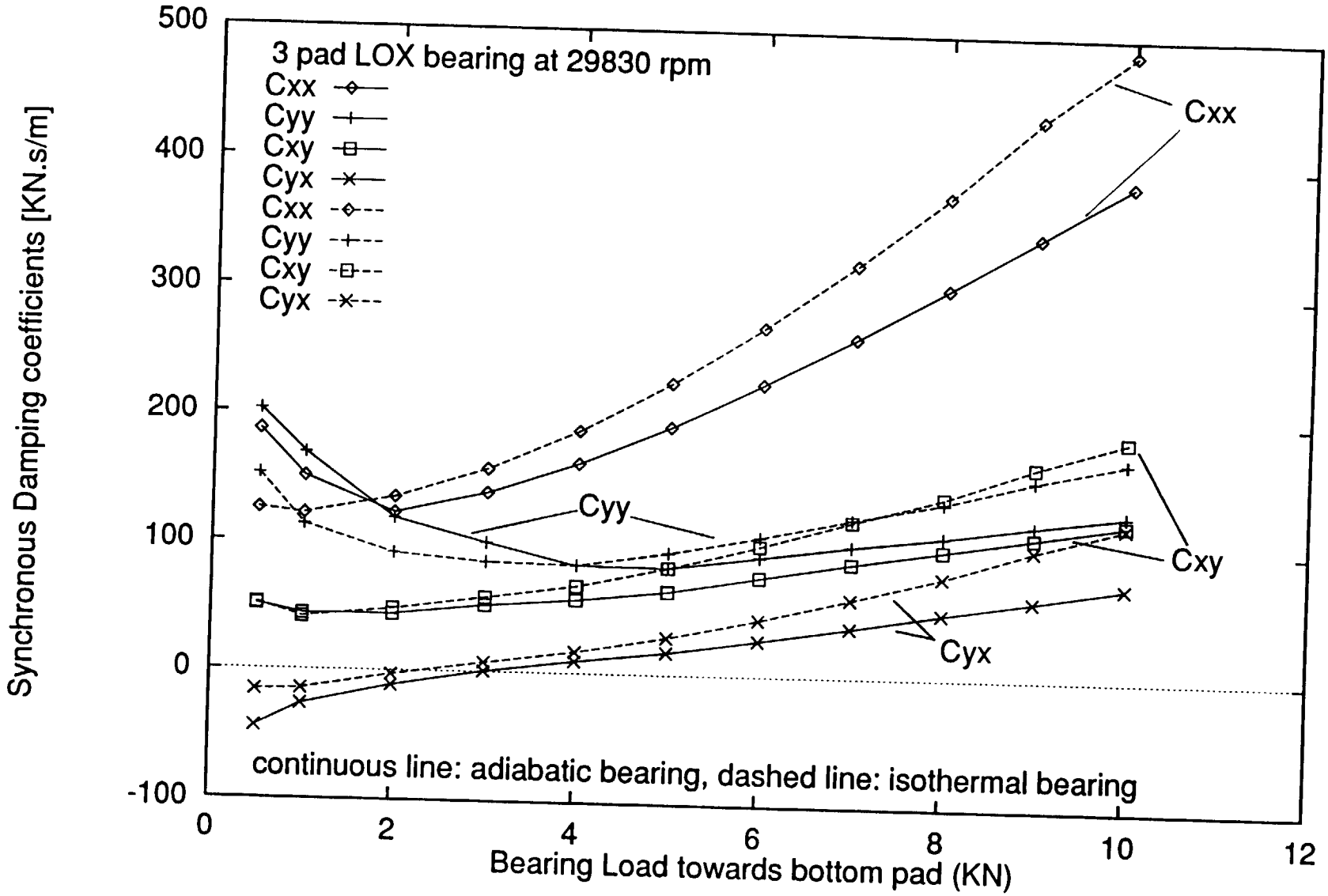

Fig 24. Synchronous dampig coefficients vs. applied load for LOX 3-pad bearing. Journal speed 29,830 cpm. (A) adiabatic bearing, (I) isothermal bearing

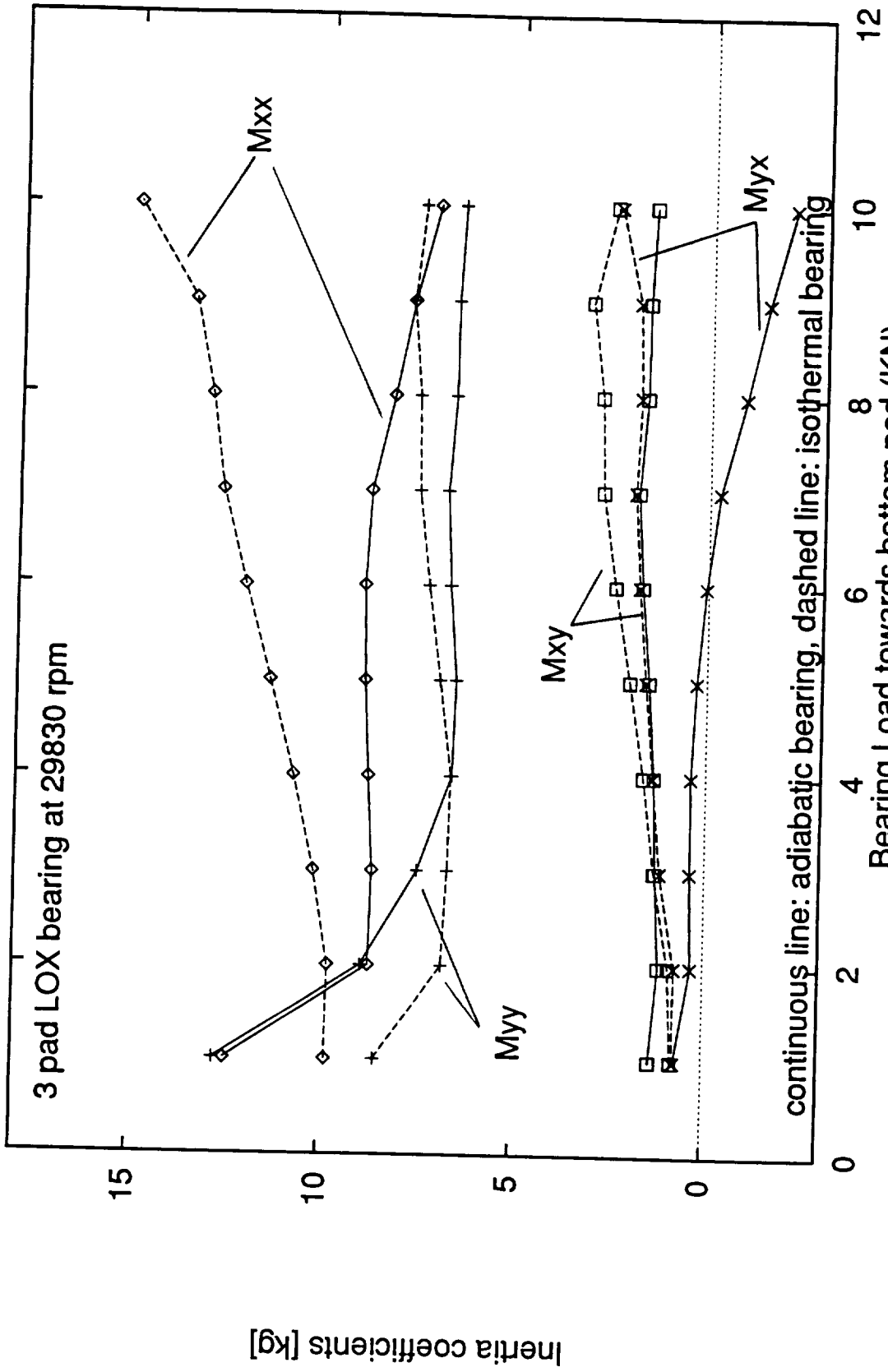

Fig 25. Inertia force coefficients vs. applied load for LOX 3-pad bearing. Journal speed 29,830 cpm. (A) adiabatic bearing, (I) isothermal bearing

shows a larger equivalent stiffness, its critical mass would be lower since the WFR is larger than the adiabatic flow model.

The LO_x bearing examples have shown that a cryogenic hydrodynamic journal bearing is able to support large loads if the bearing clearance is very small and its projected area (L x D) is large. However, these same requirements cause thermal effects to be of importance on the static and dynamic force performance of the bearing. The actual thermal model to be used for a cryogenic hydrodynamic bearing still needs to be determined by considering the thermal paths across the bearing and journal surfaces.

To close this section it is noted that no examples have been presented for bearing applications with liquid hydrogen. The ommission has been involuntary and several relevant cases can be found in the Examples Manual (San Andres 1993e) and also in the reference of Yang et al. (1993c). However, it is here advanced that thermal effects are rather insignificant for externally pressurized LH_2 bearings since the specific heat of this fluid is much larger than that of LO_2. On the other hand, fluid compressibility considerations and a Joule-Thompson like effect rule the performance of LH_2 bearings.

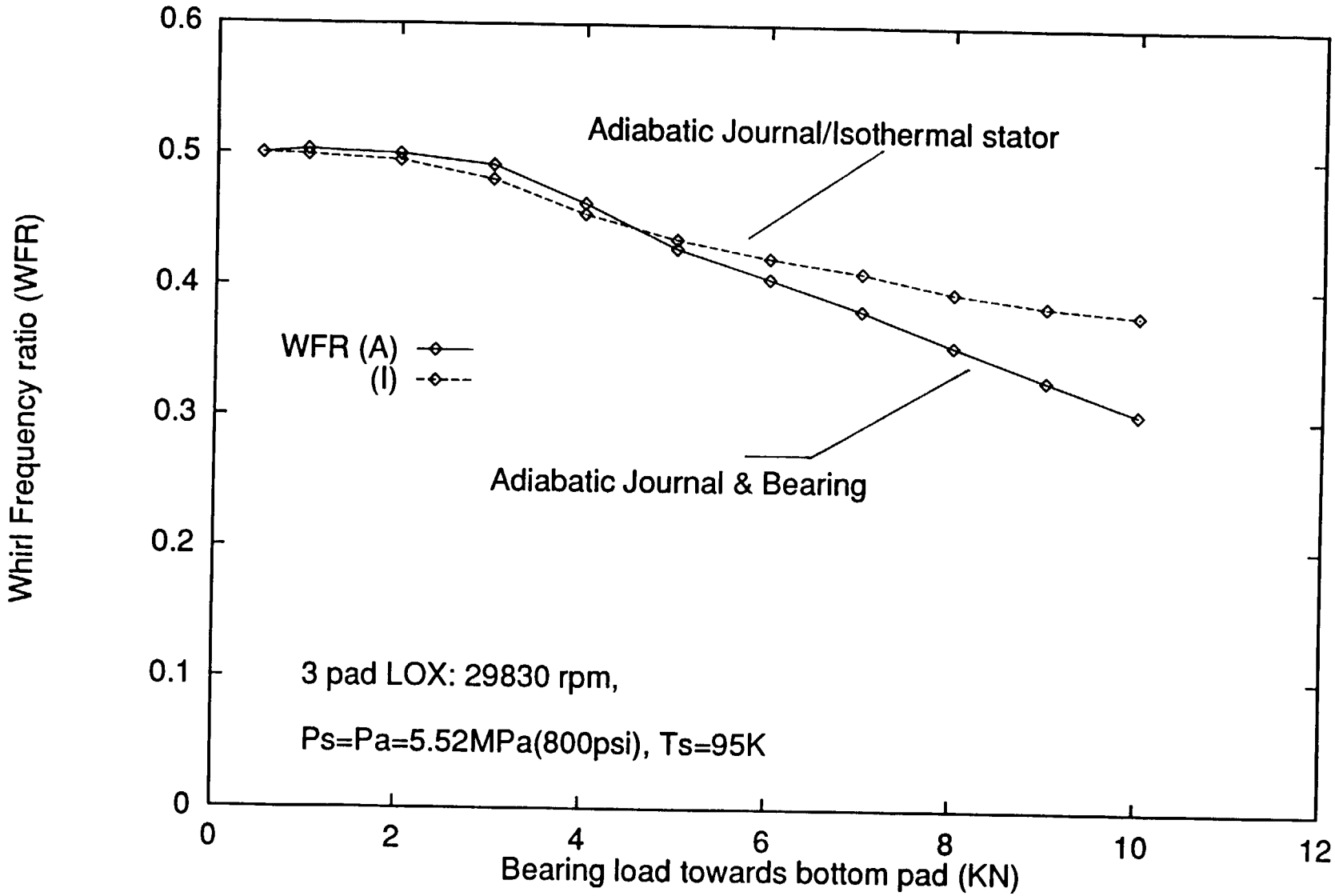

Fig 26. Whirl frequency ratio (WFR) vs. applied load for LOX 3-pad bearing. Journal speed 29,830 cpm. (A) adiabatic bearing, (I) isothermal bearing

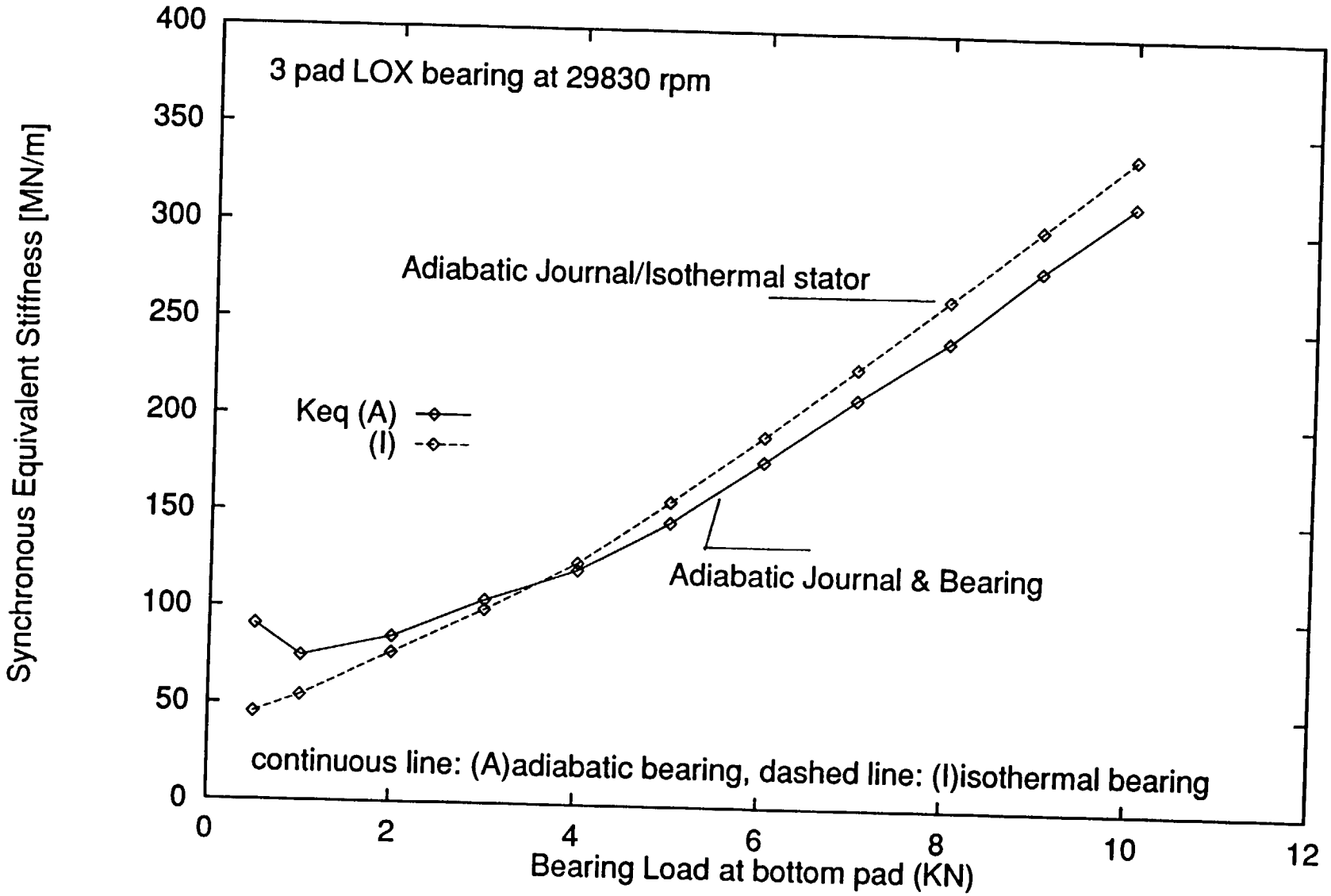

Fig 27. Equivalent stiffness coefficient vs. applied load for LOX 3-pad bearing. Journal speed 29,830 cpm. (A) adiabatic bearing, (I) isothermal bearing

CONCLUSIONS AND RECOMMENDATIONS

A thermohydrodynamic analysis and computer code for the prediction of the static and dynamic force response of fluid film bearings for cryogenic applications have been developed. The motion of a cryogenic liquid on the thin film annular region of a fluid film bearing is described by a set of mass and momentum conservation, and energy transport equations for the primitive turbulent bulk-flow variables, and accompanied by thermophysical state equations for evaluation of the fluid material properties. Zeroth-order equations describe the fluid flow field for a journal equilibrium position, while first-order linear equations govern the fluid flow for small amplitude journal center translational motions and journal axis conical motions. Solution to the zeroth-order flow field equations provides the bearing flow rate, load capacity, restoring moments and torque. Solution to the first-order equations determines the 32 rotordynamic force and moment coefficients due to journal lateral and angular motions. The analysis includes the effects of flow turbulence, fluid inertia, liquid compressibility and thermal energy transport on the performance of cryogenic liquid bearings.

The current technological needs call for reliable and resilient fluid film bearing designs to provide maximum operating life with optimum rotordynamic characteristics at the lowest cost. The analysis and computer code developed constitute practical tools for the performance prediction and design of cryogenic liquid hydrostatic journal bearings, annular pressure seals, and cylindrical pad bearings.

The numerical predictions from the program developed correlate favorably with experimental results available in the literature. The comparisons performed demonstrate the generality of the analysis and validate the computational model, and also extend the range of applicability of the program to conventional bearings

handling viscous lubricants.

The computer program developed named as *hydrosealt* calculates:

1) bearing flowrate (seal leakage),
2) friction torque and temperature rise,
3) load capacity (fluid film forces) and restoring moments,
4) rotordynamic force coefficients due to journal center displacements,
5) rotordynamic force coefficients due to journal axis rotations,
6) rotordynamic moment coefficients due to journal center displacements,
7) rotordynamic moment coefficients due to journal axis rotations,
8) Complete pressure and temperature fields on the bearing surface, as well as density and viscosity field variations, with ranges of fluid flow Reynolds numbers and Mach numbers.

for isothermal or adiabatic journal and bearing surface conditions.

as a function of:

a) journal (rotor) center eccentricity and journal axis misalignment.
b) inlet specified circumferential pre-swirl velocity.
c) general clearance function in the axial direction.
d) mean surface roughness on bearing and journal film lands.

The fluid properties (density, viscosity and specific heat) are calculated from the 32 term Benedict-Webb-Rubin equations of state as given by NBS Standard Reference Database 12 (McCarty, 1986) for the following cryogenic liquids: LO_2, LH_2, LN_2, and methane. Other fluids included in the program are water, mineral oils and air.

The analytical research and computational program development need urgent support from a complimentary experimental research effort directed to measure the dynamic force performance of high speed fluid film bearings with flow conditions similar to those found in cryogenic environments. Some empirical flow parameters need to be identified from the test data. These coefficients, like for example orifice discharge coefficients, recess edge entrance loss factors and shear friction coefficients, and thermal mixing groove coefficients are of fundamental

importance for the accurate prediction of the flow and force dynamics in high-speed, turbulent flow fluid film bearings.

Further research is needed to continue the development of advanced analysis and computer codes for the prediction of the force response of other fluid film bearing geometries for cryogenic applications. The study should consider extension of the analytical models and program developed on Phase I to include rigid and flexure pivot tilt-pad (hydrostatic) bearings, as well as bearing shells with a simple elastic structural matrix (foil–bearings). The current THD model must be advanced to account for radial heat transfer through the bearing walls.

There is also the need to develop a sound analysis and efficient computer code to calculate the transient fluid film bearing force response due to time-varying journal displacements and velocities. The analysis should be coupled to the dynamics of a rotor–bearing system for prediction of rotor lift–off, calculation of synchronous unbalance frequency response curves, and transient responses due to abnormal shock and maneuvering loads.

The mechanics of two-phase flow phenomena and choked flow operation in unique cryogenic conditions should be addressed in the near future. A fundamental analysis is required with emphasis on the calculation of dynamic force coefficients and determination of stable regimes of operation.

REFERENCES

Adams, M., J. T. Sawicki, and R. Capaldi, 1992, "Experimental Determination of Hydrostatic Journal Bearing Coefficients," Proc. of ImechE, Paper C432/145, International Conference in Vibrations in Rotating Machinery, IMechE 1992-6, September.

Arauz, G., and L. San Andres, 1993, "Effect of a Circumferential Feeding Groove on the Force Response of a Short Squeeze Film Damper," ASME Paper 93–Trib–15.

Artiles,A., Walowit,J., and Shapiro,W., 1982, "Analysis of Hybrid Fluid Film Journal Bearings with Turbulence and Inertia Effects," *Advances in Computer Aided Bearing Design*, ASME Press.

Beatty, P.A., and W.F. Hughes, 1987, "Turbulent Two-Phase Flow in Annular Seals," *STLE Tribology Transactions*, Vol. 30, pp.11–18.

Beatty, P.A., and W.F. Hughes, 1990, "Stratified Two-Phase Flow in Annular Seals," ASME Journal of Tribology, Vol. 112, pp.372–381.

Bird,R.B., Stewart,W.E., and Lightfoot,E.N., 1960, *Transport Phenomena*, John Wiley & Son, New York.

Braun,M.J., Wheeler,R.L.III, and Hendricks,R.C., 1987a, "A Fully Coupled Variable Properties Thermohydraulic Model for a Cryogenic Hydrostatic Journal Bearing," ASME Journal of Tribology, Vol. 109, pp.405–416.

Braun,M.J., Wheeler,R.L.III, and Hendricks,R.C., 1987b, "Thermal Shaft Effects on Load-Carrying Capacity of a Fully Coupled, Variable Properties Cryogenic Journal Bearing," *STLE Tribology Transactions*, Vol. 30, pp.282–292.

Braun,M.J., Don, Q., and Choy, F.K., 1993, "The Effects of a Hydrostatic Pocket Aspect Ratio, and its Supply Orifice Position and Attack Angle on Steady-State FLow Patterns, Pressure and Shear Characteristics," ASME Journal of Tribology, Vol. 115, pp.

Burton,R.A., and Carper,H.J., 1967, "An Experimental Study of Annular Flows with Applications in Turbulent Film Lubrication," ASME Journal of Lubrication Technology, Vol. 89, pp.381–391.

Childs,D., 1989, "Fluid-Structure Interaction Forces at Pump-Impeller-Shroud Surfaces for Rotordynamic Calculations," ASME Journal of Vibration, Acoustics, Stress and Reliability in Design, Vol. 111, PP.216–225.

Chaomleffel, J.P., and Nicholas, D., 1986, "Experimental Investigation of

Hybrid Journal Bearings," Tribology International, Vol. 19, No. 5, PP. 253–259.

Constantinescu,V.N., 1973, "Basic Relationships in Turbulent Lubrication and Their Extension to Include Thermal Effects," ASME JOURNAL OF LUBRICATION TECHNOLOGY, Vol. 95, pp.147–154.

Constantinescu,V.N., and Galetuse,S., 1975, "Pressure Drop due to Inertia Force in Step Bearings," ASME Papers, 75-Lub-34.

Di Pasquantonio,F., and Sala,P., 1984, "Influence of Thermal Field on the Resistance Law in Turbulent Bearing-Lubrication Theory," ASME JOURNAL OF TRIBOLOGY, Vol. 106, pp.368–376.

Ettles,C., and Cameron,A., 1968, "Considerations of Flow Across a Bearing Groove," ASME JOURNAL OF LUBRICATION TECHNOLOGY, Vol. 90, pp.312–319.

Franchek,N., Childs, D., 1993, "Experimental Test Results for Four High-Speed, High-Pressure, Orifice–Compensated Hybrid Bearings," ASME Paper 93-Trib-24.

Ghosh,M.K., Majumdar,B.C., and Rao,J.S., 1979, "Steady-State and Dynamic Behavior of Multi-Recess Hybrid Oil Journal Bearings," *J. Mech. Engng. Sci.*, Vol. 21, pp.345–351.

Ghosh,M.K., and Viswanath,N.S., 1987, "Recess Volume Fluid Compressibility Effect on the Dynamic Characteristics of Multirecess Hydrostatic Journal Bearings With Journal Rotation," ASME JOURNAL OF TRIBOLOGY, Vol. 109, pp.417–426.

Heshmat, H., 1991, "Investigation of Foil Bearings for Use in High-Thrust Liquid Rocket Engines," NASA Contractor Report CR-197099, MTI 90-TR58, April.

Hill, D. E. Baskharone, and L. San Andres, 1993, "Inertia Effects in a Hybrid Bearing with a 45 degree Entrance Region," submitted to ASME JOURNAL OF TRIBOLOGY, October.

Hirs,G.G., 1973, "A Bulk-Flow Theory for Turbulence in Lubricant Films," ASME JOURNAL OF LUBRICATION TECHNOLOGY, Vol. 95, pp.137–146.

Ho,Y.S., and Chen,N.N., 1984, "Pressure Distribution in a Six-Pocket Hydrostatic Journal Bearing," *Wear*, Vol. 98, pp.89–100.

Holman,J.P., 1986, *Heat Transfer* (Sixth Edition), McGraw-Hill Book Company, New York.

Khonsari, M., 1987, "A Review of Thermal Effects in Hydrodynamic Bearings, I: Slider/Thrust Bearings, II: Journal Bearings" *STLE Tribology Transactions*, Vol. 30, pp.26-33.

Knight, J. and A.J. Niewiarowski, 1990, "Effect of Two Film Rupture Models

on the Thermal Analysis of a Journal Bearing", ASME JOURNAL OF TRIBOLOGY, , Vol. 112, pp.183–188.

Kurtin,K.A., Childs,D., San Andres,L., and Hale,K., 1993, "Experimental Versus Theoretical Characteristics of a High-Speed Hybrid (Combination Hydrostatic and Hydrodynamic) Bearing," ASME JOURNAL OF TRIBOLOGY, Vol. 115, pp.160-168.

Launder,B.E., and Leschziner,M., 1978, "Flow in Finite Width Thrust Bearings Including Inertial Effects, I– Laminar Flow, II– Turbulent Flow," ASME JOURNAL OF LUBRICATION TECHNOLOGY, Vol. 100, pp.330–345.

Lindsey, T., 1993, "Experimental vs. Theoretical Comparison of the Effects of Taper on the Rotordynamic Coefficients in Short Smooth Annular Seals Used in High–Speed Turbomachinery," Master Thesis, May, Texas A&M University, College Station, TX 77843.

Lund, J.W., and J. Tonnesen, 1984, "An Approximate Analysis of the Temperature Conditions in a Journal Bearing, II: Application", ASME JOURNAL OF LUBRICATION TECHNOLOGY, , Vol. 106, pp.237–245.

Massey,B.S., 1983, *Mechanics of Fluids*, Van Nostrand Reinhold (UK) Co. Ltd., Workingham, Berkshire, England.

McCarty,R.D., NBS Standard Reference Data Base 12, 1986, "Thermophysical Properties of Fluids, MIPROPS-86," Thermophysics Div., Center for Chemical Engineering, National Bureu of Standards, Colorado.

Mitsui,J., Hori,Y., and Tanaka,M., 1983, "Thermohydrodynamic Analysis of Cooling Effect of Supply Oil in Circular Journal Bearing," ASME JOURNAL OF LUBRICATION TECHNOLOGY, Vol. 105, pp.414-421.

Mori,A., Makino,T., and Mori,H., 1991, "Entry Flow and Pressure Jump in Submerged Multi-Pad Bearings and Grooved Bearings," ASME Paper 90-Trib-42.

Mosher,P., 1993, "Effect of Design Parameter Variations on Hybrid (Combination Hydrostatic and Hydrodynamic) Bearings for Use in High Speed Turbomachinery," Master Thesis, May, Texas A&M University, College Station, TX 77843.

Nolan, S., R. Hibbs, and G. Genge, 1993, "Hotfire Testing of a SSME HPOTP with an Anular Hydrostatic Bearing," Proceedings of the 7th Workshop on Rotordynamic Instability Problems in High Performance Turbomachinery, Texas A&M University, May.

O'Connor,Leo, 1993, "Fluid-Film Foil Bearings Control Engine Heat," *Mechanical Engineering*, Vol. 115, No. 5, pp.72–75.

Pinkus,O., 1990, *Thermal Aspects of Fluid Film Tribology*, ASME Press, New York.

Reddecliff,J.M., and Vohr,J.H., 1969, "Hydrostatic Bearings for Cryogenic Rocket Engine Turbopumps," ASME JOURNAL OF LUBRICATION TECHNOLOGY, Vol. 91, pp.557-575.

Roach,P.J., 1976, *Computational Fluid Dynamics*, Hermosa Publishers, Albuquerque, N.M.

Rohde,S.M., and Ezzat,H.A., 1976, "On the Dynamic Behavior of Hybrid Journal Bearings," ASME JOURNAL OF LUBRICATION TECHNOLOGY, Vol. 98, pp.557–575.

Safar, Z., and A. Z. Szeri, "Thermohydrodynamic Lubrication in Laminar and Turbulent Regimes," ASME JOURNAL OF LUBRICATION TECHNOLOGY, Vol. 96, pp.48–57.

San Andres,L., 1990a, "Turbulent Hybrid Bearings with Fluid Inertia Effects," ASME JOURNAL OF TRIBOLOGY, Vol. 112, pp.699–707.

San Andres,L., 1990b, "Approximate Analysis of Turbulent Hybrid Bearings: Static and Dynamic Performance for Centered Operation," ASME JOURNAL OF TRIBOLOGY, Vol. 112, pp.692–698.

San Andres,L., 1990c, "Improved Analysis of High Speed, Turbulent Hybrid Bearings" 4th NASA Conference on Advanced Earth-to-Orbit Propulsion Technology, NASA CP 3092, Vol. 2, pp. 414–431, May

San Andres, Luis A., 1991a, "Effect of Fluid Compressibility on the Dynamic Response of Hydrostatic Journal Bearings," *Wear*, Vol. 146, pp.269–283.

San Andres, Luis A., 1991b, "Effect of Eccentricity on the Force Response of a Hybrid Bearing," *STLE Tribology Transactions*, Vol. 34, 4, pp.537–544.

San Andres, Luis A., 1991c, "Analysis of Variable Fluid Properties, Turbulent Annular Seals," ASME JOURNAL OF TRIBOLOGY, Vol. 113, pp.694–702.

San Andres, Luis A., 1992a, "Analysis of Turbulent Hydrostatic Bearings with a Barotropic Cryogenic Fluid," ASME JOURNAL OF TRIBOLOGY, Vol. 114, pp.755–765.

San Andres,L., 1992b, "Analysis of Hydrostatic Bearings with End Seals," ASME JOURNAL OF TRIBOLOGY, Vol. 114, pp. 802–811.

San Andres,L., 1993a, "The Effect of Journal Misalignment on the Operation of Turbulent Flow Hydrostatic Bearings," ASME JOURNAL OF TRIBOLOGY, Vol. 115, pp. 355–363.

San Andres,L., 1993b, "Effect of Shaft Misalignment on the Dynamic Response

of Annular Pressure Seals," *STLE Tribology Transactions*, Vol. 36, pp. 173-182.

San Andres,L., 1993c, "Dynamic Force and Moment Coefficients for Short Length Annular Seals," ASME JOURNAL OF TRIBOLOGY, Vol. 115, pp. 134–140.

San Andres,L., 1993d, "hydrosealt User's Manual and Tutorial," Texas A&M University, Mechanical Engineering Department, December.

San Andres,L., 1993e, "hydrosealt Examples," Texas A&M University, Mechanical Engineering Department, December.

San Andres,L., 1993f, "Turbulent Flow Foil Bearings for Cryogenic Applications," submitted for review to ASME JOURNAL OF TRIBOLOGY, December.

San Andres,L., and Velthuis,J.F.M., 1992, "Laminar Flow in a Recess of a Hydrostatic Bearing," *Tribology Transactions*, Vol. 35, pp.736–744.

Scharrer,J.K., and Hibbs,R.I., 1990, "Flow Coefficients for the Orifice of a Hydrostatic Bearing," *STLE Tribology Transactions*, Vol. 33, pp.543–550.

Scharrer,J.K., R. Hecht, and Hibbs,R.I., 1991a, "The Effects of Wear on the Rotordynamic Coefficients of a Hydrostatic Bearing," ASME JOURNAL OF TRIBOLOGY, , Vol. 113, pp.210–21.

Scharrer,J.K., J. Tellier, and Hibbs, R.I., 1991b, "A Study of the Transient Performance of Hydrostatic Journal Bearings, I: Test Apparatus and Facility, II: Experimental Results, " *STLE Tribology Transactions*, Preprint 91-TC-3B-2

Scharrer,J.K., and T.W. Henderson, 1992a, "Hydrostatic Bearing Selection for the STME Hydrogen Turbopump," AIAA Paper 92-3283, 28th AIAA/SAE/ASME /ASEE Joint Propulsion Conference, July 6-8, Tennese.

Scharrer,J.K., Hibbs,R.I., and San Andres,L., 1992b, "The Axisymmetrically Stepped, Orifice Compensated Hydrostatic Bearings," AIAA Paper 92-3405, 28th AIAA/SAE/ASME/ASEE Joint Propulsion Conference, July 6-8, Tennese.

Scharrer,J.K., Hibbs,R.I., and Nolan, S., 1992c, "Extending the Life of the SSME HPOTP through the Use of Annular Hydrostatic Bearings," AIAA Paper 92-3401, 28th AIAA/SAE/ASME /ASEE Joint Propulsion Conference, July 6-8, Tennese.

Scharrer,J.K., J. Tellier, and R. Hibbs, 1992d, "Start Transient of an Annular Hydrostatic Bearing in Liquid Oxygen," AIAA Paper 92-3404, 28th AIAA/SAE/ASME /ASEE Joint Propulsion Conference, July 6-8, Tennese.

Shoup, T., Private Communication, 1993, Sverdrup–NASA Marshall Space Center, October 15.

Simon, J., and J. Frene, 1989, "Static and Dynamic Characteristics of Turbulent

Annular Eccentric Seals: Effect of Convergent-Tapered Geometry and Variable Fluid Properties" ASME JOURNAL OF TRIBOLOGY, Vol. 111, pp.378-385.

Smalley,A.J., Vohr,J.H., Castelli,V. and Wachtmann,C., 1974, "An Analytical and Experimental Investigation of Turbulent Flow in Bearing Films Including Convective Fluid Inertia Forces," ASME JOURNAL OF LUBRICATION TECHNOLOGY., Vol. 96, pp.151-157.

Suganami,T., and Szeri,A.Z., 1979, "A Thermohydrodynamic Analysis of Journal Bearings," ASME JOURNAL OF LUBRICATION TECHNOLOGY, Vol. 101, pp.21-27.

Tonnesen, J., and P.K. Hansen, 1981, "Some Experiments on the Steady State Characteristics of a Cylindrical Fluid-Film Bearing Considering Thermal Effects," ASME JOURNAL OF LUBRICATION TECHNOLOGY, Vol. 103, pp. 107-114.

Van Doormaal,J.P., and Raithby,G.D., 1984, "Enhancements of the SIMPLE Method for Predicting Incompressible Fluid Flows," *Numerical Heat Transfer*, Vol. 7, pp.147-163.

Van Doormaal,J.P., and Raithby,G.D., 1985, "An Evaluation of the Segregated Approach for Predicting Incompressible Fluid Flow," ASME Papers, 85-HT-9.

Von Pragenau,G.L., 1982, "Damping seals for Turbomachinery," NASA TP 1987.

Von Pragenau,G.L., 1990, "Damping bearings for Turbomachinery," NASA TP 3092, Vol. II, pp. 155-162.

Whitaker,S., 1977, *Fundamental Principles of Heat Transfer*, Pergamon Press Inc., New York.

Yang,Z., San Andres,L., and Childs,D., 1993a, "Thermal Effects in Cryogenic Liquid Annular Seals, Part I: Theory and Approximate Solution; Part II: Numerical Solution and Results" ASME JOURNAL OF TRIBOLOGY, Vol. 115, pp.267-284.

Yang,Z., San Andres,L., and Childs,D., 1993b, "Importance of Heat Transfer from Fluid Film to Stator in Turbulent Annular Seals," *Wear*, Vol. 160, pp.269-277.

Yang,Z., San Andres,L., and Childs,D., 1993c, "Thermohydrodynamic Analysis of Process Liquid Hydrostatic Bearings in Turbulent Regime, I: Theory, II: Numerical solution and Results", accepted for publication at ASME *Journal of Applied Mechanics*, December.

Yang,Z., San Andres,L., and Childs,D., 1993d, "Process Liquid Turbulent Flow Hydrostatic Bearings: Analysis and Tests for Rotordynamic Coefficients", accepted for presentation at 1994 *IFToMM Rotordynamics Conference*, December.

Zeidan, F., 1992, "Developments in Fluid Film Bearing Technology," *Turboma-*

chinery International, September/October.

APPENDIX A

NOMENCLATURE

A	πDL, journal or bearing surface area $[m^2]$
A_o	$C_d \pi d_o^2/4$, equivalent orifice area $[m^2]$
A_r	bl, recess area $[m^2]$
b	recess circumferential length [m]
$c, c_*, \bar{c}$	radial clearance, characteristic clearance $(=\{c(y)\}_{min})$ [m], c/c_*
C_d	empirical orifice discharge coefficient
$C_p, \bar{C}_p$	specific heat [J/kg·K],C_p/C_{p*} nondimensional specific heat
$C_{XX}, \ldots, C_{\delta_Y \delta_Y}$	damping coefficients
D	journal diameter [m]
d_o	orifice diameter [m]
e_X, e_Y	displacements of the journal in X and Y direction [m]
E_c	$U_*^2/T_* C_{p*}$, Eckert number
f_J, f_B	$a_m[1 + (c_m r_{J,B}/H + b_m/R_{J,B})^{e_m}]$, turbulent friction factors at journal and bushing surfaces based on Moody's equation, a_m=0.001375; b_m=5×10^5; c_m=10^4; e_m=1/2.65
f_{rj}	$\int_{\Gamma_r} h_j \, d\theta$
F_X, F_Y, M_X, M_Y	film forces(moments) along(around) $\{X,Y\}$ axes [N,N-m]
H, h	film thickness [m], H/c_*
H_r	recess depth [m]
h_0, h_1,	zeroth- and first-order film thicknesses
h_B, h_J	heat transfer coefficients to bearing, journal surfaces [W/$m^2 \cdot K$]
$\bar{h}_B, \bar{h}_J$	$(h_B, h_J)c_*/(\wp_e^* K_*)$, dimensionless bulk heat transfer coefficients
$h_X, h_Y, h_{\delta_X}, h_{\delta_Y}$	$\cos\theta, \sin\theta, \sin\theta, \cos\theta$, perturbed film thickness components

$K, \bar{K}$	thermal conductivity of liquid [W/m·K], K/K_*
K_{xx},...,$K_{\delta_Y \delta_Y}$	stiffness coefficients
k_x,k_y	$(k_j + k_B)/2$, dimensionless shear parameters in X, Y directions
k_j,k_B	$f_j R_j$,$f_B R_B$, turbulent shear parameters at journal, bearing surfaces
k_r	$Re_r^{0.681}/7.753$, turbulent shear flow parameter
L, L_L, L_R	bearing axial length [m], $L = L_L + L_R$
l	recess axial length [m]
$\dot{m}$	mass flow rate over differential segments [kg/s]
$\dot{M}$	mass flow rate of a hydrostatic journal bearing [kg/s]
M_r	$\alpha R\Omega\sqrt{\beta\rho_r}$, recess flow Mach number due to rotation
M_{xx},...,$M_{\delta_Y \delta_Y}$	inertia or added mass coefficients [kg]
$\vec{n}$	normal vector to recess boundary
P,p	fluid pressure [N/m^2]; $(P - P_a)/\Delta P$, dimensionless pressure
p_X,p_Y	dimensionless dynamic pressures for perturbation
$\wp_e^*$	$Re_p^* \wp_r^* = \rho_* U_* c_*^2 Cp_*/(K_* R)$, Peclet number
P_L,P_R	discharge pressures on left, right sides of bearing [N/m^2]
P_s,P_a,P_r	external supply, ambient and recess pressures [N/m^2]
$\wp_r$	$C_p\mu/K$, Prandtl number
Q_{in}	mass flow rate supplied to a recess/groove [kg/s]
q_{in}	$Q_{in}/(\rho_* c_* R U_*)$
Q_r	recess to land mass flow rate [kg/s]
q_r	$Q_r/(\rho_* c_* R U_*) = \int \bar{\rho} h(\vec{\mathbf{u}} \cdot \vec{\mathbf{n}})\, d\Gamma_r$
Q_s	heat flux to the bounding surfaces [W/m^2]
$\bar{Q}_s$	dimensionless heat flux to the bounding surfaces
R	journal radius [m]
Re_c	$\rho_* R\Omega c_*/\mu_*$, nominal circumferential flow Reynolds number

Re_H	$\rho_e R\Omega H_e/\mu_e$, Reynolds number at recess edges
Re_p	$\rho_* U_* c_*/\mu_*$, reference pressure flow Reynolds number
Re_p^*	$Re_p(c_*/R)$, modified reference pressure flow Reynolds number
Re_r	$\rho_r R\Omega(H_r + H)/\mu_r$, Reynolds No. at recess volume due to rotation
Re_s	$\rho_* \omega c_*^2/\mu_*$, nominal squeeze film Reynolds number
R_J	$\rho H\sqrt{(U - \Omega R)^2 + V^2}/\mu$ Reynolds number to journal surface
R_B	$\rho H\sqrt{U^2 + V^2}/\mu$, Reynolds number relative to bearing surface
r_J,r_B	mean roughness depth at journal and bearing surfaces [m]
S_t	$h_t/\rho C_p V_t$, Stanton number
T,$\bar{T}$	two-dimensional bulk temperature in the fluid film $[K]$, T/T_*
T_*	T_s, characteristic temperature $[K]$
$\tilde{T}$	$\tilde{T}(x, y, z, t)$, three-dimensional temperature $[K]$
t	time [sec]
T_B,T_J	temperatures at the bearing and the journal surfaces [K]
T_s	inlet supply temperature at the orifice [K]
T_u,T_d,T_{side}	temperatures at the up-, down-stream and side recess edges [K]
T_{or}	fluid film resistant torque [N-m]
T_{or}^r	$\tau_{xz}^H A_r R$, friction torque over a recess area [N-m]
U,V	mean flow circumferential and axial velocities [m/s]
u,v	(U,V)$/U_*$, dimensionless mean flow velocities
$\vec{U}$,$\vec{V}_r$	$U\vec{i} + V\vec{j}$, $R\Omega\vec{i} + 0\vec{j}$
$\tilde{U}$,$\tilde{V}$,$\tilde{W}$	three-dimensional velocities in x,y,z directions [m/s]
U_*	$\Delta P c_*^2/(\mu_* R)$, characteristic velocity [m/s]
$\vec{V}$	$\{\tilde{U}, \tilde{V}, \tilde{W}\}$
$\forall_r$	$(H_r + H)A_r + \forall_s$, total recess volume $[m^3]$
$\bar{\forall}_r$	$\forall_r/(c_* R^2)$, dimensionless recess volume

$\forall_s$	volume of orifice supply line $[m^3]$
V_t,v_t	$\sqrt{U^2+V^2}$ [m/s], $\sqrt{u^2+v^2}$, fluid speed
X,Y,Z	inertial coordinates defining journal position in bearing
x,y,z	(0,πD),($-L_L$,L_R),(0,H(x,y,t)), coordinates defining flow regions
Z_0,$\bar{Z}_0$,$\bar{Z}$	distance to center of journal angular motions, Z_0/R, Z/R
$\bar{x}$,$\bar{y}$	$(x/R=\theta)$, y/R, dimensionless x, y coordinates
β_p	$\frac{1}{\rho}(\partial\rho/\partial P)_T$, liquid compressibility factor $[m^2/N]$
$\bar{\beta}_p$	$\beta_p \Delta P$, dimensionless liquid compressibility factor $[m^2/N]$
β_t	$-\frac{1}{\rho}(\partial\rho/\partial T)_p$, volumetric expansion coefficient $[1/K]$
$\bar{\beta}_t$	$\beta_t T_*$, dimensionless volumetric expansion coefficient
α	$(U\|_{y=0})/(\Omega R)$, circumferential velocity entrance swirl factor
α_y	$\frac{1}{2}(1+\xi)Re_p^*$, axial entrance loss coefficient
Λ	$\Omega R/U_*$, dimensionless journal velocity or speed parameter
σ	$\omega R/U_*$, dimensionless frequency parameter at film land
λ	thermal mixing coefficient for groove heat carry-over
λ_1	$\sigma\bar{\forall}_r$, dimensionless frequency parameter at recess volume
λ_{11}	$\sigma l/R$, modified frequency parameter at recess volume
λ_2	$\lambda_1\bar{\beta}_{pr}$, combination of compressibility & frequency parameters
Ω	rotational speed of journal [rad/sec]
ω	excitation or whirling frequency [rad/sec]
ρ,ρ_*,$\bar{\rho}$	fluid density, characteristic density [kg/m^3], ρ/ρ_*
μ,μ_*,$\bar{\mu}$	fluid viscosity, characteristic viscosity [Ns/m^2], μ/μ_*
ϕ_r	$k_r(b/D)(\eta/h)^2/(1-M_r^2)$, recess volume shear coefficient
$\phi_{x,y}$	$Re_p^*(1+\zeta_{x,y})(1+\xi_{x,y})[1-(\eta\rho_e/\rho_r)^2]$, recess entrance loss factors
$\zeta_{x,y}$	$1.95/Re_H^{0.43}$, 0
$\xi_{x,y}$	empirical entrance loss coefficients in X, Y directions

$\xi_{xu,d}$	ξ_x at up- and down-stream of recess/land entrance, respectively
δ_*	$A_o\mu_*\sqrt{2}/[c_*^3\sqrt{\rho_*\Delta P}]$, dimensionless orifice parameter
$\varepsilon_X, \varepsilon_Y$	$e_X/c_*, e_Y/c_*$, dimensionless journal eccentricities in X, Y directions
δ_X, δ_Y	journal axis angular rotations around X, Y axes
$\Delta\varepsilon_X, \Delta\varepsilon_Y$	dimensionless dynamic (perturbed) eccentricities
$\Delta\delta_X, \Delta\delta_Y$	dynamic (perturbed) journal angular rotations
τ	ωt, dimensionless time coordinate
τ_c^h	$\bar{\mu}[uk_B - (u-\Lambda)k_J]/4h$, dimensionless shear stress on journal
τ_{xz}, τ_{yz}	wall shear stresses in X and Y directions
η	$H/(H_r + H)$, ratio of land film thickness to recess depth
γ	first order turbulent shear coefficients
$\mathcal{K}_P$	pad leading edge pressure recovery factor
$\mathcal{K}_L, \mathcal{K}_R$	discharge coefficients for end seal restrictions

Scripts:

0	refers to zeroth-order solution
j	refers to first-order perturbations($j \rightarrow X, Y$ direction)
e	refers to entrance or recess edge conditions
r	refers to recess conditions
J	refers to journal
B	refers to bushing
*	refers to characteristic values or supply conditions
-	refers to three-dimensional variables
-	refers to dimensionless variables or parameters

APPENDIX B

HEAT TRANSFER TO BUSHING AND JOURNAL

For the lumped fluid film model assumption, the heat transfer from fluid film to the bounding surfaces has been expressed as

$$Q_s = h_B(T - T_B) + h_J(T - T_J) \tag{B.1}$$

where, h_B and h_J are the heat–transfer coefficients to the bushing and journal, respectively. They can be found through the Reynolds-Colburn analogy between fluid friction and heat transfer (Holman, 1986). The average heat transfer over the entire laminar/turbulent boundary layer is

$$S_t \wp_r^{2/3} = f/2 \tag{B.2}$$

where

$$S_t = \frac{h_t}{\rho C_p V_t} \qquad (\text{ Stanton number }), \tag{B.3}$$

$$\wp_r = \frac{C_p \mu}{K} \qquad (\text{ Prandtl number }), \text{ and} \tag{B.4}$$

$$f = a_m \left[1 + \left(c_m \frac{r}{H} + \frac{b_m}{R_e}\right)^{e_m}\right] \tag{B.5}$$

is the Fanning friction factor Based on Moody's Equation (Massey,1983).

So, the heat transfer coefficient can be written as

$$h_t = \frac{1}{2}\rho C_p V_t f / \wp_r^{2/3} \tag{B.6}$$

$$h_B = \frac{1}{2}\rho C_p V_B f_B / \wp_r^{2/3} \tag{B.7}$$

$$h_J = \frac{1}{2}\rho C_p V_J f_J / \wp_r^{2/3} \tag{B.8}$$

Actually, there are plenty of formulae for turbulent heat transfer coefficients (Holman, 1986). The above expressions are used because of the simplicity and the ability to include the surface roughness effects.

APPENDIX C

ZEROTH– AND FIRST-ORDER EQUATIONS

C.1 Zeroth-Order Equations on Film Lands

- Continuity Equation

$$\frac{\partial}{\partial \bar{x}}(\bar{\rho}_0 h_0 u_0) + \frac{\partial}{\partial \bar{y}}(\bar{\rho}_0 h_0 v_0) = 0\,; \tag{C.1}$$

- Circumferential-Momentum Equation

$$-h_0 \frac{\partial p_0}{\partial \bar{x}} = \frac{\bar{\mu}_0}{h_0}(k_{x0} u_0 - k_{r0}\frac{\Lambda}{2}) + Re_p^*[\frac{\partial}{\partial \bar{x}}(\bar{\rho}_0 h_0 u_0^2) + \frac{\partial}{\partial \bar{y}}(\bar{\rho}_0 h_0 u_0 v_0)]\,; \tag{C.2}$$

- Axial-Momentum Equation

$$-h_0 \frac{\partial p_0}{\partial \bar{y}} = \frac{\bar{\mu}_0}{h_0}(k_{y0} v_0) + Re_p^*[\frac{\partial}{\partial \bar{x}}(\bar{\rho}_0 h_0 u_0 v_0) + \frac{\partial}{\partial \bar{y}}(\bar{\rho}_0 h_0 v_0^2)]\,; \tag{C.3}$$

- Energy-Transport Equation

$$\begin{aligned}
&\frac{Re_p^*}{E_c}\Big\{\bar{C}_{p0}[\frac{\partial}{\partial \bar{x}}(\bar{\rho}_0 h_0 u_0 \bar{T}_0) + \frac{\partial}{\partial \bar{y}}(\bar{\rho}_0 h_0 v_0 \bar{T}_0)] + (\bar{h}_{B0} + \bar{h}_{J0})\bar{T}_0\Big\} \\
&= \bar{\beta}_{t0}\bar{T}_0 h_0(u_0\frac{\partial p_0}{\partial \bar{x}} + v_0\frac{\partial p_0}{\partial \bar{y}}) + h_0\frac{\Lambda}{2}\frac{\partial p_0}{\partial \bar{x}} + \frac{Re_p^*}{E_c}(\bar{h}_{B0}\bar{T}_{B0} + \bar{h}_{J0}\bar{T}_{J0}) \\
&\quad + \frac{\bar{\mu}_0}{h_0}[k_{x0}(v_{t0}^2 + \frac{1}{2}u_0\Lambda) + k_{r0}(\frac{1}{4}\Lambda^2 - u_0\Lambda)]
\end{aligned} \tag{C.4}$$

C.2 Zeroth-Order Equations at HJB Recesses

- Mass Conservation at a Recess

$$\delta_* \sqrt{\bar{\rho}_{r0}(1 - p_{r0})} = q_{r0} = \int_{\Gamma_r} \bar{\rho}_0 h_0 (\vec{\mathbf{u}}_0 \cdot \vec{\mathbf{n}})\, d\bar{\Gamma} \tag{C.5}$$

- Global Energy Balance Equation at a Recess

$$\begin{aligned}
&\bar{C}_{p0}\Big(\sum \bar{m}_{d0}\bar{T}_{d0} + 2\sum \bar{m}_{side0}\bar{T}_{side0}\Big) \\
&= \bar{C}_{p0}\Big(\sum \bar{m}_{u0}\bar{T}_{u0} + q_{in0}\Big) + (\bar{T}^r_{or0}\Lambda)E_c/Re_p^*
\end{aligned} \tag{C.6}$$

The recess temperature can be found from the above energy balance equation as follows.

In a hydrostatic journal bearing, flow supply enters the recess through an orifice restrictor. Temperatures at the downstream and side edges of the recess are approximately equal to the recess temperature due to the high pressure gradient:

$$\bar{T}_{d0} = \bar{T}_{side0} = \bar{T}_{r0} = Constant \tag{C.7}$$

Substituting Eq.(C.7) into Eq.(C.6), the recess temperature is then given by:

$$\bar{T}_{r0} = \frac{1}{2q_{side0} + q_{d0}} \left[q_{in0} + \sum \bar{\dot{m}}_{u0} \bar{T}_{u0} + \frac{\bar{T}^r_{or0}}{\bar{C}_{p0}} \frac{\Lambda E_c}{Re^*_p} \right] \tag{C.8}$$

where

$$\bar{T}_{u0} = \begin{cases} \bar{T}_{r0}, & \text{if } (\vec{U}_0 \cdot \vec{\mathbf{n}}) > 0; \\ \text{Upstream Film Values on Film Lands,} & \text{otherwise.} \end{cases} \tag{C.9}$$

The above equations show that if fluid flows out of all the four recess edges (as in a pure hydrostatic beairng), the edge temperatures are equal to the recess temperature. If the hot lubricant left the upstream film lands enters the recess at the trailing edge due to journal rotation, then an averaged uniform recess temperature can be obtained from the mixing of upstream and inlet temperatures.

- Global Energy Balance Equation at a Groove

$$\sum \bar{\dot{m}}_{d0} \bar{T}_{d0} = \sum \bar{\dot{m}}_{u0} \bar{T}_{u0} + q_{in0} \bar{T}_{in0} \tag{C.10}$$

where

$$q_{in0} = \sum \bar{\dot{m}}_{d0} - \sum \bar{\dot{m}}_{u0} = q_{d0} - q_{u0}. \tag{C.11}$$

If

$$q_{u0} = \sum \bar{\dot{m}}_{u0} > 0, \tag{C.12}$$

then,

$$\bar{T}_{u0} = \text{Upstream Film Values on Upstream Pad} \tag{C.13}$$

and

(a) If $q_{d0} > q_{u0}$, then

$$\bar{T}_{d0} = \lambda \frac{\sum \bar{m}_{u0} \bar{T}_{u0}}{q_{d0}} + \left(1 - \lambda \frac{q_{u0}}{q_{d0}}\right) \bar{T}_{in0} \tag{C.14}$$

where

$$\bar{T}_{in0} = 1.0. \tag{C.15}$$

(b) If $q_{d0} < q_{u0}$, then

$$\bar{T}_{d0} = \begin{cases} \lambda \bar{T}_{u0}, & \text{if } q_{d0} \geq 0; \\ \text{Upstream Film Values on Downstream Pad}, & \text{if } q_{d0} < 0. \end{cases} \tag{C.16}$$

- Recess/Film Entrance Pressure Rise/Drop

$$\bar{p}_{e0} = \begin{cases} p_{r0} - \bar{\mu}_{r0} \phi_r \vec{\mathbf{n}} \cdot \left[\vec{\mathbf{u}}_0 \eta \left(\frac{\bar{\rho}_e}{\bar{\rho}_r} \right) - \frac{\bar{\Lambda}}{2} \right], & (\vec{\mathbf{u}}_0 \cdot \vec{\mathbf{n}}) > 0, \quad \text{in x direction} \\ p_{r0}, & \text{in y direction;} \end{cases} \tag{C.17}$$

$$p^{+}_{e0} = \bar{p}_{e0} - \frac{\phi_i \cdot \bar{\rho}_{e0}}{2} (\vec{\mathbf{u}}_0 \cdot \vec{\mathbf{n}})^2, \quad (\vec{\mathbf{u}}_0 \cdot \vec{\mathbf{n}}) > 0 \tag{C.18}$$

C.3 First-Order Equations on Film Lands

The fist-order equations are obtained from the perturbations in the film thickness due to journal displacements (Δe_X,Δe_Y) and rotations ($\Delta \delta_X$,$\Delta \delta_X$). The perturbed (dynamic) film thickness in the following first-order equations can be expressed as

$$h_j = \begin{cases} h_X, h_Y, & \text{for journal displacements about (X,Y) axes;} \\ (\bar{Z} - \bar{Z}_0)\{h_{\delta_X}, h_{\delta_Y}\}, & \text{for journal axis rotations around (X,Y).} \end{cases} \tag{C.19}$$

where

$$h_X = h_{\delta_Y} = \cos\theta, \quad h_Y = -h_{\delta_X} = \sin\theta \tag{C.20}$$

- Continuity Equation

$$\frac{\partial}{\partial \bar{x}}(\bar{\rho}_0 u_0 h_j + \bar{\rho}_0 u_j h_0 + \bar{\rho}_j u_0 h_0) + \frac{\partial}{\partial \bar{y}}(\bar{\rho}_0 v_0 h_j + \bar{\rho}_0 v_j h_0 + \bar{\rho}_j v_0 h_0) + \mathbf{i}\sigma(\bar{\rho}_0 h_j + \bar{\rho}_j h_0) = 0 \qquad (C.21)$$

- Circumferential-Momentum Equation

$$-h_0 \frac{\partial p_j}{\partial \bar{x}} = (\gamma_{uu} + \mathbf{i}\bar{\rho}_0 h_0 Re_s) u_j + \gamma_{uv} v_j + \gamma_{uh} h_j + \gamma_{u\rho}\bar{\rho}_j + \gamma_{u\mu}\bar{\mu}_j + Re_p^*[\frac{\partial}{\partial \bar{x}}(\bar{\rho}_0 h_0 u_0 u_j) + \frac{\partial}{\partial \bar{y}}(\bar{\rho}_0 h_0 v_0 u_j) + \bar{\rho}_0 h_0 u_j \frac{\partial u_0}{\partial \bar{x}} + \bar{\rho}_0 h_0 v_j \frac{\partial u_0}{\partial \bar{y}}] \qquad (C.22)$$

- Axial-Momentum Equation

$$-h_0 \frac{\partial p_j}{\partial \bar{y}} = (\gamma_{vv} + \mathbf{i}\bar{\rho}_0 h_0 Re_s) v_j + \gamma_{vu} u_j + \gamma_{vh} h_j + \gamma_{v\rho}\bar{\rho}_j + \gamma_{v\mu}\bar{\mu}_j + Re_p^*[\frac{\partial}{\partial \bar{x}}(\bar{\rho}_0 h_0 u_0 v_j) + \frac{\partial}{\partial \bar{y}}(\bar{\rho}_0 h_0 v_0 v_j) + \bar{\rho}_0 h_0 u_j \frac{\partial v_0}{\partial \bar{x}} + \bar{\rho}_0 h_0 v_j \frac{\partial v_0}{\partial \bar{y}}] \qquad (C.23)$$

- Energy-Transport Equation

$$\bar{C}_{p_0} \frac{Re_p^*}{E_c}[\frac{\partial}{\partial \bar{x}}(\bar{\rho}_0 h_0 u_0 \bar{T}_j) + \frac{\partial}{\partial \bar{y}}(\bar{\rho}_0 h_0 v_0 \bar{T}_j)] + (\gamma_{tt} + \mathbf{i}\bar{\rho}_0 h_0 \bar{C}_{p_0} Re_s / E_c)\bar{T}_j + \gamma_{tu} u_j + \gamma_{tv} v_j + (\gamma_{tp} - \mathbf{i}\sigma\bar{\beta}_{t0}\bar{T}_0 h_0) p_j + \gamma_{th} h_j - h_0 \frac{\Lambda}{2}\frac{\partial p_j}{\partial \bar{x}} = \bar{\beta}_{t0}\bar{T}_0 h_0 (u_0 \frac{\partial p_j}{\partial \bar{x}} + v_0 \frac{\partial p_j}{\partial \bar{y}}) + \frac{Re_p^*}{E_c}(\bar{h}_{B_0}\bar{T}_{B_j} + \bar{h}_{J_0}\bar{T}_{J_j}) \qquad (C.24)$$

where, the subscript "j"($=X, Y, \delta_X, \delta_Y$) denotes the direction of perturbation for the first-order variables. The γ coefficients arise from the perturbation of the turbulent shear parameters k_x and k_y and are given in this Appendix. The perturbed first-order liquid properties are evaluated from relationships like

$$\phi_j = \left[\frac{\partial \phi}{\partial p}\right]_0 p_j + \left[\frac{\partial \phi}{\partial \bar{T}}\right]_0 \bar{T}_j \,, \quad \phi = \bar{\rho}, \bar{\mu}, ..., etc. \qquad (C.25)$$

C.4 First-Order Equations at HJB Recesses

- Mass Conservation at a Recess

$$
\begin{aligned}
&-p_{rj}\left\{\frac{\delta_*^2\bar{\rho}_{r0}}{2q_{r0}}[1-\bar{\beta}_{pr0}(1-p_{r0})]+\mathbf{i}\lambda_2\bar{\rho}_{r0}\right\}\\
&=q_{rj}+\mathbf{i}\bar{\rho}_{r0}\lambda_{11}f_{rj}+\left[(1-p_{r0})\frac{\delta_*^2\bar{\rho}_{r0}}{2q_{r0}}-\mathbf{i}\lambda_1\bar{\rho}_{r0}\right]\bar{\beta}_{tr0}\bar{T}_{rj}
\end{aligned}
\tag{C.26}
$$

where

$$
f_{rj}=\int_{\Gamma_r}h_j\,d\bar{x}\ , \tag{C.27}
$$

and

$$
q_{rj}=\int_{\Gamma_r}(\bar{\rho}_0h_j\vec{\mathbf{u}}_0+\bar{\rho}_0h_0\vec{\mathbf{u}}_j+\bar{\rho}_jh_0\vec{\mathbf{u}}_0)\cdot\vec{\mathbf{n}}\,d\bar{\Gamma}\ , \tag{C.28}
$$

$$
\lambda_{11}=\sigma l/R\ , \tag{C.29}
$$

$$
\lambda_2=\lambda_1\bar{\beta}_{pr0}=\sigma\bar{\forall}_r\bar{\beta}_{pr0} \tag{C.30}
$$

are the perturbed recess mass flow rate, a modified frequency parameter, and a combination of the frequency and compressibility parameters at recess volume, respectively.

- Global Energy Balance Equation at a Recess

$$
\begin{aligned}
&\sum\left(\dot{\bar{m}}_{d0}\bar{T}_{dj}+\dot{\bar{m}}_{dj}\bar{T}_{d0}-\dot{\bar{m}}_{u0}\bar{T}_{uj}-\dot{\bar{m}}_{uj}\bar{T}_{u0}+2\dot{m}_{side0}\bar{T}_{sidej}+2\dot{m}_{sidej}\bar{T}_{side0}\right)\\
&=q_{rj}-\mathbf{i}\sigma\bar{\forall}_r(\bar{T}_{r0}\bar{\rho}_{rj}+\bar{\rho}_{r0}\bar{T}_{rj})+\left(\frac{\bar{T}^r_{orj}}{\bar{T}^r_{or0}}-\frac{\bar{C}_{prj}}{\bar{C}_{pr0}}\right)\frac{\bar{T}^r_{or0}}{\bar{C}_{pr0}}\frac{E_c\Lambda}{Re^*_p}
\end{aligned}
\tag{C.31}
$$

Assuming

$$
\bar{T}_{uj}=\bar{T}_{dj}=\bar{T}_{sidej}=\bar{T}_{rj}, \tag{C.32}
$$

then, the perturbed recess temperature can be calculated as

$$
\begin{aligned}
\bar{T}_{rj}=\frac{1}{q_{r0}+\mathbf{i}\sigma\bar{\forall}_r\bar{\rho}_{r0}}\Big[&q_{rj}-2q_{sidej}\bar{T}_{r0}+\sum\dot{\bar{m}}_{uj}\bar{T}_{u0}-\sum\dot{\bar{m}}_{dj}\bar{T}_{d0}\\
&-\mathbf{i}\sigma\bar{\forall}_r\bar{T}_{r0}\bar{\rho}_{rj}+\left(\frac{\bar{T}^r_{orj}}{\bar{T}^r_{or0}}-\frac{\bar{C}_{prj}}{\bar{C}_{pr0}}\right)\frac{\bar{T}^r_{or0}}{\bar{C}_{pr0}}\frac{E_c\Lambda}{Re^*_p}\Big]
\end{aligned}
\tag{C.33}
$$

where

$$\bar{T}^r_{orj} = \bar{T}^r_{or0}\Big[\Big(1+\frac{\gamma_s b_m}{k_{Bo}}\Big)\frac{\bar{\rho}_j}{\bar{\rho}_0} - \Big(\frac{\gamma_s b_m}{k_{Bo}}\Big)\frac{\bar{\mu}_j}{\bar{\mu}_0} + \Big(\frac{2C_{cs}}{k_{Bo}}\Big)\frac{h_j}{h_0}\Big]_r \qquad (C.34)$$

is the perturbed dimensionless torque.

- Global Energy Balance Equation at a Groove

  Assuming

$$(\bar{T}_{in})_j = 0$$

then

$$\sum\Big(\bar{\dot{m}}_{d0}\bar{T}_{dj} + \bar{\dot{m}}_{dj}\bar{T}_{d0} - \bar{\dot{m}}_{u0}\bar{T}_{uj} - \bar{\dot{m}}_{uj}\bar{T}_{u0}\Big) = \sum\Big(\bar{\dot{m}}_{dj} - \bar{\dot{m}}_{uj}\Big)\bar{T}_{in0} \qquad (C.35)$$

If

$$q_{u0} = \sum \bar{\dot{m}}_{u0} > 0,$$

then

$$\bar{T}_{uj} = \text{Upstream Film Values on Upstream Pad,} \qquad (C.36)$$

and

(a) If $q_{d0} = \sum \bar{\dot{m}}_{d0} > q_{u0}$, then

$$\bar{T}_{dj} = \frac{1}{q_{d0}}\Big[\sum \lambda(\bar{\dot{m}}_{u0}\bar{T}_{uj} + \bar{\dot{m}}_{uj}\bar{T}_{u0} - \bar{\dot{m}}_{dj}\bar{T}_{d0}\Big) + (q_{dj} - \lambda q_{uj})\bar{T}_{in0}\Big] \qquad (C.37)$$

(b) If $q_{d0} < q_{u0}$, then

$$\bar{T}_{dj} = \begin{cases} \lambda\bar{T}_{uj}, & \text{if } q_{d0} \geq 0; \\ \text{Upstream Film Values on Downstream Pad,} & \text{if } q_{d0} < 0. \end{cases} \qquad (C.38)$$

- Recess/Film Entrance Pressure Rise/Drop

$$\bar{p}_{ej} = \begin{cases} p_{rj} - \bar{\mu}_r\phi_r\eta\big(\frac{\bar{\rho}_e}{\bar{\rho}_r}\big)(\vec{\mathbf{u}}_j\cdot\vec{\mathbf{n}}), & \vec{\mathbf{u}}_0\cdot\vec{\mathbf{n}} > 0, \quad \text{in x direction} \\ p_{rj}, & \text{in y direction;} \end{cases} \qquad (C.39)$$

$$p_{ej}^{+} = p_{ej}^{-} - \phi_i[\bar{\rho}_{e0}(\vec{\mathbf{u}}_0 \cdot \vec{\mathbf{n}})(\vec{\mathbf{u}}_j \cdot \vec{\mathbf{n}}) + \bar{\rho}_{ej}(\vec{\mathbf{u}}_0 \cdot \vec{\mathbf{n}})^2/2]\,; \quad \vec{\mathbf{u}}_0 \cdot \vec{\mathbf{n}} > 0 \qquad (C.40)$$

C.5 Perturbed Shear Coefficients

The perturbed shear coefficients for the first-order solution are given for a general fluid by:

$$\gamma_{uu} = \Big[\frac{k_{x0}}{h_0} + f_{r1}(u_0 - \Lambda)^2 + f_{s1}u_0^2\Big]\bar{\mu}_0 \qquad (C.41)$$

$$\gamma_{vv} = \Big[\frac{k_{y0}}{h_0} + (f_{r1} + f_{s1})v_0^2\Big]\bar{\mu}_0 \qquad (C.42)$$

$$\gamma_{uv} = \gamma_{vu} = \big[f_{r1}(u_0 - \Lambda) + f_{s1}u_0\big]v_0\bar{\mu}_0 \qquad (C.43)$$

$$\gamma_{uh} = \Big[u_0(-k_{x0} + C_{cr} + C_{cs}) - \Lambda(C_{cr} - k_{J0}/2)\Big]\frac{\bar{\mu}_0}{h_0^2} \qquad (C.44)$$

$$\gamma_{vh} = \frac{v_0}{h_0^2}(-k_{y0} + C_{cr} + C_{cs})\bar{\mu}_0 \qquad (C.45)$$

$$\gamma_{u\rho} = \frac{b_m}{2h_0}\frac{\bar{\mu}_0}{\bar{\rho}_0}[u_0(\gamma_r + \gamma_s) - \Lambda_1\gamma_s] - \frac{h_0}{\bar{\rho}_0}\frac{\partial \bar{p}_0}{\partial \bar{x}} \qquad (C.46)$$

$$\gamma_{v\rho} = \frac{b_m}{2h_0}\frac{\bar{\mu}_0}{\bar{\rho}_0}[v_0(\gamma_r + \gamma_s)] - \frac{h_0}{\bar{\rho}_0}\frac{\partial \bar{p}_0}{\partial \bar{y}} \qquad (C.47)$$

$$\gamma_{u\mu} = \frac{-b_m}{2h_0}[u_0(\gamma_r + \gamma_s) - \Lambda_1\gamma_s] \qquad (C.48)$$

$$\gamma_{v\mu} = \frac{-b_m}{2h_0}[v_0(\gamma_r + \gamma_s)] \qquad (C.49)$$

$$\begin{aligned}\gamma_{tu} = \frac{Re_p^*}{E_c}\Big\{\bar{C}_{p_0}\bar{\rho}_0 h_0\frac{\partial \bar{T}_0}{\partial \bar{x}} + 2h_0\Big[\frac{f_{s1}u_0}{k_{Bo}}\bar{Q}_{Bo} + \frac{f_{r1}(u_0 - \Lambda)}{k_{Jo}}\bar{Q}_{Jo}\Big]\Big\} \\ - \bar{\beta}_{t0}\bar{T}_0 h_0\frac{\partial \bar{p}_0}{\partial \bar{x}} - \frac{\bar{\mu}_0}{h_0}\Big[k_{x0}\Big(2u_0 + \frac{\Lambda}{2}\Big) - \Lambda k_{Jo}\Big] \\ - \bar{\mu}_0[(u_{c0} + 2u_{c1})(u_0 - \Lambda)f_{r1} + u_{c0}u_0 f_{s1}]\end{aligned} \qquad (C.50)$$

$$\begin{aligned}\gamma_{tv} = \frac{Re_p^*}{E_c}\Big[\bar{C}_{p_0}\bar{\rho}_0 h_0\frac{\partial \bar{T}_0}{\partial \bar{y}} + 2h_0 v_0\Big(\frac{f_{s1}}{k_{Bo}}\bar{Q}_{Bo} + \frac{f_{r1}}{k_{Jo}}\bar{Q}_{Jo}\Big)\Big] - \bar{\beta}_0\bar{T}_0 h_0\frac{\partial \bar{p}_0}{\partial \bar{y}} \\ - \frac{\bar{\mu}_0}{h_0}(2k_{y0}v_0) - \bar{\mu}_0 v_0[(u_{c0}(f_{r1} + f_{s1}) + 2u_{c1}f_{r1}]\end{aligned} \qquad (C.51)$$

$$\gamma_{tp} = \gamma_{t\rho}\frac{\partial \bar{\rho}}{\partial p} + \gamma_{t\mu}\frac{\partial \bar{\mu}}{\partial p} + \gamma_{t\beta}\frac{\partial \bar{\beta}}{\partial p} + \gamma_{tk}\frac{\partial \bar{K}}{\partial p} + \gamma_{C_p}\frac{\partial \bar{C}_p}{\partial p} \qquad (C.52)$$

$$\gamma_{tt} = \frac{Re_p^*}{E_c}(\bar{h}_{Bo} + \bar{h}_{Jo}) - \bar{\beta}_0 h_0 (u_0 \frac{\partial \bar{p}_0}{\partial \bar{x}} + v_0 \frac{\partial \bar{p}_0}{\partial \bar{y}}) + \gamma_{t\rho} \frac{\partial \bar{\rho}}{\partial t} + \gamma_{t\mu} \frac{\partial \bar{\mu}}{\partial t} + \gamma_{t\beta} \frac{\partial \bar{\beta}}{\partial t} + \gamma_{tk} \frac{\partial \bar{K}}{\partial t} + \gamma_{C_p} \frac{\partial \bar{C}_p}{\partial t} \quad (C.53)$$

$$\gamma_{th} = \frac{Re_p^*}{E_c}\Big[\bar{C}_{p_0}\bar{\rho}_0(u_0 \frac{\partial \bar{T}_0}{\partial \bar{x}} + v_0 \frac{\partial \bar{T}_0}{\partial \bar{y}}) + \frac{2}{h_0}(\frac{C_{cs}}{k_{Bo}}\bar{Q}_{Bo} + \frac{C_{cr}}{k_{Jo}}\bar{Q}_{Jo})\Big] - \frac{\Lambda}{2}\frac{\partial \bar{p}_0}{\partial \bar{x}} - \bar{\beta}_0 \bar{T}_0 (u_0 \frac{\partial \bar{p}_0}{\partial \bar{x}} + v_0 \frac{\partial \bar{p}_0}{\partial \bar{y}}) - \frac{\bar{\mu}_0}{h_0^2}[u_{c0}(C_{cr} + C_{cs}) + 2u_{c1}C_{cr}] \quad (C.54)$$

$$\gamma_{t\mu} = \frac{b_m}{h_0}[\frac{1}{2}u_{c0}(\gamma_r + \gamma_s) + u_{c1}\gamma_r] - \frac{Re_p^*}{\bar{\mu}_0 E_c}\Big[\frac{2}{3}\bar{Q}_{s0} + \frac{\gamma_s b_m}{k_{Bo}}\bar{Q}_{Bo} + \frac{\gamma_r b_m}{k_{Jo}}\bar{Q}_{Jo}\Big] \quad (C.55)$$

$$\gamma_{t\rho} = \frac{Re_p^*}{E_c}[\bar{C}_{p_0} h_0 (u_0 \frac{\partial \bar{T}_0}{\partial \bar{x}} + v_0 \frac{\partial \bar{T}_0}{\partial \bar{y}}) + (\bar{Q}_{s0} + \frac{\gamma_s b_m}{k_{Bo}}\bar{Q}_{Bo} + \frac{\gamma_r b_m}{k_{Jo}}\bar{Q}_{Jo})/\bar{\rho}_0] - \frac{\bar{\mu}_0}{\bar{\rho}_0 h_0}\{u_{c0}[k_{x0} + \frac{b_m}{2}(\gamma_r + \gamma_s)] + u_{c1}(k_{Jo} + b_m\gamma_r)\} \quad (C.56)$$

$$\gamma_{t\beta} = -h_0 \bar{T}_0 (u_0 \frac{\partial \bar{p}_0}{\partial \bar{x}} + v_0 \frac{\partial \bar{p}_0}{\partial \bar{y}}) \quad (C.57)$$

$$\gamma_{tk} = \frac{2}{3}\frac{Re_p^*}{E_c}\frac{\bar{Q}_{s0}}{\bar{K}_0} \quad (C.58)$$

$$\gamma_{C_p} = \frac{Re_p^*}{E_c}\Big[\bar{\rho}_0 h_0 \Big(u_0 \frac{\partial \bar{T}_0}{\partial \bar{x}} + v_0 \frac{\partial \bar{T}_0}{\partial \bar{y}}\Big) + \frac{1}{3}\bar{Q}_{s0}/\bar{C}_{p0}\Big] \quad (C.59)$$

where

$$C_{cr} = \frac{1}{2}[R_{Jo}C_r + b_m]\gamma_r\,; \quad C_{cs} = \frac{1}{2}[R_{Bo}C_s + b_m]\gamma_s, \quad (C.60)$$

$$C_r = c_m \frac{r_r}{c_* h_0}\,; \quad C_s = c_m \frac{r_s}{c_* h_0}, \quad (C.61)$$

$$R_{Jo} = Re_p(\bar{\rho}_0/\bar{\mu}_0)h_0[(u_0 - \Lambda)^2 + v_0^2]^{1/2},$$
$$R_{Bo} = Re_p(\bar{\rho}_0/\bar{\mu}_0)h_0[u_0^2 + v_0^2]^{1/2}, \quad (C.62)$$

$$\gamma_r = \frac{-a_m \cdot e_m}{[f_{r0}/a_m - 1]^{(1/e_m - 1)}}\,;$$
$$\gamma_s = \frac{-a_m \cdot e_m}{[f_{s0}/a_m - 1]^{(1/e_m - 1)}}, \quad (C.63)$$

$$f_{r1} = \frac{(Re_p \bar{\rho}_0 / \bar{\mu}_0)^2 h_0}{2R_{J0}} [f_{r0} + \beta_r \gamma_r];$$
$$f_{s1} = \frac{(Re_p \bar{\rho}_0 / \bar{\mu}_0)^2 h_0}{2R_{B0}} [f_{s0} + \beta_s \gamma_s], \qquad (C.64)$$

$$\beta_r = b_m / R_{J0}; \quad \beta_s = b_m / R_{B0}, \qquad (C.65)$$

$$u_{c0} = u_0^2 + v_0^2 + u_0 \frac{\Lambda}{2}; \quad u_{c1} = \frac{\Lambda^2}{4} - u_0 \Lambda, \qquad (C.66)$$

$$\bar{Q}_{B0} = \bar{h}_{B0}(\bar{T}_0 - \bar{T}_{B0}); \quad \bar{Q}_{J0} = \bar{h}_{J0}(\bar{T}_0 - \bar{T}_{J0}); \quad \bar{Q}_{s0} = \bar{Q}_{B0} + \bar{Q}_{J0} \qquad (C.67)$$

APPENDIX D

ALGEBRAIC EQUATIONS FOR THIN FILM FLUID FLOWS

For convenience, the subscript "0" is omitted for all the zeroth-order variables.

D.1 Dimensionless Zeroth-Order Discretization Equations

a) Circumferential u-momentum equation:

$$A_P^u u_P = A_E^u u_E + A_W^u u_W + A_S^u u_S + A_N^u u_N + S_c^u \tag{D.1}$$

where

$$A_P^u = \sum A_{nb}^u + S_P^u \tag{D.2}$$

$$\sum A_{nb}^u = A_E^u + A_W^u + A_S^u + A_N^u \tag{D.3}$$

$$\begin{aligned} A_E^u &= Re_p^* \mathrm{Max}(-F_e^u, 0); \quad A_W^u = Re_p^* \mathrm{Max}(F_w^u, 0); \\ A_N^u &= Re_p^* \mathrm{Max}(-F_n^u, 0); \quad A_S^u = Re_p^* \mathrm{Max}(F_s^u, 0) \end{aligned} \tag{D.4}$$

$$\begin{aligned} F_e &= (\bar{\rho} h u)_e \Delta \bar{y}; \quad F_w = (\bar{\rho} h u)_w \Delta \bar{y}; \\ F_n &= (\bar{\rho} h v)_n \Delta \bar{x}; \quad F_s = (\bar{\rho} h v)_s \Delta \bar{x} \end{aligned} \tag{D.5}$$

$$S_P^u = \left[\frac{\bar{\mu}}{h} k_x\right]_P^u \Delta \bar{x}_u \Delta \bar{y}_u \tag{D.6}$$

$$S_c^u = \left[\frac{\bar{\mu}}{h} k_r \frac{\Lambda}{2}\right]_P^u \Delta \bar{x}_u \Delta \bar{y}_u - h_P^u (p_e - p_w) \Delta \bar{y}_u \tag{D.7}$$

b) Axial v-momentum equation:

$$A_P^v v_P = A_E^v v_E + A_W^v v_W + A_S^v v_S + A_N^v v_N + S_c^v \tag{D.8}$$

where

$$A_P^v = \sum A_{nb}^v + S_P^v \tag{D.9}$$

$$A_E^v = Re_p^* \text{Max}(-F_e^v, 0); \quad A_W^v = Re_p^* \text{Max}(F_w^v, 0);$$
$$A_N^v = Re_p^* \text{Max}(-F_n^v, 0); \quad A_S^v = Re_p^* \text{Max}(F_s^v, 0) \tag{D.10}$$

$$S_P^v = \left[\frac{\bar{\mu}}{h} k_y\right]_P^v \Delta\bar{x}_v \Delta\bar{y}_v \tag{D.11}$$

$$S_c^v = -h_P^v (p_n - p_s)\Delta\bar{x}_v \tag{D.12}$$

c) Correction-p equation(from the continuity equation):

$$A_P^p p'_P = A_E^p p'_E + A_W^p p'_W + A_S^p p'_S + A_N^p p'_N + S_c^p \tag{D.13}$$

where

$$A_P^p = \sum A_{nb}^p \tag{D.14}$$

$$A_E^p = (\bar{\rho}h)_e^p \Delta\bar{y}_p D_p^u; \quad A_S^p = (\bar{\rho}h)_s^p \Delta\bar{x}_p D_p^v; \ldots\ldots \tag{D.15}$$

$$D_p^u = \frac{h_p^u \Delta\bar{y}_p}{A_p^u - \sum A_{nb}^u}; \quad D_p^v = \frac{h_p^v \Delta\bar{x}_p}{A_p^v - \sum A_{nb}^v}; \ldots\ldots \tag{D.16}$$

Note that the denominators of D_p^u and D_p^v will not be zero due to under-relaxation and source terms.

$$S_c^p = -(F_e^p - F_w^p + F_n^p - F_s^p) \tag{D.17}$$

d) Energy equation:

$$A_P^t \bar{T}_P = A_E^t \bar{T}_E + A_W^t \bar{T}_W + A_S^t \bar{T}_S + A_N^t \bar{T}_N + S_c^t \tag{D.18}$$

$$A_P^t = \sum A_{nb}^t + S_{P1}^t + \text{Max}(S_{P2}^t, 0) \tag{D.19}$$

$$A_E^t = \bar{C}_p (Re_p^*/E_c)\text{Max}(-F_e^t, 0); \quad A_W^t = \bar{C}_p (Re_p^*/E_c)\text{Max}(F_w^t, 0);$$
$$A_N^t = \bar{C}_p (Re_p^*/E_c)\text{Max}(-F_n^t, 0); \quad A_S^t = \bar{C}_p (Re_p^*/E_c)\text{Max}(F_s^t, 0) \tag{D.20}$$

$$S_{P1}^t = Re_p^*/E_c (\bar{h}_B + \bar{h}_j)\Delta\bar{x}_p \Delta\bar{y}_p \tag{D.21}$$

$$S_{P2}^t = -\bar{\beta}_P h_P [u_P (p_e - p_w)\Delta\bar{y}_p + v_P (p_n - p_s)\Delta\bar{x}_p] \tag{D.22}$$

$$S_c^t = S_{c1}^t + S_{c2}^t + S_{c3}^t + \mathrm{Max}(-S_P^t, 0)\bar{T}_P^{(0)} \qquad (D.23)$$

$$S_{c1}^t = \left\{ \frac{\bar{\mu}}{h}[k_x(u^2 + v^2 + \frac{1}{2}u\Lambda) + k_r(\frac{\Lambda^2}{4} - u\Lambda)] \right\}_P \Delta\bar{x}_p \Delta\bar{y}_p \qquad (D.24)$$

$$S_{c2}^t = \frac{\Lambda}{2} h_P (p_e - p_w)\Delta\bar{y}_p \qquad (D.25)$$

$$S_{c3}^t = Re_p^*/E_c(\bar{h}_B\bar{T}_B + \bar{h}_j\bar{T}_j)\Delta\bar{x}_p\Delta\bar{y}_p \qquad (D.26)$$

D.2 Dimensionless First-Order Discretization Equations

a) u-momentum equation:

$$A_{Pj}^u u_{jP} = A_E^u u_{jE} + A_W^u u_{jW} + A_S^u u_{jS} + A_N^u u_{jN} + S_{cj}^u \qquad (D.27)$$

where

$$A_{Pj}^u = \sum A_{nb}^u + S_{Pj}^u \qquad (D.28)$$

$$\begin{aligned} A_E^u &= Re_p^* \mathrm{Max}(-F_e^u, 0); \quad A_W^u = Re_p^* \mathrm{Max}(F_w^u, 0); \\ A_N^u &= Re_p^* \mathrm{Max}(-F_n^u, 0); \quad A_S^u = Re_p^* \mathrm{Max}(F_s^u, 0) \end{aligned} \qquad (D.29)$$

$$S_{Pj}^u = (\gamma_{uu} + \mathrm{i}\bar{\rho}hRe_s)\Delta\bar{x}_u\Delta\bar{y}_u + \mathrm{Max}(S_{P2j}^u, 0) \qquad (D.30)$$

$$S_{P2j}^u = Re_p^*\bar{\rho}h(u_e - u_w)\Delta\bar{y}_u \qquad (D.31)$$

$$\begin{aligned} S_{cj}^u = &-(\gamma_{uv}v_j + \gamma_{uh}h_j + \gamma_{u\rho}\bar{\rho}_j + \gamma_{u\mu}\bar{\mu}_j)\Delta\bar{x}_u\Delta\bar{y}_u \\ &- Re_p^*\bar{\rho}h(u_n - u_s)\Delta\bar{x}_u v_j + \mathrm{Max}(-S_{P2j}^u, 0)u_j \\ &- h_P^u(p_{jE} - p_{jP})\Delta\bar{y}_u \end{aligned} \qquad (D.32)$$

b) v-momentum equation :

$$A_{Pj}^v v_{jP} = A_E^v v_{jE} + A_W^v v_{jW} + A_S^v v_{jS} + A_N^v v_{jN} + S_{cj}^v \qquad (D.33)$$

where

$$A_{Pj}^v = \sum A_{nb}^v + S_{Pj}^v \qquad (D.34)$$

$$A_E^v = Re_p^* \mathrm{Max}(-F_e^v, 0); \quad A_W^v = Re_p^* \mathrm{Max}(F_w^v, 0);$$
$$A_N^v = Re_p^* \mathrm{Max}(-F_n^v, 0); \quad A_S^v = Re_p^* \mathrm{Max}(F_s^v, 0) \tag{D.35}$$

$$S_{Pj}^v = (\gamma_{vv} + \mathrm{i}\bar{\rho}hRe_s)\Delta\bar{x}_v\Delta\bar{y}_v + \mathrm{Max}(S_{P2j}^v, 0) \tag{D.36}$$

$$S_{P2j}^v = Re_p^*\bar{\rho}h(v_n - v_s)\Delta\bar{x}_v \tag{D.37}$$

$$\begin{aligned} S_{cj}^v = &-(\gamma_{vu}u_j + \gamma_{vh}h_j + \gamma_{v\rho}\bar{\rho}_j + \gamma_{v\mu}\bar{\mu}_j)\Delta\bar{x}_v\Delta\bar{y}_v \\ &- Re_p^*\bar{\rho}h(v_e - v_w)\Delta\bar{y}_v u_j + \mathrm{Max}(-S_{P2j}^v, 0)v_j \\ &- h_P^v(p_{jP} - p_{jS})\Delta\bar{x}_v \end{aligned} \tag{D.38}$$

c) Correction-p equation(from the continuity equation):

$$A_P^p p'_{jP} = A_E^p p'_{jE} + A_W^p p'_{jW} + A_S^p p'_{jS} + A_N^p p'_{jN} + S_{cj}^p \tag{D.39}$$

where

$$A_P^p = \sum A_{nb}^p \tag{D.40}$$

$$A_E^p = (\bar{\rho}h)_e^p \Delta\bar{y}_p D_p^u; \quad A_S^p = (\bar{\rho}h)_s^p \Delta\bar{x}_p D_p^v; \ldots\ldots \tag{D.41}$$

$$D_p^u = \frac{h_p^u \Delta\bar{y}_p}{A_p^u - \sum A_{nb}^u}; \quad D_p^v = \frac{h_p^v \Delta\bar{x}_p}{A_p^v - \sum A_{nb}^v}; \ldots\ldots \tag{D.42}$$

$$\begin{aligned} S_{cj}^p = &-(F_{ej}^p - F_{wj}^p + F_{nj}^p - F_{sj}^p) - (\bar{\rho}uh_j + \bar{\rho}_j uh)_w^e \Delta\bar{y} \\ &- (\bar{\rho}vh_j + \bar{\rho}_j vh)_s^n \Delta\bar{x} - \mathrm{i}\sigma(\bar{\rho}_j h + \bar{\rho}h_j)\Delta\bar{x}\Delta\bar{y} \end{aligned} \tag{D.43}$$

$$\begin{aligned} F_{ej}^p &= (\bar{\rho}hu_j)_e \Delta\bar{y}; \quad F_{wj}^p = (\bar{\rho}hu_j)_w \Delta\bar{y}; \\ F_{nj}^p &= (\bar{\rho}hv_j)_n \Delta\bar{x}; \quad F_{sj}^p = (\bar{\rho}hv_j)_s \Delta\bar{x} \end{aligned} \tag{D.44}$$

d) Energy equation:

$$A_{Pj}^t \bar{T}_{jP} = A_E^t \bar{T}_{jE} + A_W^t \bar{T}_{jW} + A_S^t \bar{T}_{jS} + A_N^t \bar{T}_{jN} + S_{cj}^t \tag{D.45}$$

where

$$A_{Pj}^t = \sum A_{nb}^t + \gamma_{tt}\Delta\bar{x}_p\Delta\bar{y}_p \tag{D.46}$$

$$A_E^t = \bar{C}_p(Re_p^*/E_c)\mathrm{Max}(-F_e^t, 0)\,; \quad A_W^t = \bar{C}_p(Re_p^*/E_c)\mathrm{Max}(F_w^t, 0)\,;$$
$$A_N^t = \bar{C}_p(Re_p^*/E_c)\mathrm{Max}(-F_n^t, 0)\,; \quad A_S^t = \bar{C}_p(Re_p^*/E_c)\mathrm{Max}(F_s^t, 0) \tag{D.47}$$

$$\begin{aligned} S_{cj}^t = [&-(\gamma_{tu}u_j + \gamma_{tv}v_j + \gamma_{tp}p_j + \gamma_{th}h_j) \\ &+ \bar{h}_{Bj}(\bar{T}_{B0} - \bar{T}_0) + \bar{h}_{Jj}(\bar{T}_{J0} - \bar{T}_0)]\Delta\bar{x}_p\Delta\bar{y}_p \\ &+ (\bar{\beta}\bar{T}hu + h\frac{\Lambda}{2})(p_{je} - p_{jw})\Delta\bar{y}_p + \bar{\beta}\bar{T}hv(p_{jn} - p_{js})\Delta\bar{x}_p \end{aligned} \tag{D.48}$$